

POLITECNICO DI TORINO

Master Course in Mathematical Engineering

Master Thesis

**Mathematical Models of Crowd-to-Structure Action in Footbridges  
at Different Scales**



**Supervisor:**

Andrea Tosin

**Co-supervisor:**

Fiammetta Venuti

**Candidate:**

Luca Lanzilao

*Academic Year 2018-2019*



*The first step is to establish that something is possible;  
then probability will occur.*  
— *Elon Musk*



# Acknowledgement

First and foremost, I am very grateful to my supervisor, prof. Andrea Tosin, and co-supervisor, prof. Fiammetta Venuti, for guiding me in this Master Thesis work. I really appreciated the fact that they were always available and enthusiast to discuss new results and to help me when I could not achieve a goal by myself. They also guided me through the conception, the development, and the improvement of the present work, and they finally proofread the whole thesis to lead it to its best possible form. I truly benefited from their high standards.

I would also like to thank my family, who always have supported my studies and my decisions; surely without them nothing of this would have been possible.

I am also very grateful to all friends and colleagues with who i shared the last five years; a special thanks goes to Alessandro, Dario, Domenica, Giada, Luca, Mattia and Michele, with who I did many team work projects, exams and shared unforgettable moments, in and out of university.

Last but not least, I would like to extend my gratitude to my girlfriend, who constantly believed in my skills, gave me the right advice when needed and helped me to afford life decision. I would not be here without your support.



# Abstract

The problem of footbridge vibrations due to pedestrian motion is largely studied nowadays. This intensive attention is due to the construction of increasingly daring structures which has led to build very slender footbridges. Mathematical frameworks that aim to simulate this phenomenon should include suitable models to describe the crowd system, the structure system and the dynamic force exerted by the crowd on the structure.

In this thesis a comparison is made between results provided by approaching the problem from two different points of view, respectively a microscopic and a macroscopic one, in a one-dimensional domain. Regarding the microscopic scale, a first-order crowd model is used accompanied by a force model which uses the positions and velocities of pedestrians for evaluating the dynamic load exerted on the structure. In the macroscopic scale, a first-order crowd model is used, which is directly derived from the microscopic one by means of an upscaling procedure that relies on notions of kinetic theory.

The scale passage allows us to get a macroscopic crowd model that is a generalization of the microscopic one, and they can be considered as equivalent; also the macroscopic crowd model is accompanied by a force model which evaluates the dynamic load exerted on the structure, once that the pedestrian velocity and density are given. In both frameworks, the footbridge is modelled as a single degree of freedom system which is used for computing the vertical acceleration of the structure. Finally, the response in both frameworks is studied when the number of pedestrians  $N$  on the footbridge varies.

Since the two types of models are equivalent, their dynamics are similar for large times when  $N \rightarrow \infty$ ; in this work, it is demonstrated that this hypothesis is met with good approximation also for finite  $N$  and, in particular, proper estimates of  $N$  are derived. Moreover, results concerning vertical

accelerations are discussed.

# Contents

<b>1</b>	<b>Introduction</b>	<b>1</b>
<b>2</b>	<b>Literature review</b>	<b>9</b>
2.1	Microscopic crowd models . . . . .	9
2.1.1	First-order models . . . . .	10
2.1.2	Second-order models . . . . .	12
2.1.2.1	Social force model . . . . .	12
2.1.2.2	Other force models . . . . .	19
2.2	Macroscopic crowd models . . . . .	20
2.2.1	Fundamental diagram . . . . .	21
2.2.2	First-order models . . . . .	23
2.2.2.1	Colombo and Rosini's model . . . . .	24
2.2.2.2	Coscia and Canavesio's Model . . . . .	25
2.2.2.3	Maury et al.'s model . . . . .	26
2.2.2.4	Non-local models . . . . .	27
2.2.3	Second-order models . . . . .	29
2.3	Mesoscopic crowd models . . . . .	31
2.3.1	Common features . . . . .	32
2.3.2	Dogbè's model . . . . .	34
2.4	Force models . . . . .	36
2.5	Structure models . . . . .	39
<b>3</b>	<b>Description of the modelling framework</b>	<b>45</b>
3.1	The microscopic crowd model . . . . .	45
3.2	The mesoscopic crowd model . . . . .	49
3.2.1	Weak form of a Boltzmann-type equation . . . . .	49
3.2.2	Statistical moments . . . . .	54

---

3.2.3	Fokker-Planck equation . . . . .	56
3.3	The macroscopic crowd model . . . . .	61
3.4	Equivalence of crowd models . . . . .	65
3.4.1	Wasserstein metric . . . . .	66
3.5	The structure model . . . . .	72
3.6	The force model . . . . .	73
3.6.1	The microscopic force model . . . . .	73
3.6.2	The macroscopic force model . . . . .	74
3.6.3	Equivalence of force models . . . . .	75
<b>4</b>	<b>Numerical results</b>	<b>79</b>
4.1	Macroscopic model results . . . . .	79
4.1.1	Burger's equation . . . . .	80
4.1.2	Crowd model . . . . .	83
4.1.3	Force model . . . . .	89
4.1.4	Structure model . . . . .	90
4.2	Microscopic model results . . . . .	93
4.2.1	Crowd model . . . . .	94
4.2.2	Force model . . . . .	98
4.2.3	Structure model . . . . .	99
4.3	Comparing results . . . . .	102
<b>5</b>	<b>Conclusions and future works</b>	<b>113</b>
5.1	Summary of results . . . . .	113
5.2	Suggestions for future research . . . . .	117
<b>A</b>	<b>Finite Volume Method</b>	<b>119</b>
A.0.1	Two-dimensional case . . . . .	121
A.0.2	One-dimensional case . . . . .	123
A.0.2.1	Example: . . . . .	124
	<b>Bibliography</b>	<b>129</b>

---

# List of Figures

1.1	Footbridges affected by excessive vibration problems. . . . .	2
1.2	Comparison of main lateral and vertical natural frequency of different types of footbridges, respectively in graph (a) and (b); the data are provided in [98, 101]. . . . .	3
1.3	Comparison among the three modelling approaches. . . . .	5
2.1	Pedestrian size and relative notations. . . . .	11
2.2	Path for reaching the target destination $\mathbf{r}_i^K$ in a domain with obstacles. .	13
2.3	Repulsion forces between two interacting pedestrians. . . . .	13
2.4	Sensory region of the $i$ -th pedestrian; $R$ is the length, $\theta$ is the angle representing the breadth, $j$ and $k$ are two other pedestrians within the sensory region. . . . .	14
2.5	Repulsion forces due to domain boundaries acting on the $i$ -th pedestrian.	15
2.6	Crowd dynamics on a two-dimensional domain. . . . .	16
2.7	Possible choices for expressing the velocity as dependent from the pedestrian density. . . . .	21
2.8	Velocity-density relations in literature [83–93]: linear laws are shown in (a) while non-linear ones are shown in (b). . . . .	23
2.9	Mass conservation due to incoming and outgoing flux of pedestrians across domain boundaries. . . . .	24
2.10	Example of admissible flow. . . . .	25
2.11	Examples of localizations strategies on a one-dimensional domain; the black lines represent the density while the red points/lines represent the perceived density within the sensory region $R_s$ of the $i$ -th pedestrian. . .	28
2.12	Walking force time history generated by a single pedestrian walking at 1.39 m/s and 1.81 Hz pacing rate [115]. . . . .	37
2.13	Moving force model in graph (a); moving mass model in graph (b). . . .	38

---

2.14	Single degree of freedom pedestrian model in graph (a); inverted-pendulum pedestrian model in graph (b). . . . .	39
2.15	Modulus and phase of the dynamic amplification factor for a single degree of freedom system for different values of $\xi$ . . . . .	43
3.1	Schematic description of the modelling framework. . . . .	46
3.2	Example of a suitable interaction kernel. . . . .	48
3.3	Pedestrian in position $x_j(t)$ is within the sensory region $R_s(x_i)$ of pedestrian in position $x_i(t)$ ; $R$ is the length of the sensory region. . . . .	50
3.4	In (a) the total mass $M$ of the system is constant while the mass $m$ of each pedestrian becomes infinitesimal as $N$ increases. In (b) the mass $m$ of each pedestrian is constant while $M$ grows when $N$ increases. . . . .	64
3.5	$h(x)$ and $s(x)$ are two normal probability distributions with $\sigma = 0.2$ , $\mu_h = 1$ and $\mu_s = 3$ in (a), and with $\sigma = 0.2$ , $\mu_h = 1.5$ and $\mu_s = 2.5$ in (b). . . . .	67
3.6	Graphical representation of how the Wasserstein metric operate. . . . .	69
4.1	Discontinuity evolution with initial condition $\rho_L = 0.6$ , $\rho_R = 0.2$ in (a) and $\rho_L = 0.2$ , $\rho_R = 0.6$ in (b). In both graphs the solution is plotted at time $t = 0.5$ s. . . . .	81
4.2	Comparison between the exact and approximate solutions of Burger's equation. In both graphs the solution is plotted at time $t = 0.5$ s. . . . .	82
4.3	Time evolution of the pedestrian density. . . . .	86
4.4	Time evolution of the pedestrian velocity. . . . .	87
4.5	Time evolution of the pedestrian pacing frequency. . . . .	88
4.6	Dynamic load exerted by pedestrians on the footbridge. . . . .	90
4.7	Vertical acceleration of the footbridge due to pedestrian motion. . . . .	92
4.8	Total mass of the system. . . . .	93
4.9	$N = 100$ pedestrians walking along a footbridge with length $L = 100$ m and width $B = 2$ m. Due to the assumption of one-dimensional domain, pedestrians can walk only along a straight line. . . . .	94
4.10	In graph (a) the pedestrian positions are distributed according to a uniform distribution; in graph (b) they follow a Beta distribution. In both cases the total number of pedestrians is $N = 100$ . . . . .	95
4.11	Time evolution of the pedestrian positions. In blue and red is represented a generic couple of pedestrian $i$ and $j$ ; the total number of pedestrians is $N = 125$ . . . . .	96

---

4.12	Velocities and pacing frequencies of a generic couple of pedestrians $i$ and $j$ marked respectively in blue and red in Fig.(4.11); the total number of agents on the footbridge is $N = 125$ and the desired velocity is $v_d = 1.41$ m/s. . . . .	97
4.13	Velocities and pacing frequencies of a generic couple of pedestrians; the total number of agents on the footbridge is $N = 70$ and the desired velocity is $v_d = 1.41$ m/s. . . . .	98
4.14	Dynamic load exerted by $N = 125$ pedestrians on the footbridge; the force is obtained with the assumption of $M = 1$ . . . . .	99
4.15	Vertical acceleration of the footbridge due to pedestrian motion under the assumption of $M = 1$ ; the system is exerted by the force $F(t)$ and the total number of pedestrian is $N = 125$ . . . . .	100
4.16	Vertical accelerations generated by $N = 125$ pedestrians, and relative force and force spectrum; in (a) the desired velocity is set to $v_d = 1.05$ m/s while in (b) is set to $v_d = 1.50$ m/s. N.a. is the acronym of normalized amplitude. . . . .	101
4.17	In blue are reported the maximum values in modulus of force and vertical acceleration provided by the microscopic force and structural models during a time simulation of 1000 s; In red are reported the maximum values in modulus of force and vertical acceleration provided by the macroscopic force and structural models during a time simulation of 1000 s. A logarithmic scale on the $y$ -axis is used in graph (b). . . . .	103
4.18	In histogram (a) it is reported $\rho_{micro}(t, x)$ in blue and $\rho_{macro}(x)$ in red; the time evolution of the Wasserstein metric is shown in (b); the pedestrian positions on the footbridge are shown in (c). All graph are obtained with $N = 50$ . . . . .	105
4.19	In histogram (a) it is reported $\rho_{micro}(t, x)$ in blue and $\rho_{macro}(x)$ in red; the time evolution of the Wasserstein metric is shown in (b); the pedestrian positions on the footbridge are shown in (c). All graph are obtained with $N = 100$ . . . . .	106
4.20	Time evolution of the Wasserstein metric as $N$ varies. . . . .	108
4.21	In histogram (a) it is reported $\rho_{micro}(t, x)$ in blue and $\rho_{macro}(x)$ in red; the time evolution of the Wasserstein metric is shown in (b); the pedestrian positions on the footbridge are shown in (c). All graph are obtained with $N = 550$ . . . . .	109

---

4.22	Wasserstein metric computed at time $t_0(N)$ for increasing values of $N$ . . .	111
A.1	Spatial discretization of a two-dimensional domain. . . . .	121
A.2	Spatial discretization of a one-dimensional domain. . . . .	123
A.3	Solutions of initial-value problem (A.12) plotted at time $t = 4.5$ s and obtained with different numerical fluxes; the exact solution in red is given by (A.14). . . . .	126

---

# List of Tables

4.1	Parameter values used in numerical simulations. . . . .	85
4.2	Dynamic properties of the structure model. . . . .	91
4.3	Defined comfort classes and related vertical acceleration values [79]. . . .	102
4.4	Values of mean velocity $\bar{v}(N)$ in m/s, crossing time $T(N)$ in seconds, reference time $t_0(N)$ in seconds and Wasserstein metric $W_1(N)$ as $N$ varies.	110



# Chapter 1

## Introduction

In the last twenty years, excessive footbridge vibrations induced by walking pedestrians have become one of the leading research topic in structural dynamics.

This relatively young research topic has grown very fast after that some footbridges have been closed due to excessive vibrations. It is well known the case of the Millennium Bridge in London, which was closed immediately after the opening day; the bridge is shown in Fig.(1.1a) and a deep analysis and discussion about the manifested problem is made by P. Dallard et al. in [98]. The same phenomenon has occurred on the Solferino Bridge in Paris; also this footbridge, which is shown in Fig.(1.1b), was affected by excessive lateral vibrations when a huge number of pedestrians walked on it; the reasons which triggered this behaviour are amply explained in [99]. Many other cases which did not lead to a complete closure of the footbridge but still required structural interventions are known, such as the T-Bridge in Tokyo in Fig.(1.1c), the Alexandra Bridge in Ottawa or the Queens Park Bridge in Chester; analysis and information about them can be found in [100].

Experimental data reported in [114] confirm that the pacing vertical frequency is usually in the range  $1.7 - 2.1$  Hz, depending on the pedestrian velocity, while the pacing lateral frequency is half the vertical one. Consequently, recent footbridge design guidelines, e.g. [79, 110], identify vertical vibration modes in the range  $1.7 - 2.1$  Hz and lateral vibration modes in the range  $0.5 - 1.1$  Hz as the ones characterized by the maximum risk of resonance. Values of the vertical and lateral natural frequency for different types for footbridges are reported in Fig.(1.2). Therefore, as discussed in [101], a



(a) Millennium Bridge, London



(b) Solferino Bridge, Paris



(c) T-Bridge, Tokyo

Figure 1.1: Footbridges affected by excessive vibration problems.

footbridge can have the vertical natural frequency and/or the lateral natural frequency within the respectively range above-mentioned, depending on the type and length, and as a consequence it can be affected by excessive vertical and/or lateral vibrations when pedestrians walk on it. In this thesis we will treat only the phenomenon of excessive vertical vibrations.

In recent years, a considerable number of articles has been published and remarkable advances have been made in the experimental characterization and mathematical modelling of footbridge vertical vibrations induced by pedestrian walking. Despite these advances, there is still a lack of reliable methods and adequate design guidelines relevant to serviceability of light and slender footbridges that may vibrate when occupied by pedestrians.

In order to evaluate the effect of multiple pedestrians walking on a lively

---

structure, we have to consider the following three models:

- Crowd model: it is important to describe how pedestrians move on the footbridge; indeed, each pedestrian has its own strategy, which may be perturbed by interactions with other walkers or with the environment. In order to evaluate the generated vibrations, we should be able to predict the pedestrians distribution along the footbridge over time.
- Force model: we should be able to evaluate the force exerted on the footbridge due to pedestrian walking; this dynamic load strongly depends on the pedestrian velocities, which are given by the crowd model.
- Structure model: we have to introduce a model able to evaluate the vertical acceleration of the footbridge, and consequently the vertical vibrations, when it is excited by a dynamic load described by the force model.

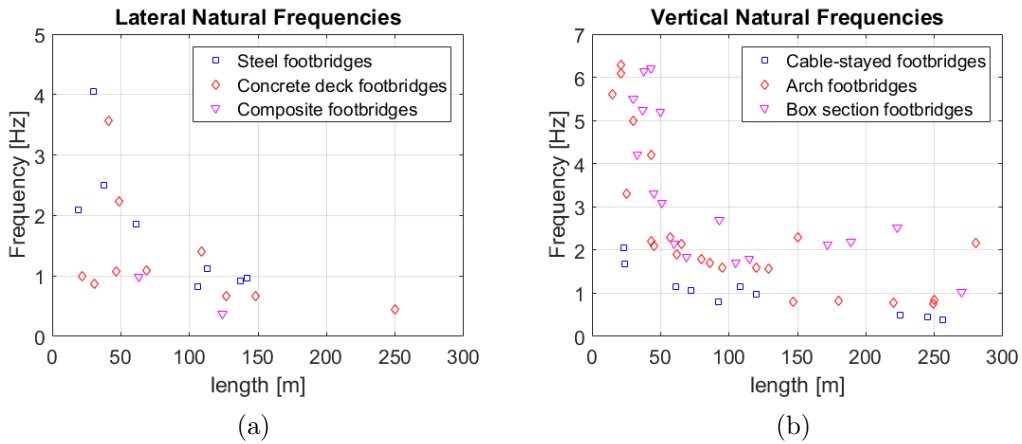


Figure 1.2: Comparison of main lateral and vertical natural frequency of different types of footbridges, respectively in graph (a) and (b); the data are provided in [98, 101].

In the following, we will discuss more in details the above-mentioned models.

The collective dynamics of crowd systems depend strongly on the behaviour of the individuals which constitute them; indeed pedestrians have different strategies and different goals and, depending on the situations, they

interact in different ways. For these reasons a crowd is classified as a complex system, that is a system composed by several individuals which evolves through self-organization. A first attempt to model pedestrian motion could be by treating pedestrians as particles; but, unlike particles, human beings react to internal influences or preferences. Indeed pedestrians are defined as intelligent agents who react to what they perceive around them.

The modelling of crowd dynamics can be tackled at three different scales of observation:

- Microscopic scale: this is the most precise scale, which allows one to track the position and the velocity of each pedestrian, and to define his/her strategy. Moreover, this approach accounts explicitly for the inter-subject variability of pedestrians, so that particular features for each agent can be considered. A typical example of model which uses this approach is the social force model by Helbing and co-authors [4, 102, 103].
  - Macroscopic scale: models that use this approach aim to describe the global dynamics of the system without direct reference to the behaviour of individuals; consequently, we do not have information about position and velocity of each single pedestrian, but instead the system is usually described in term of pedestrian density. These models are based on the analogy between a flow of pedestrians and a continuous flow of a fluid; thus crowd movements are described by equations similar to those found in fluid mechanics. Examples of macroscopic crowd models are given in [36, 38, 41, 43, 45, 48, 84, 104].
  - Mesoscopic scale: this is an intermediate scale, also defined as kinetic scale. A statistical representation is used, in which the state of the whole system is described by a suitable probability distribution over the microscopic state of the interacting elements. Indeed, by analogy with the kinetic theory of rarefied gas, it is assumed that pedestrians change their microscopic state after each interaction; only pairwise interactions are considered. Thanks to this approach, we can study how a single pedestrian interacts with others nearby, and consequently how their statistical distribution evolves in time. Examples of mesoscopic crowd models are given in [28, 74, 76–78, 105].
-

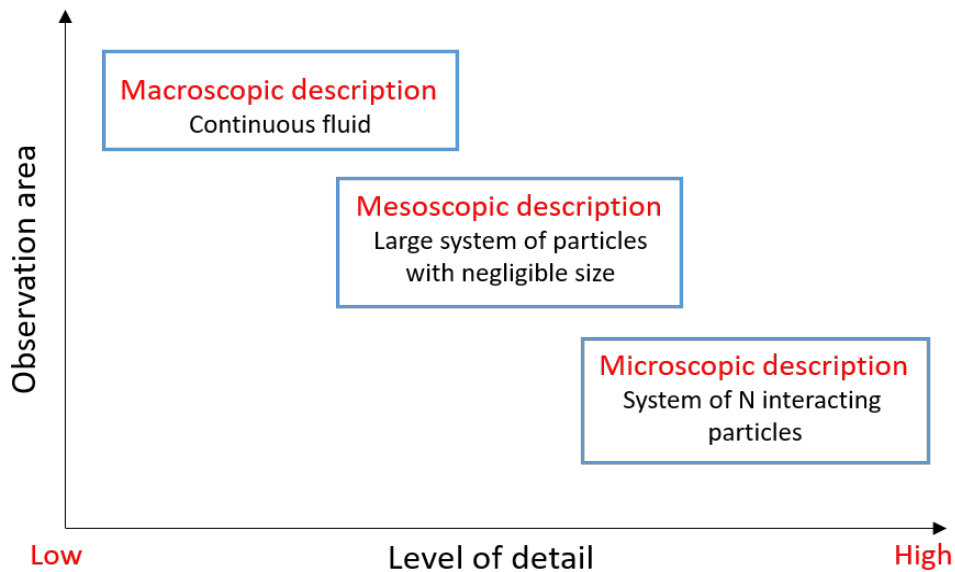


Figure 1.3: Comparison among the three modelling approaches.

As shown in Fig.(1.3), by passing from a microscopic to a mesoscopic scale and finally to a macroscopic one, we lose precision in the description of the crowd, although the modelling becomes less and less costly from the numerical point of view; on the contrary, the observation area increases, which means that we describe the crowd firstly by looking at how one single pedestrian behaves, then by looking at how groups of walkers interact and finally by looking at the whole crowd as a continuous fluid. Therefore, it is usually advisable to use a macroscopic crowd model when we are dealing with a huge number of pedestrians, while a microscopic crowd model is more suitable for problems that deals with a restricted number of pedestrians.

Concerning the footbridge vibration problem, strong arguments in favour of one modelling approach instead of another still cannot be found; indeed in literature the analysis is carried out both with macroscopic crowd models used in [51,52,54,57] and microscopic crowd models used in [2,55,56]. Up to now, no mesoscopic crowd models have been applied for modelling footbridge vibration problem, but instead they are used to realize the scaling passage from microscopic to macroscopic models.

As previously said, also the choice of the force model is fundamental in modelling footbridge vibration problems; indeed, according to how the

dynamic load due to pedestrian walking is evaluated, results can strongly differ.

Starting from the excessive lateral vibration problem shown in the Millennium Bridge in 2000, a lot of work has been made in order to understand how pedestrian walking induces lateral oscillation in the structures; different models and deep analysis of the problem can be found in [43, 54, 55, 106]. On the other hand, only little is known about the way in which pedestrians interact with structures in the vertical direction. By the way, few attempts to model this phenomenon have been done in the past and nowadays there are several models which tackle it.

The simplest model is the moving force one, in which each pedestrian is described as a concentrated load that travels at a certain velocity on the structure. Even if this model does not take into account pedestrian-structure interactions, it is by far the most used due to its simplicity. More realistic models are the ones which try to include pedestrian-structure interactions, because it is proved that pedestrians change the dynamic properties of the structure on which they are walking. Examples of these models are the moving mass one, developed by Biggs [112], or the spring-mass-damper one, introduced by Caprani et al. [108, 111] and further adopted in [56, 109]. Other models have been proposed in literature, and the description of some of them can be found in [111].

Finally, a structure model is needed in order to evaluate the vertical acceleration of the footbridge. Two different types of models are used in literature; the bridge can be modelled using either a formulation in modal coordinates or Finite Element (FE) methods [111]. Since experimental data often confirm that there is only a single mode which dominates the footbridge response, a single degree of freedom system is usually adopted to model the structure.

This thesis is organized as follows: the useful notions for fully understanding our work are introduced in chapter 2; moreover, a literature review is made, which gives an idea of the evolution over the years of each field that composes this research topic. In chapter 3 the modelling framework used in this work is presented in detail. The microscopic crowd model is introduced and a scale passage is made in order to derive the evolution equation valid at the macroscopic scale; moreover, also the force and structure models are

---

discussed. Finally, an analytical comparison between the microscopic and macroscopic frameworks is made. Numerical results are reported and discussed in chapter 4; the data provided by the crowd, force and structure models at the microscopic and macroscopic levels are compared when the number of pedestrians  $N$  varies and it is proved that the systems on the two scales have the same dynamics. Moreover, by using the microscopic crowd model an estimate of the number of pedestrians from which a macroscopic approximation is valid is obtained. Finally, in chapter 5 the main results are summarized and future research perspective are proposed.

---



# Chapter 2

## Literature review

The purpose of this chapter is to give an overview of the literature inherent to problems treated in this thesis, and to provide the necessary theory for understanding it. In particular, in sections 2.1, 2.2 and 2.3 examples are given of crowd models based on microscopic, macroscopic and mesoscopic scales. This helps to get a better idea of the main differences among the three scales, and provides an overview of the current achievements reached in this field. Moreover, in section 2.4 some force models are reported, which allow us to understand how walking pedestrians on footbridges are modelled. Finally, in section 2.5 we will examine the structure model adopted in this work.

### 2.1 Microscopic crowd models

The dynamics of a crowd can be modelled at different levels. If the interest is in a detailed comprehension of the characteristics of each individual, then a description based on a microscopic scale must be chosen. Indeed this allows one to track each pedestrian, and to keep a detailed focus over all the simulated crowd.

In literature a certain number of articles regarding crowd dynamics models based on a microscopic description is available. Among these ones, a great part are inherent to crowd force models. The social force model was introduced by Helbing and Molnàr [4], and was further developed in many ways, for instance by adding waiting pedestrians [6], signalized cross-

walks [5] or information transmission mechanisms [7]. The magnetic force model, where it is assumed that pedestrians behave as magnets, were introduced by Okazaki [8–10], Okazaki and Matsushita [11] and Okazaki and Yamamoto [12]. The centrifugal force model, which is more recent, differs from the social force model mainly in the definition of the repulsive force, and was introduced by Yu et al. [13]. Other microscopic crowd models are the cellular automata models, in which the concept of repulsion force does not exist but instead each pedestrian is represented by a cell of a spatial grid, and the way to move is decided on the basis of the state of the surrounding cells. These types of models were introduced by Kirchner and Schadschneider [14], Blue and Adler [15–17] and Burstedde et al. [18].

In the next paragraphs we will discuss the main features of some of the above-mentioned models. We will denote by  $\mathbf{r}_i(t)$  and  $\mathbf{v}_i(t)$  respectively the position and velocity of the  $i$ -th pedestrian; in general  $\mathbf{r}_i : [0, \infty) \rightarrow \mathbb{R}^d$  and  $\mathbf{v}_i : [0, \infty) \rightarrow \mathbb{R}^2$ , where  $d$  is the dimension of the domain. Since pedestrian motion normally takes place on two-dimensional domains, in the following we will set  $d = 2$ .

### 2.1.1 First-order models

A first-order differential model is described by  $2N$  scalar ordinary differential equations

$$\dot{\mathbf{r}}_i(t) = \mathbf{v}_i(t, \mathbf{r}_1, \dots, \mathbf{r}_N), \quad i = 1, \dots, N \quad (2.1)$$

accompanied by the initial conditions  $\mathbf{r}_{0,i}$ . In this framework it is possible to predict only the time evolution of the pedestrian position  $\mathbf{r}_i(t)$ , which depends on the velocity; indeed there are no other equations that express the time derivative of the velocity in function of external forces.

An example of first-order model is the Maury and Venel's one, introduced by the authors in [20]. In the following only the main concepts are reported. In this model pedestrians are identified as rigid disks, all with common radius value  $s$  and center  $\mathbf{r}_i(t)$ . For the sake of simplicity, in the following the time dependence will be omitted. It is reasonable to assume that a pedestrian cannot walk over other pedestrians, therefore the set of feasible configurations is given by

$$\mathcal{R} = \{\mathbf{r} \in \mathbb{R}^{2N} : D_{i,j}(\mathbf{r}) \geq 0, \forall i, j, i \neq j\}, \quad \forall t > 0$$


---

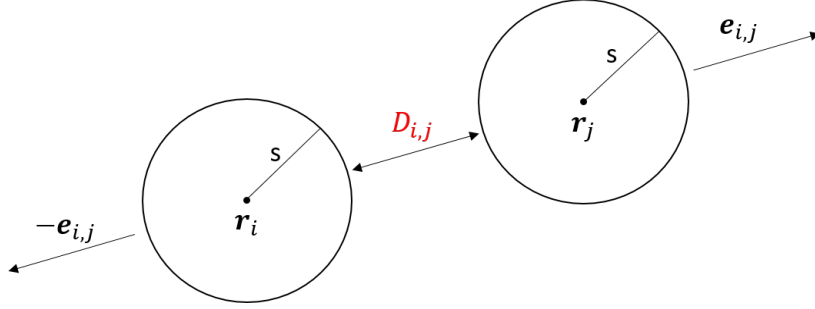


Figure 2.1: Pedestrian size and relative notations.

where  $\mathbf{r} = (\mathbf{r}_1, \dots, \mathbf{r}_N) \in \mathbb{R}^{2N}$  is the position vector and  $D_{i,j}(\mathbf{r}) = |\mathbf{r}_i - \mathbf{r}_j| - 2s$  is the distance between a couple of pedestrians  $i$  and  $j$ . If we assume that pedestrians do not have all the same size, then  $D_{i,j}(\mathbf{r}) = |\mathbf{r}_i - \mathbf{r}_j| - s_i - s_j$ . In this model pedestrians are treated as points with volume, like represented in Fig.(2.1).

This is a first-order model, therefore it is not possible to refer at the pedestrian acceleration; for this reason it is assumed that a pedestrian-independent desired velocity field  $\mathbf{v}_d$  is given. Hence, once the specific position  $\mathbf{r}_i$  of the  $i$ -th pedestrian is computed, we can evaluate his/her velocity  $\mathbf{v}_i$ , which is given by the projection of  $\mathbf{v}_d(\mathbf{r}_i)$  on a space of admissible velocity. This projection is made for taking into account the fact that if the velocity  $\mathbf{v}_d(\mathbf{r}_i)$  is assigned directly, it may happen that pedestrians collide.

The cone of admissible velocities  $C(\mathbf{r})$  on which  $\mathbf{v}_d(\mathbf{r}_i)$  is projected is given by

$$C(\mathbf{r}) = \{ \mathbf{z} \in \mathbb{R}^{2N} : D_{i,j}(\mathbf{r}) = 0 \Rightarrow \mathbf{z}_i \cdot \mathbf{e}_{i,j}(\mathbf{r}) + \mathbf{z}_j \cdot \mathbf{e}_{j,i}(\mathbf{r}) \geq 0, \forall i < j \}$$

where

$$\mathbf{e}_{i,j}(\mathbf{r}) = \frac{\mathbf{r}_i - \mathbf{r}_j}{|\mathbf{r}_i - \mathbf{r}_j|}$$

and is properly defined so that whenever two pedestrians  $i$  and  $j$  enter in contact, their velocities  $\mathbf{v}_i$  and  $\mathbf{v}_j$  will make their mutual distance  $D_{i,j}(\mathbf{r})$  immediately increase, and so collisions are avoided. Hence, Eq.(2.1) becomes

$$\dot{\mathbf{r}} = P_{C(\mathbf{r})} \mathbf{v}_d(\mathbf{r}) \quad (2.2)$$

where  $P_{C(\mathbf{r})}$  is the projection operator on set  $C(\mathbf{r})$ . Eq.(2.2) describes the dynamics of all  $N$  pedestrians.

### 2.1.2 Second-order models

A second-order differential model is described by  $4N$  scalar ordinary differential equations, where  $N$  is the number of pedestrians. There are  $2N$  equations regarding the evolution of the position  $\mathbf{r}(t) \in \mathbb{R}^2$  of each pedestrian and  $2N$  equations for the velocity  $\mathbf{v}(t) \in \mathbb{R}^2$ . The model can be written as

$$\begin{cases} \dot{\mathbf{r}}_i(t) = \mathbf{v}_i(t) \\ \dot{\mathbf{v}}_i(t) = \mathbf{F}_i(t, \mathbf{r}_1, \dots, \mathbf{r}_N, \mathbf{v}_1, \dots, \mathbf{v}_N) \end{cases} \quad (2.3)$$

where  $i = 1, \dots, N$ . The initial conditions  $\mathbf{r}(0) = \mathbf{r}_{0,i}$  and  $\mathbf{v}(0) = \mathbf{v}_{0,i}$  provide an initial configuration of the crowd and starting from this point the system will simulate a possible evolution. The total force  $\mathbf{F}_i$  exerted on the  $i$ -th pedestrian can be expressed in many ways; in the following we will analyse some of them.

#### 2.1.2.1 Social force model

The social force model introduced by Helbing and Molnàr in [4] is characterized by a particular choice of total force. In the following we will give a detailed description of each force term which composes  $\mathbf{F}_i$ .

##### 1. Desired velocity:

Each pedestrian has a specified target to reach. We will denote by  $\mathbf{r}_{K,i}$  the target destination of the  $i$ -pedestrian, which can be for instance the exit of a room. As represented in Fig.(2.2), the domain in which pedestrians walk can have obstacles, therefore he/she is forced to set intermediate target destinations  $\mathbf{r}_{1,i}, \mathbf{r}_{2,i}$  in order to arrive at the final destination  $\mathbf{r}_{K,i}$ . Note that in general the target destinations  $\mathbf{r}_{k,i}$  with  $k = 1, \dots, K$  are time independent, because it is reasonable to assume that each pedestrian knows his/her goals before moving.

It is useful to define a unit vector

$$\mathbf{e}_i(t) = \frac{\mathbf{r}_{k,i} - \mathbf{r}_i(t)}{|\mathbf{r}_{k,i} - \mathbf{r}_i(t)|}, \quad k = 1, 2, \dots, K \quad (2.4)$$

which expresses the direction along which a pedestrian would move if interactions did not take place. It is easy to see that (2.4) is a unit vector, indeed  $|\mathbf{e}_i(t)| = 1, \forall t$ .

---

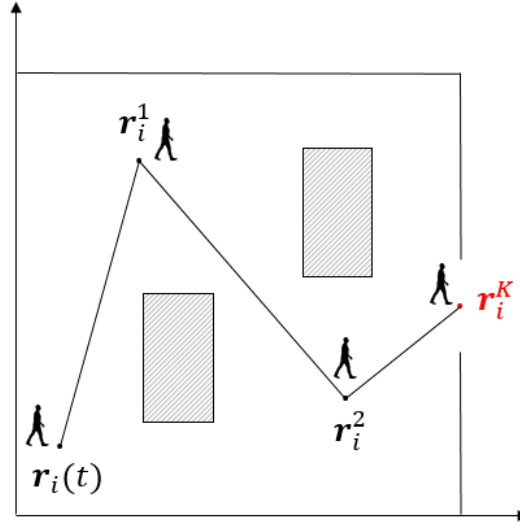


Figure 2.2: Path for reaching the target destination  $\mathbf{r}_i^K$  in a domain with obstacles.

In order to allow a pedestrian to effectively go toward a target destination, the following force is introduced

$$\mathbf{F}_i^{des} = \frac{1}{\tau_i} (v_{d,i} \mathbf{e}_i(t) - \mathbf{v}_i(t))$$

which tends to direct the  $i$ -th pedestrian toward the direction  $\mathbf{e}_i(t)$  with velocity  $\mathbf{v}_{d,i}$ . With  $v_{d,i}$  we denote the modulus of the vector  $v_{d,i} \mathbf{e}_i(t)$  and it represents the desired velocity. If the  $i$ -th pedestrian has a velocity such that  $\mathbf{v}_i(t) = v_{d,i} \mathbf{e}_i(t)$ , then  $\mathbf{F}_i^{des} = 0$ . On the other hand if  $\mathbf{v}_i(t) \neq v_{d,i} \mathbf{e}_i(t)$ , then  $\mathbf{F}_i^{des} \neq 0$  and a deceleration or acceleration process starts, which leads to approach the velocity  $v_{d,i}$  within a certain relaxation time  $\tau_i$ .

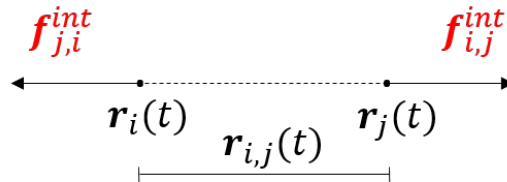


Figure 2.3: Repulsion forces between two interacting pedestrians.

## 2. Interactions among pedestrians:

A crowd is composed by a huge number of pedestrians, and it is legitimate to think that there are interactions among them; in particular, between two pedestrians in positions  $\mathbf{r}_i$  and  $\mathbf{r}_j$ , a repulsion force acts, as shown in Fig.(2.3). This force can be mathematically formulated as

$$\mathbf{f}_{i,j}^{int} = -\nabla_{\mathbf{r}_{i,j}} V_{i,j}, \quad i \neq j$$

where  $V_{i,j}$  is the repulsive potential, which is a monotonically decreasing function of  $\mathbf{r}_{i,j}$ , and  $-\nabla_{\mathbf{r}_{i,j}}$  is the gradient computed with respect to  $\mathbf{r}_{i,j}$ , so that

$$\nabla_{\mathbf{r}_{i,j}} V_{i,j} = (\nabla V_{i,j} \cdot \mathbf{r}_{i,j}) \frac{\mathbf{r}_{i,j}}{|\mathbf{r}_{i,j}|} = \frac{\partial V_{i,j}}{\partial \mathbf{r}_{i,j}} \frac{\mathbf{r}_{i,j}}{|\mathbf{r}_{i,j}|}.$$

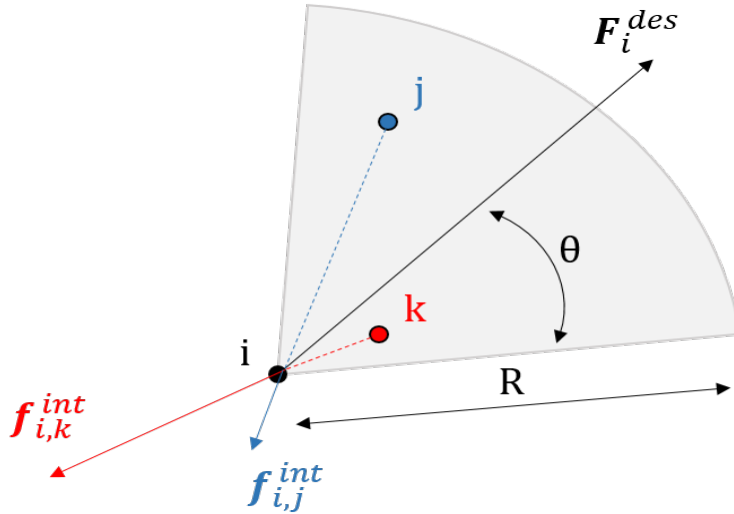


Figure 2.4: Sensory region of the  $i$ -th pedestrian;  $R$  is the length,  $\theta$  is the angle representing the breadth,  $j$  and  $k$  are two other pedestrians within the sensory region.

The quantity  $\mathbf{r}_{i,j}$  represents the reciprocal distance between the  $i$ -th and  $j$ -th pedestrian. Obviously, this case is inherent to a couple of interacting pedestrians, but the  $i$ -th pedestrian does not necessarily interact only with the  $j$ -th. Indeed in principle he/she can interact with all the  $N$  pedestrians

---

present in the domain; therefore the total interaction force is given by

$$\begin{aligned}\mathbf{F}_i^{int} &= \sum_{i \neq j} \mathbf{f}_{i,j}^{int} \\ &= - \sum_{i \neq j} \nabla_{\mathbf{r}_{i,j}} V_{i,j}.\end{aligned}$$

Surely a pedestrian does not interact with other members that are far from him/her, instead it is normal to assume that he/she feels increasingly uncomfortable the closer he/she gets to another person. Thus, the magnitude of the interaction force  $\mathbf{F}_i^{int}$  depends only on the number of members which are close to the  $i$ -th pedestrian, basically inside his/her sensory region. An example of sensory region is shown in Fig.(2.4); the dimension of this region depends on the applications, but in general is assumed to be long from 2 to 10 meters. In more complex cases, the dimension can depend on the pedestrian density value.

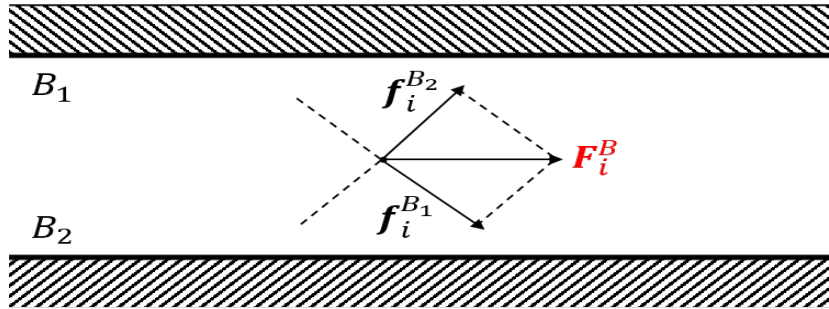


Figure 2.5: Repulsion forces due to domain boundaries acting on the  $i$ -th pedestrian.

### 3. Interactions with domain boundaries:

Crowd dynamics are strongly influenced by the shape of the walking area, and in particular by the boundaries and obstacles present within it. Pedestrians have constraints, indeed they cannot go out of the considered domain, and they cannot walk on obstacles. Therefore, as shown in Fig.(2.5), it is assumed that on the  $i$ -th pedestrian in position  $\mathbf{r}_i$  close to obstacles/boundaries a force

$\mathbf{F}_i^B$  is exerted; this force is given by

$$\begin{aligned}\mathbf{F}_i^B &= \sum_{l=1}^L \mathbf{f}_i^{B_l} \\ &= - \sum_{l=1}^L \nabla_{\mathbf{r}_{i,B_l}} U_{i,B_l}\end{aligned}$$

where  $U_{i,B_l}$  is again a repulsive and monotonically decreasing potential and is a function of  $\mathbf{r}_{i,B_l}$ , which is the distance between the pedestrian position and the boundary  $B_l$ . Finally,  $L$  represents the total number of obstacles/boundaries with which the  $i$ -th pedestrian interacts.

Fig.(2.6) shows the numerical result of a simulation on a two-dimensional domain. Pedestrians are walking from left to right and they enter the domain with a uniform distribution along the cross section; due to boundary repulsions, it is possible to see that near the exit they tend to walk far enough from the lateral side.



Figure 2.6: Crowd dynamics on a two-dimensional domain.

#### 4. Attractions among pedestrians:

Not always pedestrians feel uncomfortable when near to others, but instead they can be attracted. This phenomenon is manifested in case of group of friends, tourist guides or families. These attractive effects can be modelled by a force

$$\mathbf{F}_i^A = - \sum_{i \neq j} \nabla_{\mathbf{r}_{i,j}} W_{i,j}$$

where the index  $j$  represents the members by which the  $i$ -th pedestrian is attracted, while  $W_{i,j}$  is an attractive monotonic increasing potential function of the distance  $\mathbf{r}_{i,j}$ .

---

All these factors influence the decisions of each pedestrian at any moments and for this reason they are included in a unique term, the total force  $\mathbf{F}_i$ , that now can be expressed as

$$\mathbf{F}_i = \mathbf{F}_i^{des} + \mathbf{F}_i^{int} + \mathbf{F}_i^B + \mathbf{F}_i^A \quad (2.5)$$

and is the so-called social force.

In case of we consider non-interacting pedestrians on an unbounded domain, the model (2.3) becomes

$$\begin{cases} \dot{\mathbf{r}}_i(t) = \mathbf{v}_i(t) \\ \dot{\mathbf{v}}_i(t) = \frac{1}{\tau_i} [v_{d,i} \mathbf{e}_i(t) - \mathbf{v}_i(t)]. \end{cases}$$

Let us suppose that the domain is without obstacles, then the  $i$ -th pedestrian is able to go directly toward the final target destination  $\mathbf{r}_i^K$ , hence

$$\mathbf{e}_i(t) = \frac{\mathbf{r}_i^K - \mathbf{r}_i(t)}{|\mathbf{r}_i^K - \mathbf{r}_i(t)|} \quad (2.6)$$

with desired velocity

$$v_{d,i} = \alpha |\mathbf{r}_i^K - \mathbf{r}_i(t)|, \quad \alpha > 0. \quad (2.7)$$

Relation (2.7) states that the nearer the  $i$ -th pedestrian is to his/her target destination, the slower he/she would like to walk. Consequently Eq.(2.6) becomes

$$\begin{cases} \dot{\mathbf{r}}_i(t) = \mathbf{v}_i(t) \\ \dot{\mathbf{v}}_i(t) = \frac{1}{\tau_i} [\alpha (\mathbf{r}_i^K - \mathbf{r}_i) - \mathbf{v}_i]. \end{cases} \quad (2.8)$$

We would like to prove that

$$\mathbf{r}_i(t) \rightarrow \mathbf{r}_i^K, \quad t \rightarrow \infty$$

which means that the  $i$ -th pedestrian reaches the target destination. In order to do this, we write (2.8) as

$$\ddot{\mathbf{r}}_i(t) + \frac{1}{\tau_i} \dot{\mathbf{r}}_i(t) = \frac{\alpha}{\tau_i} (\mathbf{r}_i^K - \mathbf{r}_i)$$

and so

$$\frac{d^2}{dr^2} [\mathbf{r}_i^K - \mathbf{r}_i] + \frac{1}{\tau_i} \frac{d}{dr} [\mathbf{r}_i^K - \mathbf{r}_i] + \frac{\alpha}{\tau_i} [\mathbf{r}_i^K - \mathbf{r}_i] = 0. \quad (2.9)$$


---

Let  $\mathbf{u}(t) = \mathbf{r}_i^K - \mathbf{r}_i(t)$ , then Eq.(2.9) becomes

$$\tau_i \ddot{\mathbf{u}}(t) + \dot{\mathbf{u}}(t) + \alpha \mathbf{u}(t) = 0.$$

It is reasonable to assume that the reaction time  $\tau_i$  is small enough, so

$$\dot{\mathbf{u}}(t) + \alpha \mathbf{u}(t) = 0$$

which has as a solution

$$\mathbf{u}(t) = \mathbf{u}(0)e^{-\alpha t}$$

therefore

$$\mathbf{u}(t) \rightarrow 0, t \rightarrow \infty \quad \Longrightarrow \quad \mathbf{r}_i(t) \rightarrow \mathbf{r}_i^K, t \rightarrow \infty$$

and this proves that the  $i$ -th pedestrian reaches his/her target destination.

In the following, more details are added. Indeed, it is physically reasonable to assume that a pedestrian cannot walk over a certain velocity. This means that the model need the introduction of a speed limitation, so that

$$|\dot{\mathbf{r}}_i(t)| \leq v_i^{max}, \quad \forall t \quad (2.10)$$

in order to have only pedestrians walking at velocities smaller in modulus than  $v_i^{max}$ ; usually  $v_i^{max} = 2.5$  m/s. In order to satisfy constraint (2.10), we have to assume that

$$\dot{\mathbf{r}}_i(t) = \mathbf{v}_i(t) g\left(\frac{v_i^{max}}{|\mathbf{v}_i(t)|}\right)$$

where  $g$  is a function given by

$$g\left(\frac{v_i^{max}}{|\mathbf{v}_i(t)|}\right) = \begin{cases} \frac{v_i^{max}}{|\mathbf{v}_i(t)|} & \text{if } \frac{v_i^{max}}{|\mathbf{v}_i(t)|} \leq 1 \\ 1. & \text{if } \frac{v_i^{max}}{|\mathbf{v}_i(t)|} > 1 \end{cases}$$

In this way if

$$\frac{v_i^{max}}{|\mathbf{v}_i(t)|} < 1 \quad \Longrightarrow \quad |\mathbf{v}_i(t)| > v_i^{max}$$

then

$$g\left(\frac{v_i^{max}}{|\mathbf{v}_i(t)|}\right) = \frac{v_i^{max}}{|\mathbf{v}_i(t)|} \quad \Longrightarrow \quad |\dot{\mathbf{r}}_i(t)| = v_i^{max}$$

so that the inequality (2.10) is satisfied.

---

Till this point the model is fully deterministic, but in such context which involves also decisional aspect of pedestrians, it is expected that a stochastic behaviour takes place. Hence, we have to add at the dynamics of the model a new term  $\Theta_i$ , which is a fluctuation term that takes into account random variations of the pedestrian behaviours.

In the end, the social force model (2.3) introduced by Helbing in [4] becomes

$$\begin{cases} \dot{\mathbf{r}}_i(t) = \mathbf{v}_i(t) \\ \dot{\mathbf{v}}_i(t) = \frac{1}{\tau_i} (v_{d,i} \mathbf{e}_i(t) - \mathbf{v}_i(t)) - \sum_{i \neq j} \nabla_{\mathbf{r}_{i,j}} V_{i,j} - \nabla_{\mathbf{r}_{i,B}} U_{i,B} - \sum_{i \neq j} \nabla_{r_{i,j}} W_{i,j} + \Theta_i \end{cases}$$

accompanied by suitable initial conditions  $\mathbf{r}_{0,i}$  and  $\mathbf{v}_{0,i}$ .

### 2.1.2.2 Other force models

The expression of the total force given in (2.5) is only one among the endless possibilities. For instance, Okazaki [8–10], Okazaki and Matsushita [11] and Okazaki and Yamamoto [12] introduced the idea to consider pedestrians as magnets or electrically charged particles; as a consequence they move in a certain domain by following the Coulomb's law

$$\mathbf{F}_i = \sum_{i \neq j} c q_i q_j \frac{\mathbf{r}_i(t) - \mathbf{r}_j(t)}{|\mathbf{r}_i(t) - \mathbf{r}_j(t)|^3} \quad (2.11)$$

which is the unique force exerted on themselves. In Eq.(2.11)  $c$  is a repulsion constant,  $q_i$  is the charge of pedestrian  $i$ , while  $q_j$  is the charge of the point with which he/she interacts, located in  $\mathbf{r}_j(t)$ . The idea is that all pedestrians are positive point sources so that they are repulsed from each other. Moreover, the perimeter of the domain and the obstacles within it are positive point sources too, in order to avoid that pedestrians cross it. On the other hand targets or group of friends are negative point sources, so that pedestrians are attracted.

Another type of force model is the centrifugal force model, which differs from the social force model mainly for the definition of the interacting force  $\mathbf{F}_i^{int}$ , or the model reported in [19], which differ from the social force model for the definition of the boundary force  $\mathbf{F}_i^B$ .

---

## 2.2 Macroscopic crowd models

In many contexts the need arises to simulate crowds composed by high numbers of pedestrians, and track each of them would be numerically impossible. This is the reason why it is necessary to introduce a macroscopic scale. The main assumption is the validity of the continuum hypothesis, so that the number of agents is large enough to be described by locally averaged quantities, which normally are the pedestrian density  $\rho(t, x)$  and the pedestrian velocity  $v(t, x)$ , both dependent variables of space and time. Therefore, a macroscopic level modelling is concerned with group behaviour and deals with a crowd as a whole; detailed interactions are overlooked.

Macroscopic crowd models were initially born as extensions of traffic flow models, like the Lighthill-Whitham-Richards model described in [31,32], further developed by Payne [33] and Whitham [34], or as extensions of Boltzmann-like gas kinetic model, like the model presented by Helbing in [35]. Moreover, in [35] a fluid dynamic description for the collective movement of pedestrians is given.

One of the purposes of macroscopic crowd models is to correctly reproduce fundamental diagrams obtained by experimental data, which are diagrams that show the dependence of the pedestrian velocity on the pedestrian density. Many numerical results concerning fundamental diagrams can be found in papers by Coscia and Canavesio [38] and by Bellomo and Dogbé [39,40], while some experiments are carried out and explained in papers published by Helbing et al. [41], Seyfried et al. [42], Venuti and Bruno [43] and by Daamen and Hoogendoorn [44].

In these last years many other models have been published. It is remarkable the pioneering work of Colombo et al. [36] in 2005, who introduced a macroscopic model able to simulate also the dynamics of a panicking crowd. Another model was introduced by Coscia and Canavesio [38] in 2008, which is able to include pedestrian strategies. Maury et al. [45] introduced a macroscopic version of their microscopic model described in [20] and they compared the results obtained at the different scales in [46].

Finally, even more recent are the nonlocal models, which take into account the natural anisotropic behaviour of pedestrians. Examples can be found in papers published by Cristiani et al. [47] and by Bruno et al [48], where

---

there are also applications to real world problems like pedestrian traffic along footbridges.

In the next paragraphs we will describe the main concepts and results of the more relevant models mentioned above.

### 2.2.1 Fundamental diagram

The main quantities studied by each macroscopic crowd model are the density, the velocity and the flow of pedestrians, which are also the quantities used in assessing the performance of pedestrian facilities. The relations among these variables constitute the fundamental diagrams relative to pedestrian traffic. Each real world problem has different shape of fundamental diagrams, because obviously the flow of pedestrians in a corridor of a shopping center is very different from the flow of pedestrians at the entrance of a stadium.

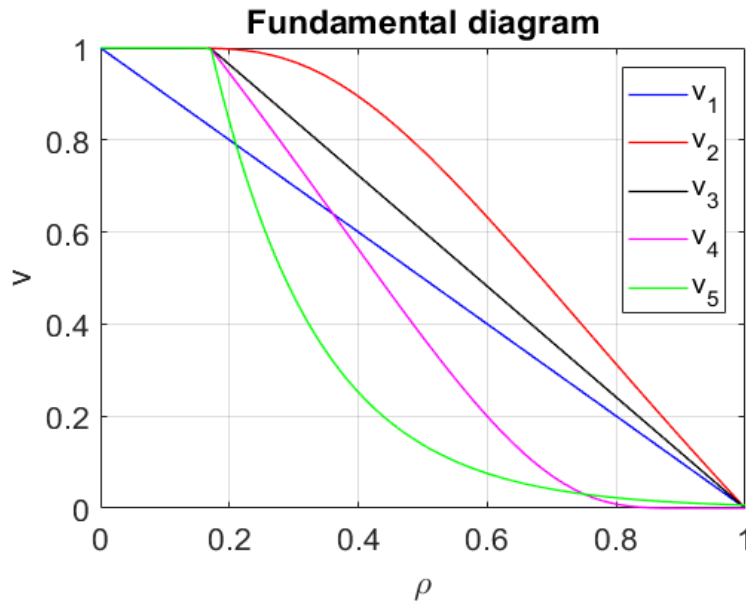


Figure 2.7: Possible choices for expressing the velocity as dependent from the pedestrian density.

The pedestrian flow can be defined as

$$F[\rho] = \rho v[\rho] \quad (2.12)$$

where  $\rho = \rho(t, x)$  is the pedestrian density at time  $t$  in point  $x$  and  $v[\rho]$  is the pedestrian velocity, which depends on the density. Square brackets denote functional dependence. Relation (2.12) is mainly studied in one-dimensional problems; since it is more realistic to assume that a vehicle can move only along one direction, this relation is widely studied in traffic flow problems. In case of we are dealing with pedestrians, it is usually assumed that they can walk on a two-dimensional domain, and consequently the fundamental diagram is given only by the relationship between the speed  $v$  and the density  $\rho$ .

In the following some possible choices for the function  $v = v[\rho]$  used in [50, 51] are reported. The subscript  $v_i[\rho], i = 1, 2, 3, 4, 5$  has the unique function to make the laws recognizable in Fig.(2.7). The plotted relations are

$$\begin{aligned}
 v_1[\rho] &= 1 - \rho \\
 v_2[\rho] &= 1 - \exp\left(-\alpha \frac{1 - \rho}{\rho}\right) \\
 v_3[\rho] &= \begin{cases} 1 & \text{if } \rho \leq \rho_c \\ \frac{1 - \rho}{1 - \rho_c} & \text{if } \rho > \rho_c \end{cases} \\
 v_4[\rho] &= \begin{cases} 1 & \text{if } \rho \leq \rho_c \\ \exp\left(-\alpha \frac{\rho - \rho_c}{1 - \rho}\right) & \text{if } \rho > \rho_c \end{cases} \\
 v_5[\rho] &= \begin{cases} 1 & \text{if } \rho \leq \rho_c \\ 1 + \frac{\exp(-\beta(\rho - \rho_c)/(1 - \rho_c))}{1 - \exp(-\beta)} & \text{if } \rho > \rho_c \end{cases}
 \end{aligned} \tag{2.13}$$

where both the density and the speed are normalized, so that  $v, \rho \in [0, 1]$ . Regarding the parameters,  $\alpha \in [0, 2.5]$  and is set to be  $\alpha = 1.5$ , while  $\beta \in [0, 10]$  and is set to be  $\beta = 5$ ;  $\rho_c$ , defined also as critical density, represents the value over which the velocity starts to be affected by the pedestrian density, and it usually assumes the value of  $\rho_c = 0.17$ .

Other examples of velocity-density laws are reported in Fig.(2.8); in these cases both the quantities are not normalized. In particular, Fig.(2.8a) shows many linear relationships between velocity and density present in literature of the form  $v = v_d - k\rho$ , where  $v_d$  represents the desired velocity, while  $k$  is a non-negative parameter. On the other hand, Fig.(2.8b) shows non-linear

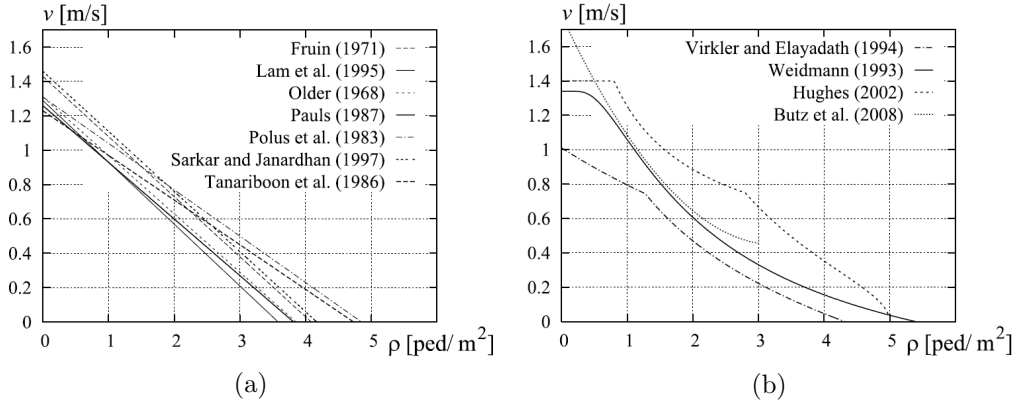


Figure 2.8: Velocity-density relations in literature [83–93]: linear laws are shown in (a) while non-linear ones are shown in (b).

laws or multi-regime models.

It is worth to point out that all the laws above-mentioned are correct, even if in general the non-linear multi-regime models are more accurate than the linear laws, because they better fit the observation data.

### 2.2.2 First-order models

In a first-order model the dynamics of the crowd are described by the initial/-boundary-value problem

$$\begin{cases} \frac{\partial}{\partial t} \rho(t, x) + \nabla \cdot F[\rho](t, x) = 0 & \text{in } \Omega \times (0, T] \\ \rho(t, x) = g(t, x) & \text{in } \partial\Omega \times (0, T] \\ \rho(0, x) = \rho_0(x) & \text{in } \Omega \end{cases} \quad (2.14)$$

where  $\rho(t, x)$  is the pedestrian density,  $F[\rho](t, x)$  is the flux of pedestrian in the point  $x$  at time  $t$ ,  $\rho_0(x)$  is the initial condition,  $g$  is the boundary condition,  $T > 0$  is a certain final time and  $\Omega \in \mathbb{R}^d$ ,  $d = 1, 2, 3$  is the domain. This equation is a conservation law, which states that variations of density  $\rho$  are due to incoming or outgoing flux of pedestrians across the domain boundaries. Indeed, in a two-dimensional framework, Eq.(2.14) can be derived from Fig.(2.9).

As discussed in section 2.2.1, the flux  $F[\rho]$  is given by the relation

$$F[\rho] = \rho v[\rho].$$

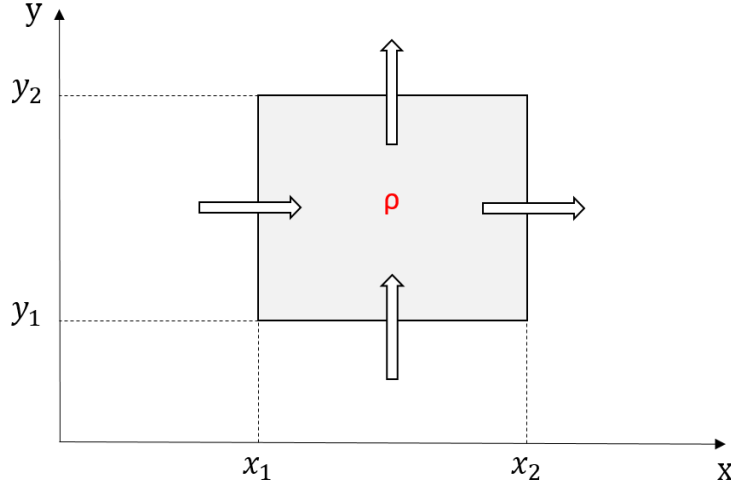


Figure 2.9: Mass conservation due to incoming and outgoing flux of pedestrians across domain boundaries.

Therefore, all first-order models are governed by the conservation law (2.14), but their performances can strongly change according to the way of expressing  $v[\rho]$ . In the following we will see some interpretations.

### 2.2.2.1 Colombo and Rosini's model

The main purpose of this model is to include the possibility to simulate some special features of the pedestrian behaviour in panic conditions. The complete version is reported by the authors in [36]; in the following we will give only the main concepts, in order to understand the dynamics.

The model is based on the assumptions that the total mass of the system is conserved and the velocity  $v$  depends only on  $\rho$ . The analysis is carried out in a one-dimensional domain, but further extensions can be found in [63]. This model mostly differ from others in the choice of a non-standard relationship  $v[\rho]$ . Indeed, it is introduced a  $\rho_{max}$  which is the maximum density in normal conditions, but also a  $\rho_{max}^*$ , which is the maximum density allowed in special conditions, with  $\rho_{max} < \rho_{max}^*$ . Therefore, in normal circumstances,  $\rho \in [0, \rho_{max}]$ , but in exceptional situations such as panic, then  $\rho \in [\rho_{max}, \rho_{max}^*]$ . More precisely, the flow  $F[q]$  must satisfy the following properties:

1.  $F : [0, \rho_{max}^*] \mapsto [0, \infty[$ , with  $F \in C^0([0, \rho_{max}^*]) \cap C^2([0, \rho_{max}^*] \setminus \{\rho_{max}\})$ .

2.  $F[\rho] = 0 \iff \rho \in \{0, \rho_{max}, \rho_{max}^*\}$
3.  $F'$  is bounded on  $[0, \rho_{max}^*]$ . Moreover  $F'$  is null at a single point  $\rho_M$  in  $[0, \rho_{max}]$  and at a single point  $\rho_M^*$  in  $[\rho_{max}, \rho_{max}^*]$ .
4.  $F$  has at most one inflection point  $\rho_P$  in  $[0, \rho_{max}]$  and at most another one  $\rho_P^*$  in  $[\rho_{max}, \rho_{max}^*]$ .

An example of admissible flow is reported in Fig.(2.10), where the notations used are also shown. It is worth mentioning that the assumption  $F[\rho_{max}] = 0$  can be relaxed with the hypothesis that  $F[\rho_{max}]$  must be small enough; also the presence of other inflection points can be managed. Since is physically reasonable to avoid discontinuity in  $F[\rho]$ , the boundedness of  $F'$  is required. Possible solutions of Eq.(2.14) with such a choice of  $F[\rho]$  are discussed in [36].

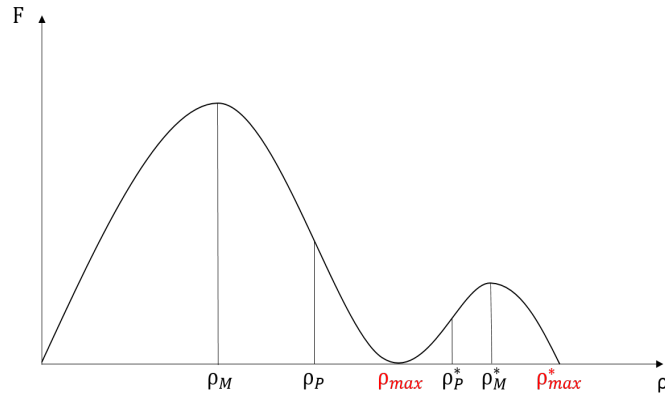


Figure 2.10: Example of admissible flow.

### 2.2.2.2 Coscia and Canavesio's Model

This model, which is amply discussed in [38], is conceived such that the pedestrian velocity  $v$  has dependence not only from the density  $\rho$ , but also from the density gradient  $\nabla\rho$ . Indeed when the pedestrian density approaches high values, pedestrians feel the danger and try moving toward the target in a way that depends not only on the local density but also on its spatial gradient in the direction of the target. Therefore, the governing equation used is always the one reported in (2.14) with  $\Omega \in \mathbb{R}^2$ , but  $\mathbf{v} = \mathbf{v}[\rho, \nabla\rho]\nu(\mathbf{x})$ ,

where  $\boldsymbol{\nu}$  is a unit vector expressing the direction along which the density gradient is evaluated.

Possible choices of velocity  $v$  given in [38] are

$$\begin{aligned} v[\rho, \nabla\rho] &= (1 - \rho) - \epsilon \nabla\rho \\ v[\rho, \nabla\rho] &= (1 - \rho) - \epsilon k[\rho] \nabla\rho \end{aligned}$$

where  $\epsilon$  is a parameter, and  $k[\rho]$  must satisfy

$$\begin{cases} k[0] = 0 \\ k[1] = 0. \end{cases}$$

This model has been used in two real world applications regarding the exit from a closed domain and the passage over the Jamarat bridge; in both cases it is shown that the presence of obstacles in the domain may lead to catastrophic events.

### 2.2.2.3 Maury et al.'s model

The main purpose of this model is to handle the flow of pedestrians in emergency evacuation situations. It was introduced by the author in [20] and only the main concepts are reported in the following. The model is set in a two-dimensional environment and is the macroscopic version of the Maury and Venel's model described in paragraph 2.1.1. The idea is that the velocity  $\mathbf{v}_d(\mathbf{x})$  is given, and represents the velocity that pedestrians in position  $\mathbf{x}$  would like to have. Due to the presence of constraints and other members within the domain, this speed cannot be always realized and consequently the actual velocity of each pedestrian is chosen to be the projection of  $\mathbf{v}_d(\mathbf{x})$  onto  $C(\rho)$ , which is a set of admissible velocities. Therefore, the relationship which links the velocity to the density is given by

$$\mathbf{v}[\rho] = P_{C(\rho)} \mathbf{v}_d(\mathbf{x})$$

where  $P$  is the projection operator in the  $L^2$  sense and the set  $C(\rho)$  is the cone of admissible velocities. All speeds that belong to this set do not increase  $\rho$  in regions where the values are already high; in this model, the maximum value of density allowed is  $\rho_{max} = 1$ .

---

The set  $C(\rho)$  is given by

$$C(\rho) = \left\{ \mathbf{z} \in (L^2(\Omega))^2, \int_{\Omega} \mathbf{z} \cdot \nabla \phi \leq 0 \quad \forall \phi \in H_{\rho}^1 \right\}$$

where

$$H_{\rho}^1 = \{ \phi \in H^1(\Omega), \phi \geq 0 \text{ a.e. in } \Omega, \phi = 0 \text{ a.e. in } \{\rho < 1\} \}$$

so that  $\mathbf{v}[\rho]$  cannot have any components directed from a point where  $\rho < 1$  to a point where  $\rho = 1$ . In [46] this model is tested in cases of crowd dynamics along a convergent corridor.

#### 2.2.2.4 Non-local models

It is physically reasonable assume that pedestrians make decisions in order to the local conditions, specifically by considering the distribution of neighbours. Non-local models have been introduced for taking into account this behaviour, and examples can be found in papers published by Cristiani et al. [47] and by Bruno et al [48].

The relationship  $\mathbf{v} = \mathbf{v}[\rho]$  still holds but in this framework the velocity depends on values of the density  $\rho$  around  $\mathbf{x}$  and not only in  $\mathbf{x}$ . Obviously, there are many ways in which this relationship can be written, and in the following some will be presented.

One of these ways for taking into account non-local dynamics on a two-dimensional domain consist in expressing the velocity  $\mathbf{v}$  as function of  $\rho_p$  and not  $\rho$ , where  $\rho_p = \rho_p(t, \mathbf{x})$  is the perceived density that a pedestrian located in  $\mathbf{x}$  feels within his/her sensory region. The perceived density comes from an intelligent evaluation process which implies some weighting of the true density  $\rho$ . The sensory region  $R_s$  will have the same shape of the one shown in Fig.(2.4), with length  $R$ ;  $\mathbf{e}_d(t)$  and  $\mathbf{e}_i(t)$  represent respectively the desired and interaction direction. In the following we will discuss four different strategies for defining the perceived density  $\rho_p(t, \mathbf{x}) = \rho(t, \mathbf{x}_p)$ :

- (a) Pedestrians evaluate the perceived density at the intersection between the far boundary of the sensory region and the desired direction, so that

$$\mathbf{x}_p = \mathbf{x} + R\mathbf{e}_d(\mathbf{x}). \quad (2.15)$$

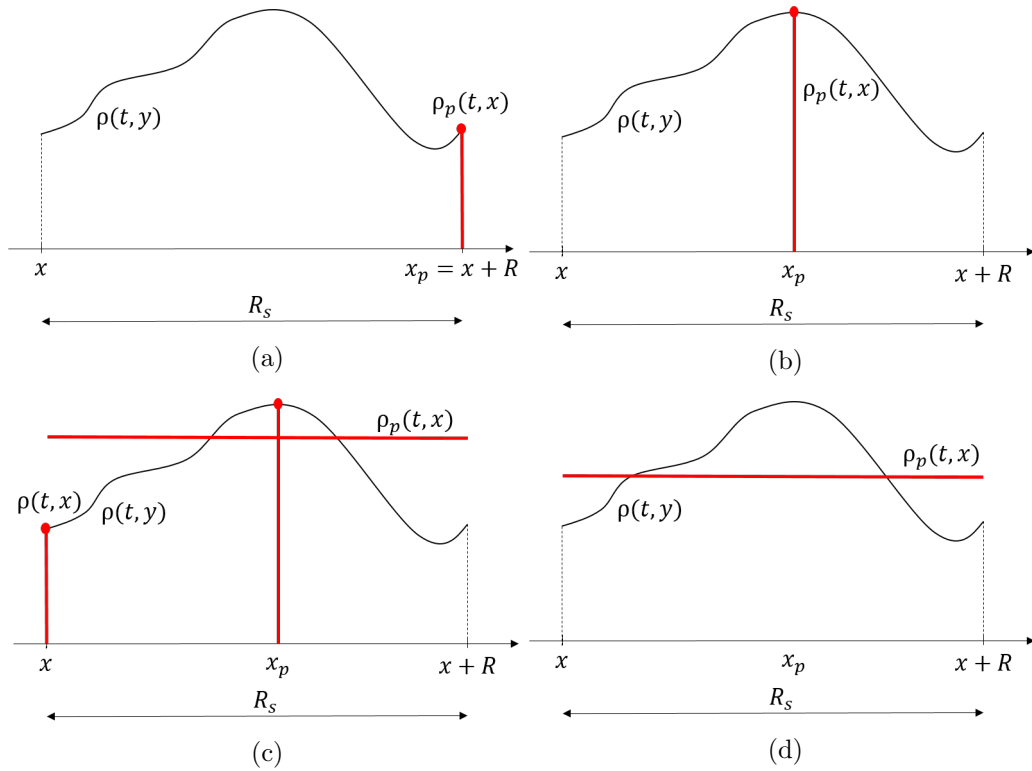


Figure 2.11: Examples of localizations strategies on a one-dimensional domain; the black lines represent the density while the red points/lines represent the perceived density within the sensory region  $R_s$  of the  $i$ -th pedestrian.

This strategy is used for pedestrians which are very determined to reach a target destination, and therefore they do not take care of surrounding regions, but they just look as far as possible toward the desired direction.

- (b) Pedestrians attention is drawn by the point in the sensory region where the maximum value of  $\rho$  is attained, so

$$\mathbf{x}_p = \operatorname{argmax}_{\mathbf{y} \in R_s} \rho(t, \mathbf{y}).$$

This strategy is able to simulate pedestrian anxiety for high crowd density; if adopted on a single agent, this will certainly try to reach his/her target by avoiding all regions with high density.

- (c) Pedestrians evaluate the perceived density as a weighted average of the

true density in  $\mathbf{x}$  and  $\mathbf{x}_p$ , so

$$\rho_p(t, \mathbf{x}) = (1 - g(R_p))\rho(t, \mathbf{x}) + g(R_p)\rho(t, \mathbf{x}_p)$$

where

$$R_p = |\mathbf{x}_p - \mathbf{x}|, \quad g(R_p) = -\frac{8}{10R}R_p + 1$$

while  $\mathbf{x}_p$  is still given by (2.15). In this strategy, pedestrians are still mainly concerned with the highest crowd density, but they are able to recognise if this regions are far or near to themselves.

- (d) Pedestrians evaluate  $\mathbf{x}_p$  as the centre of mass of the whole crowd distributed in  $R_s$ , weighted by a function  $G$  which takes into accounts the fact that an agent gives more importance at groups of people in front of him/her instead of people at the lateral boundaries of the sensory region. Therefore the perceived density results as

$$\rho_p(t, \mathbf{x}) = \frac{\int_{R_s} \rho(t, \mathbf{y})G(\alpha(\mathbf{y} - \mathbf{x}))d\mathbf{y}}{\int_{R_s} G(\alpha(\mathbf{y} - \mathbf{x}))d\mathbf{y}}.$$

This strategy is able to introduce in the model dynamics in which there are curious pedestrians, that occur for instance during shopping activity.

In Fig.(2.11) is shown a graphical version of the four strategies above mentioned, adapted in a one-dimensional context. The huge differences in the perceived density among the various strategies is evident, evaluated by starting from an equal density distribution. More analytical and numerical results can be found in [57].

### 2.2.3 Second-order models

In a second-order model the dynamics of the crowd is described by a system of partial differential equation for  $\rho$  and  $v$  of the form

$$\begin{cases} \frac{\partial}{\partial t}\rho(t, x) + \nabla \cdot F[\rho](t, x) = 0 & \text{in } \Omega \times (0, T] \\ \frac{\partial}{\partial t}v(t, x) + (v(t, x) \cdot \nabla)v(t, x) = a[\rho, v](t, x) & \text{in } \Omega \times (0, T] \\ \rho(t, x) = g(t, x) & \text{in } \partial\Omega \times (0, T] \\ \rho(0, x) = \rho_0(x) & \text{in } \Omega \end{cases} \quad (2.16)$$


---

where  $\mathbf{v} = (v_x, v_y)$ ,  $\mathbf{x} = (x_1, x_2)$  and

$$(\mathbf{v} \cdot \nabla)\mathbf{v} = \left( v_x \frac{\partial v_x}{\partial x} + v_y \frac{\partial v_x}{\partial y}, v_x \frac{\partial v_y}{\partial x} + v_y \frac{\partial v_y}{\partial y} \right)$$

if  $\Omega \subseteq \mathbb{R}^2$ . The quantities in system (2.16) are the same one discussed for the first-order models, but in addition we have a second equation. On the right-hand side of this equation there is a function denoted by  $a = a[\rho, v]$ , which represents the pedestrian acceleration (denoted by  $\mathbf{a}$  in two-dimensional context). While the first equation in (2.16) states the conservation of mass, the second equation accounts for the conservation of momentum.

Models can be classified according to the way in which the acceleration is modelled. An example is given in the model introduced by Bellomo and Dogbè [39, 40] in which are studied two different choices of acceleration functions; as a consequence, there are two classes of models:

1. Models where the pedestrians move along straight lines toward the target destination.
2. Models where pedestrians are still moving toward the target destination, but are also attracted by paths with small density gradients.

In the first class of models, pedestrians always try to minimize their travel time in order to reach a given objective by walking along the direction  $\boldsymbol{\nu}_d$ , while adjusting their velocity according to the local density. The acceleration function consists of two terms: the first one models the will to keep walking at the desired velocity in direction  $\boldsymbol{\nu}$ , while the second term represents the action of the density gradient along  $\boldsymbol{\nu}_d$ . The resulting expression of the acceleration function is

$$\mathbf{a}[\rho, \mathbf{v}] = \alpha(v_e[\rho]\boldsymbol{\nu}_d - \mathbf{v}) - \frac{k^2[\rho]}{\rho} \nabla_{\boldsymbol{\nu}_d} \rho \quad (2.17)$$

where  $\alpha$  is a parameter,  $v_e[\rho] = 1 - \rho$  but other expressions are admissible and  $k^2[\rho]$  is a scalar function; five possible different choices of relationship  $k^2[\rho]$  are reported in [40].

In the second class of models, pedestrians always try to reach as fast as possible their objectives, but meanwhile they also try to avoid regions with high density values. Pedestrians do not have a global vision of the situation,

therefore their perception of the density is only within their sensory regions. In this case the acceleration function is given by

$$\mathbf{a}[\rho, \mathbf{v}] = \alpha(v_e[\rho]\boldsymbol{\nu} - \mathbf{v}) - \frac{k^2[\rho]}{\rho} \nabla_{\boldsymbol{\nu}} \rho$$

where  $\boldsymbol{\nu}$  is the direction toward which pedestrians are walking.

In [40] are discussed further extensions of these models, including presence of obstacles and panic conditions.

## 2.3 Mesoscopic crowd models

In systems composed of huge number of living agents it is possible to identify universal interaction rules which allow the construction of a mathematical model based on notions that belong to the kinetic theory of rarefied gases. This is the main idea on which mesoscopic models are founded. Consequently, pedestrians are seen as gas particles that change their states due to interactions. Models may differ in the choice of variables which characterize the state (also called microstate) of each pedestrian. For deriving a model with such point of view, it is needed to keep a parallelism with the kinetic theory of rarefied gases, and as a consequence a statistical representation of the crowd is assumed.

The way of modelling the crowd through a mesoscopic scale is still a young research field, but it is growing very fast. Even if he did not applied this theory to pedestrian traffic, the father of the discipline is Ludwig Boltzmann, who introduced for the first time a kinetic theory of rarefied gases in [75]. The first attempt to describe crowd dynamics from a kinetic point of view is due to Henderson [76], who carried out the entire analysis by doing analogies between pedestrians and gas particles. Further developments were introduced by Dogbè in [28]; the particularity of his model is that the microstate assigned at each pedestrian is described by the position, the velocity and a variable which express the strategy/target, also called activity variable. Other variations are given in [77, 78]. Only recently a few real applications of these models are rising; for instance in [74] a mesoscopic model is used for simulating pedestrian mobility in the context of public events.

In the next paragraphs we will describe the main concepts common to all models, and we will discuss more in detail the most popular ones.

### 2.3.1 Common features

The microstate of each pedestrian is usually defined by the pair position-velocity  $(\mathbf{x}, \mathbf{v}) \in \mathbb{R}^2 \times \mathbb{R}^2$  understood as independent variables. Consequently, the distribution function  $f$  is written as  $f = f(t, \mathbf{x}, \mathbf{v})$  and is such that the infinitesimal average of pedestrians located in the space volume  $d\mathbf{x}$  centered in  $\mathbf{x}$  with velocity belonging in the volume  $d\mathbf{v}$  centered in  $\mathbf{v}$ , at time  $t$ , is given by  $f(t, \mathbf{x}, \mathbf{v})d\mathbf{x}d\mathbf{v}$ . Hence, if we define  $\Omega_{\mathbf{x}} \subseteq \mathbb{R}^2$  and  $\Omega_{\mathbf{v}} \subseteq \mathbb{R}^2$  which are respectively the space and velocity domains, the quantity

$$N(t) = \int_{\Omega_{\mathbf{x}}} \int_{\Omega_{\mathbf{v}}} f(t, \mathbf{x}, \mathbf{v})d\mathbf{x}d\mathbf{v}$$

provides the total number of pedestrians inside a domain  $\Omega \subseteq \mathbb{R}^2$  at a certain time  $t$ .

The main purpose of each kinetic model is to describe the time evolution of the distribution function  $f$ , in order to have information about how the crowd is distributed within the region of interest. The kinetic equation which describe this evolution is

$$\frac{\partial f}{\partial t} + \mathbf{v} \cdot \nabla_{\mathbf{x}} f + \nabla_{\mathbf{v}} \cdot (\mathbf{S}[f]f) = J[f] \quad (2.18)$$

where  $\nabla_{\mathbf{x}}$  denote the gradient with respect to  $\mathbf{x}$  and  $\nabla_{\mathbf{v}} \cdot$  denote the divergence with respect to  $\mathbf{v}$ . Moreover, the term

$$\frac{Df}{Dt} = \frac{\partial f}{\partial t} + \mathbf{v} \cdot \nabla_{\mathbf{x}} f$$

represents the convective derivative, which states that the distribution function  $f$  is transported in the space of microscopic states by the pedestrian velocity  $\mathbf{v}$ . Regarding the third term at the left-hand side and the first at the right-hand side of Eq.(2.18), they model the acceleration acting on pedestrians due to either external actions or mutual microscopic interactions.

Let's imagine to have a generic pedestrian defined as test pedestrian with microstate  $(\mathbf{x}, \mathbf{v})$  and sensory region  $R_s(\mathbf{x})$ . It is legitimate to assume that the test pedestrian interacts with other surrounding agents within his/her sensory region. The operator  $\mathbf{S}$  describes a mean field acceleration exerted on a test pedestrian and is expressed as

$$\mathbf{S}[f](t, \mathbf{x}, \mathbf{v}) = \int \int_{R_s(\mathbf{x}) \times \mathbb{R}^2} \theta(\mathbf{x}, \mathbf{y}, \mathbf{v}, \mathbf{w}) f(t, \mathbf{y}, \mathbf{w}) d\mathbf{y}d\mathbf{w} \quad (2.19)$$

where the function  $\theta$  defines the type of interaction between the test and the field pedestrian, with microstate  $(\mathbf{y}, \mathbf{w})$ .

Moreover, pedestrians can gain or loose the test state  $(\mathbf{x}, \mathbf{v})$  because of interactions. The operator  $J$  takes into accounts this process, and evaluates the number of pedestrians who change state. In a general form  $J$  is written as

$$J[f](t, \mathbf{x}, \mathbf{v}) = G[f, f](t, \mathbf{x}, \mathbf{v}) - f(t, \mathbf{x}, \mathbf{v})L[f](t, \mathbf{x}, \mathbf{v}) \quad (2.20)$$

where  $G$  is the bilinear gain operator which counts the number of pedestrians that acquire state  $(\mathbf{x}, \mathbf{v})$  while  $L$  is the linear loss operator which counts the number of pedestrians that loose state  $(\mathbf{x}, \mathbf{v})$ .

One of the advantages of these models relies on the fact that when the distribution function  $f$  is known, it is also possible to derive macroscopic quantities. Indeed, by computing the statistical moments of  $f$  with respect to the variable  $\mathbf{v}$ , we obtain

$$\begin{aligned} \rho(t, \mathbf{x}) &= \int_{\Omega_{\mathbf{v}}} f(t, \mathbf{x}, \mathbf{v}) d\mathbf{v} \\ \mathbf{F}(t, \mathbf{x}) &= \int_{\Omega_{\mathbf{v}}} \mathbf{v} f(t, \mathbf{x}, \mathbf{v}) d\mathbf{v} \end{aligned}$$

which represent respectively the pedestrian density and the pedestrian flow. Moreover, if we define  $\bar{\mathbf{v}}(t, \mathbf{x})$  as mean velocity given by

$$\bar{\mathbf{v}}(t, \mathbf{x}) = \frac{\mathbf{F}(t, \mathbf{x})}{\rho(t, \mathbf{x})}$$

it is also possible to derive the variance of velocity  $\mathbf{v}$ , which is

$$\sigma(t, \mathbf{x}) = \frac{1}{\rho(t, \mathbf{x})} \int_{\Omega_{\mathbf{v}}} (\mathbf{v} - \bar{\mathbf{v}}(t, \mathbf{x}))^2 f(t, \mathbf{x}, \mathbf{v}) d\mathbf{v}.$$

The various models in literature differ mainly in the choice of three factors:

- the definition of the microstate
- the form of the gain and loss operator  $G$  and  $L$
- the form of the interaction function  $\theta$

In the next paragraph we will provide an example.

---

### 2.3.2 Dogbè's model

In this paragraph we will derive the mean field acceleration operator  $\mathbf{S}$  and the interaction operator  $J$  introduced by Dogbè in [28].

Firstly, it is worth to mention that in this model the collective behavior of the system is identified by the probability distribution function which is expressed as

$$f : \mathbb{R}^+ \times \Omega_{\mathbf{x}} \times \Omega_{\mathbf{v}} \times \Omega_u \rightarrow \mathbb{R}^+ : f = f(t, \mathbf{x}, \mathbf{v}, u)$$

with  $\Omega_{\mathbf{x}} \subseteq \mathbb{R}^2$ ,  $\Omega_{\mathbf{v}} \subseteq \mathbb{R}^2$  and  $\Omega_u \subseteq \mathbb{R}$ . This means that the microstate of each pedestrian is defined by his/her position  $\mathbf{x}$ , velocity  $\mathbf{v}$  and strategy  $u$ , also called activity variable. The analysis is carried out in two different contexts, in the following analysed.

#### Long-range interactions

We are assuming that individuals develop their strategies not only by taking into account nearby pedestrians, but also those far away; moreover, only pair interactions are considered. The governing equation is

$$\frac{\partial f}{\partial t} + \mathbf{v} \cdot \nabla_{\mathbf{x}} f + \nabla_{\mathbf{v}} \cdot ((\mathbf{S}[\rho] + \mathcal{S}[f])f) + \nabla_u (\mathcal{S}[f]f) = 0 \quad (2.21)$$

where  $\mathbf{S}$  models the macroscopic acceleration while  $\mathcal{S}$  models the microscopic acceleration.

The macroscopic accelerations among pedestrians are taken into account by introducing an intensity  $\phi$  which points along the direction  $\boldsymbol{\nu}$ , that is the direction of the velocity  $\mathbf{v}$ . In this way we are able to describe the average acceleration with which the crowd changes speed. Moreover, it is assumed that the behaviour among pedestrians is influenced both by density and speed, so

$$\mathbf{S}[\rho, \mathbf{v}, v] = \phi[\rho, \nabla_{\mathbf{x}} \rho, \mathbf{v}] \boldsymbol{\nu}$$

where  $\mathbf{v}(t, \mathbf{x}) = v(t, \mathbf{x}) \boldsymbol{\nu}(\mathbf{x})$ . For instance, if we assume that the behaviour of pedestrians is influenced only by the density, a possible expression of the operator  $\mathbf{S}[\rho]$  is

$$\mathbf{S}[\rho] = \alpha(v_e[\rho] \boldsymbol{\nu} - \mathbf{v}) - \frac{k^2[\rho]}{\rho} \nabla_{\boldsymbol{\nu}} \rho \quad (2.22)$$

which assumes the same form and meaning of (2.17). Possible choices for expressing  $k^2[\rho]$  can be found in [61].

The microscopic accelerations are taken into account by the operator  $\mathcal{S}$ , which is expressed as in (2.19) (with an abuse of notation). The proposed pairwise interaction term  $\theta$ , which defines operator  $\mathcal{S}[f]$ , is

$$\theta(\mathbf{x}, \mathbf{y}, \mathbf{v}, \mathbf{w}) = -\beta_1 \left( \frac{d_c - |\mathbf{y} - \mathbf{x}|}{|\mathbf{y} - \mathbf{x}|} \right) e^{-\beta_2(d_c - |\mathbf{y} - \mathbf{x}|)^2} \frac{\mathbf{y} - \mathbf{x}}{|\mathbf{y} - \mathbf{x}|} \quad (2.23)$$

with  $\beta_1, \beta_2$  non-negative coefficients. So, the pairwise mean field microscopic interaction is attractive if  $|\mathbf{y} - \mathbf{x}| > d_c$ , repulsive if  $|\mathbf{y} - \mathbf{x}| < d_c$ , where  $d_c$  is a critical threshold distance between the couple of interacting pedestrians. The exponential function is introduced in (2.23) for considering the fact that the interaction intensity decays with the distance.

These considerations completely define Eq.(2.21), which can be used for studying the evolution of the distribution function  $f$ .

### Localized interactions

We are assuming that individuals take into account only interactions among others that occur at finite distances. So, the basic difference between localized interactions and long-range interactions is only in the evaluation of the distance limit at which interactions do not produce any effect; it is like to introduce a sensory region for each member, that we will denote as  $R_s$ .

In this case, the governing equation is

$$\frac{\partial f}{\partial t} + \mathbf{v} \cdot \nabla_{\mathbf{x}} f + \nabla_{\mathbf{v}}(\mathbf{S}[\rho]f) = J[f] \quad (2.24)$$

which is able to predict the time evolution of  $f$  while neglecting long-range interactions. The operator  $\mathbf{S}[\rho]$  is given by (2.22); the operator  $J[f]$  models the interactions among pedestrians and in the following we will define it.

In this framework, interactions between a candidate pedestrian in position  $\mathbf{x}$  and field pedestrians take place only within the sensory region  $R_s(\mathbf{x})$ . Therefore we need to introduce a function which is able to weight the intensity of this interactions by looking at the distance between the interacting agents. For this reason we define a weight function  $\omega : \mathbb{R}^2 \rightarrow \mathbb{R}^+$  such that

$$\int_{\Omega_{\mathbf{x}}} \omega(\mathbf{x}, \mathbf{y}) d\mathbf{y} = 1.$$


---

Moreover, it is also introduced a function  $\eta = \eta(\mathbf{x}, \mathbf{y}, \mathbf{v}, \mathbf{w})$  which defines the rate of encounters per unit time in the unit volume for individuals with microscopic state  $(\mathbf{x}, \mathbf{v})$  and  $(\mathbf{y}, \mathbf{w})$ .

Finally, it is defined an interaction-transition function  $\mathcal{A}$  which denotes the probability density that a candidate pedestrian with state  $(\mathbf{x}, \mathbf{v}_*)$  will fall into state  $(\mathbf{x}, \mathbf{v})$  due to interaction with a pedestrian with velocity  $\mathbf{w}$ .

As a consequence, the gain and loss operator are defined by

$$\begin{aligned} G[f, f](t, \mathbf{x}, \mathbf{v}) &= \int \int \int_{R_s(\mathbf{x}) \times \mathbb{R}^2 \times \mathbb{R}^2} \eta(\mathbf{x}, \mathbf{y}, \mathbf{v}_*, \mathbf{w}) \mathcal{A}(\mathbf{v}_* \rightarrow \mathbf{v} | \mathbf{v}_*, \mathbf{w}) \omega(\mathbf{x}, \mathbf{y}) \\ &\quad \times f(t, \mathbf{x}, \mathbf{v}_*) f(t, \mathbf{y}, \mathbf{w}) d\mathbf{y} d\mathbf{v}_* d\mathbf{w} \\ L[f](t, \mathbf{x}, \mathbf{v}) &= \int \int_{R_s(\mathbf{x}) \times \mathbb{R}^2} \eta(\mathbf{x}, \mathbf{y}, \mathbf{v}, \mathbf{w}) \omega(\mathbf{x}, \mathbf{y}) f(t, \mathbf{y}, \mathbf{w}) d\mathbf{y} d\mathbf{w} \end{aligned} \quad (2.25)$$

and by substituting (2.25) into (2.20), we get the expression of the operator  $J[f]$ . Hence, each term of Eq.(2.24) is defined, and the time evolution of  $f$  can be predicted.

## 2.4 Force models

The choice of the force model is fundamental in modelling footbridge vibration problems indeed, according to how the dynamic load due to pedestrian walking is evaluated, results can strongly differ.

Dynamic forces induced by humans walking change in time and space, being random in nature and varying considerably not only between different pedestrians but also for a single individual who cannot repeat two identical steps. An example of walking force generated by a pedestrian walking at 1.39 m/s is reported in Fig.(2.12). The total force is quasi-periodic, indeed little variations occur over time because a single individual is not able to repeat two identical steps and consequently also the pacing period  $T_i$  can slightly change, so that  $T_i \neq T_{i+1}$ ; the red line allows a better understanding of times in which a pedestrian generates forces higher than its body weight from times in which the opposite occurs. As previously stated, this force is generated by only a single pedestrian; surely other individuals with different mass and height would generate different values of force. A reliable and realistic force model should be able to take into account these facts.

---

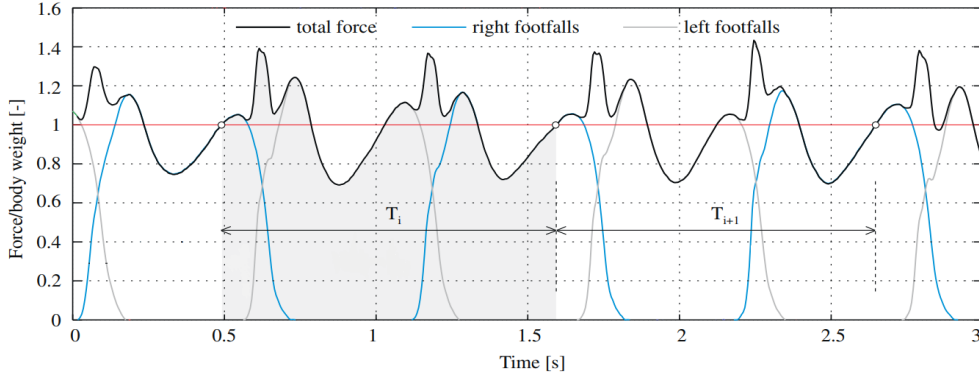


Figure 2.12: Walking force time history generated by a single pedestrian walking at 1.39 m/s and 1.81 Hz pacing rate [115].

Force models are mainly divided into two categories: time-domain and frequency-domain force models. Moreover, a time-domain model can be deterministic or probabilistic: the deterministic models make the assumption that all pedestrians apply the same dynamic load while walking, therefore random variation are not taken into account; on the other hand, the probabilistic models consider all people as individuals with distinctive parameters, therefore each pedestrian apply different load on the structure while walking.

In this thesis we will use a deterministic time-domain force model, consequently in the following we will study more in details the different types of this class of models.

The simplest model is the moving force one, in which each pedestrian is described as a concentrated load that travels at a certain velocity on the structure, as shown in graph (a) of Fig.(2.13). Moreover, this model is a deterministic one, therefore each individual generates identical and perfectly repeatable footfalls with period  $T$ . The vertical force generated by each pedestrian can be represented as a sum of Fourier harmonic components

$$F_p(t) = G + \sum_{i=1}^n G\alpha_i \sin(2\pi f_p t - \theta_i)$$

where  $G = m_p g$  is the pedestrian static weight,  $m_p$  is the pedestrian mass,  $g$  is the acceleration due to gravity,  $i$  is the order number of the harmonic,  $n$  is the total number of contributing harmonic,  $\alpha_i$  is the Fourier coefficient of the  $i$ -th harmonic also known as dynamic load factor,  $f_p$  is the pacing rate and  $\theta_i$  is the phase shift of the  $i$ -th harmonic.

The dynamic load factor, which is the ratio of the force amplitude to the weight of a person, has been studied over the years and nowadays is confirmed that it strongly depends on the pacing frequency; several methods for evaluating it are incorporated in contemporary design guidelines on vibration performance of civil engineering structures when subjected to pedestrian movement [116]. Even if the moving force model does not take into account pedestrian-structure interactions and is deterministic, it is by far the most used due to its simplicity.

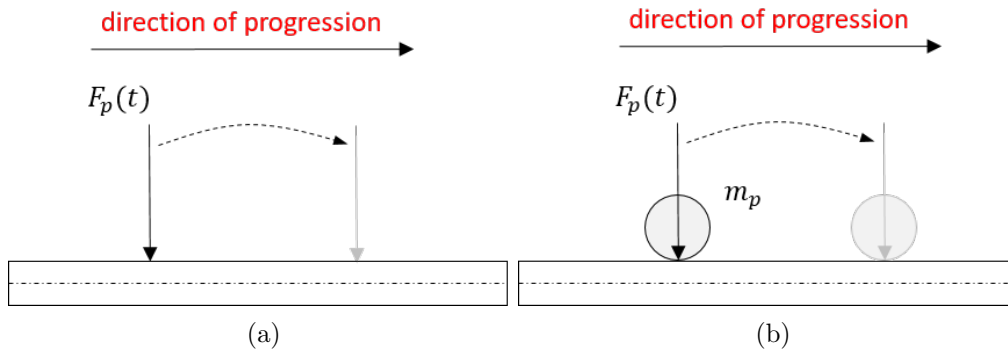


Figure 2.13: Moving force model in graph (a); moving mass model in graph (b).

A more realistic model is the moving mass one, developed by Biggs [112] and successfully adopted for studying footbridge vibration problems by O’Sullivan et al. [113]. In this case each pedestrian is seen as a moving mass which lays on the structure and moves along it, as shown in graph (b) of Fig.(2.13); thus, inertial forces are introduced and pedestrian-structure interactions are taken into account. However, the moving mass model assumes equal deflection of the centre of mass of the pedestrian and the bridge surface, therefore it would be even more realistic to model each pedestrian as a single degree of freedom system which moves along the footbridge span, as shown in graph (a) of Fig.(2.14). This model was introduced by Caprani et al. [108, 111] and it was further adopted in [56, 109]. Nowadays, this way to model pedestrian-structure interactions is finding popularity; the challenge consists in identify and calibrate the model parameters, such as the stiffness or the damping of the SDOF system which models the human body. Further, pedestrians can be described also by a simple inverted pendulum which oscillates in the vertical plane while moving along the footbridge, as shown in

graph (b) of Fig.(2.14). This idea was introduced by Bocian et al. [107]; they have shown that on the basis of the value of the ratio between the bridge vibration frequency and the pedestrian pacing frequency, a pedestrian acts as a positive or negative damper to the vertical dynamic response. Indeed, it is known that a crowd which crosses a footbridge adds mass to the structure and changes its damping coefficient.

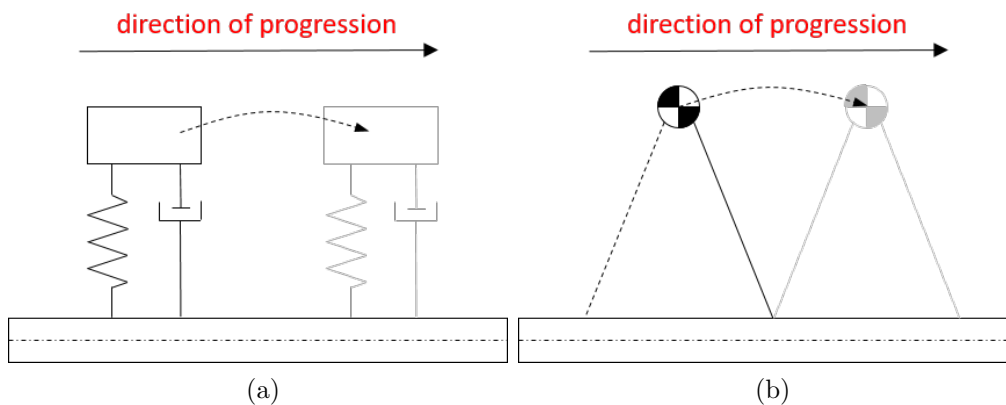


Figure 2.14: Single degree of freedom pedestrian model in graph (a); inverted-pendulum pedestrian model in graph (b).

## 2.5 Structure models

A structure model is needed in order to evaluate the vertical acceleration of the footbridge. As previously stated, there are basically two types of models used in literature, in which the structure is described either using a formulation in modal coordinates, that is, as a single degree of freedom system, or by using the Finite Element (FE) method [111].

In the following we will use the first type of model, so the footbridge is described by a single degree of freedom system excited with harmonic forces. Hence, it is useful to recall some basic concepts regarding the dynamics of these systems. More information inherent to possible extensions and further developments of the topic can be found in [68, 71, 72, 95, 96].

A structure can be modelled as a three-dimensional damped dynamical system. The equation of motion can be derived by a direct equilibration of

all the forces acting on the structure, so

$$\mathbf{F}_I(t, \mathbf{x}) + \mathbf{F}_D(t, \mathbf{x}) + \mathbf{F}_E(t, \mathbf{x}) = \mathbf{F}(t, \mathbf{x}) \quad (2.26)$$

where  $\mathbf{x} = \{x, y, z\}$  and  $t \geq 0$  are the space and time variables. In relation (2.26) the quantity  $\mathbf{F}_I(t, \mathbf{x})$  represents the inertial force,  $\mathbf{F}_D(t, \mathbf{x})$  is the damping force,  $\mathbf{F}_E(t, \mathbf{x})$  is the elastic force and  $\mathbf{F}(t, \mathbf{x})$  is the external force caused by pedestrian motion.

The inertial force is given by the product of the mass and the acceleration, therefore

$$\mathbf{F}_I(t, \mathbf{x}) = m(\mathbf{x})\ddot{\mathbf{d}}(t, \mathbf{x}) \quad (2.27)$$

where  $\mathbf{d}(t, \mathbf{x})$  is the structural displacement while  $m(\mathbf{x})$  is the footbridge's mass. If we work under the assumption of viscous damping, the damping force can be expressed as proportional to the velocity, hence

$$\mathbf{F}_D(t, \mathbf{x}) = \mathcal{C}[\dot{\mathbf{d}}(t, \mathbf{x})]$$

where  $\mathcal{C}$  is the damping operator. Moreover, the elastic force is usually expressed as proportional to the displacement, therefore

$$\mathbf{F}_E(t, \mathbf{x}) = \mathcal{L}[\mathbf{d}(t, \mathbf{x})]$$

where  $\mathcal{L}$  is the stiffness operator.

It is often assumed that the equation of motion is linear, consequently the damping and stiffness operators are assumed linear too, so

$$\begin{aligned} \mathcal{C}[\dot{\mathbf{d}}(t, \mathbf{x})] &= c(\mathbf{x})\dot{\mathbf{d}}(t, \mathbf{x}) \\ \mathcal{L}[\mathbf{d}(t, \mathbf{x})] &= k(\mathbf{x})\mathbf{d}(t, \mathbf{x}) \end{aligned} \quad (2.28)$$

where  $c(\mathbf{x})$  and  $k(\mathbf{x})$  are respectively the damping and the stiffness of the structure. On the basis of this assumption, the equation of motion can be solved while approximating the solution by the following truncating expression

$$\mathbf{d}(t, \mathbf{x}) \approx \sum_{j=1}^n \phi_j(\mathbf{x})y_j(t) \quad (2.29)$$

where  $\phi_j(\mathbf{x})$  is the eigenvector of the  $j$ -th mode of vibration while  $y_j(t)$  is the corresponding principal coordinate;  $n$  represents a suitable number of structural modes.

---

A footbridge is often characterized by a reduced width to length ratio, therefore the equation of motion (2.26) is usually expressed in one space dimension; consequently, the footbridge is modelled as a line-like structure, for instance as a simply supported beam, and the space variable  $x \in \Omega \subset \mathbb{R}$ . Under this assumption, if we substitute relations (2.27), (2.28) and (2.29) into (2.26) we obtain

$$m(x) \sum_{j=1}^n \phi_j(x) \ddot{y}_j(t) + c(x) \sum_{j=1}^n \phi_j(x) \dot{y}_j(t) + k(x) \sum_{j=1}^n \phi_j(x) y_j(t) = F(t, x). \quad (2.30)$$

Moreover, it is usually assumed that only one mode mainly contributes to the structural response in footbridge vibration problems; thus, the response can be estimated with sufficient accuracy using a single degree of freedom modal equation. Consequently,  $n = 1$  and Eq.(2.30) becomes

$$m(x)\phi(x)\ddot{y}(t) + c(x)\phi(x)\dot{y}(t) + k(x)\phi(x)y(t) = F(t, x). \quad (2.31)$$

where  $\phi(x) = \phi_1(x)$  is our mode of interest.

If we multiply both side of Eq.(2.31) by  $\phi(x)$  and we integrate over the space variable, we obtain

$$M\ddot{y}(t) + C\dot{y}(t) + Ky(t) = F(t) \quad (2.32)$$

where

$$\begin{aligned} M &= \int_0^L m(x)\phi^2(x)dx \\ C &= \int_0^L c(x)\phi^2(x)dx \\ K &= \int_0^L k(x)\phi^2(x)dx \\ F(t) &= \int_0^L F(x, t)\phi(x)dx \end{aligned}$$

are respectively the modal mass, damping, stiffness and force while  $L$  is the length of the footbridge. Eq.(2.32) must be accompanied by suitable initial conditions, such as

$$\begin{cases} y(0) &= y_0 \\ \dot{y}(0) &= \dot{y}_0 \end{cases}$$


---

with  $y_0, \dot{y}_0 \in \mathbb{R}$ .

Eq.(2.32) provides the time evolution of the modal displacement  $y(t)$  and we would like to understand how  $y(t)$  evolves once that the transitional phase ends. The following analysis is carried out under the assumption that the modal force  $F(t)$  is harmonic, hence

$$\begin{aligned} F(t) &= F_0 e^{i\omega t} \\ &= F_0 (\cos \omega t + i \sin \omega t) \end{aligned}$$

where  $i$  is the imaginary unit and  $F_0 \in \mathbb{C}$  is the force amplitude. Consequently the solution will assume the form  $y(t) = Y_0 e^{i\omega t}$ , with  $Y_0 \in \mathbb{C}$ . The amplitude of the solution  $Y_0$  is an unknown quantity, and the purpose is to derive it. Once that  $Y_0$  is known, then:

- if  $F(t) = F_0 \cos \omega t$ , the solution will be  $y(t) = \text{Re}[Y_0 e^{i\omega t}]$
- if  $F(t) = F_0 \sin \omega t$ , the solution will be  $y(t) = \text{Im}[Y_0 e^{i\omega t}]$

Since we are assuming a solution type  $y(t) = Y_0 e^{i\omega t}$ , then

$$\begin{aligned} \dot{y}(t) &= i\omega Y_0 e^{i\omega t} \\ \ddot{y}(t) &= -\omega^2 Y_0 e^{i\omega t} \end{aligned} \tag{2.33}$$

and by substituting relations (2.33) in Eq.(2.32) and while dividing both side by  $1/M$ , we obtain

$$\left( \frac{K}{M} - \omega^2 + i\omega \frac{C}{M} \right) Y_0 = F_0. \tag{2.34}$$

The natural frequency  $\omega_n$  of our mode of interest and the modal damping  $C$  can be expressed as

$$\omega_n = \sqrt{\frac{K}{M}}, \quad C = 2\xi M\omega$$

where  $\xi$  is the damping coefficient of our mode of interest. Consequently, Eq.(2.34) becomes

$$\begin{aligned} (\omega_n^2 - \omega^2 + i2\xi\omega\omega_n) Y_0 &= \frac{F_0}{M} \\ (1 - r^2 + i2\xi r) Y_0 &= \frac{F_0}{K} \end{aligned}$$


---

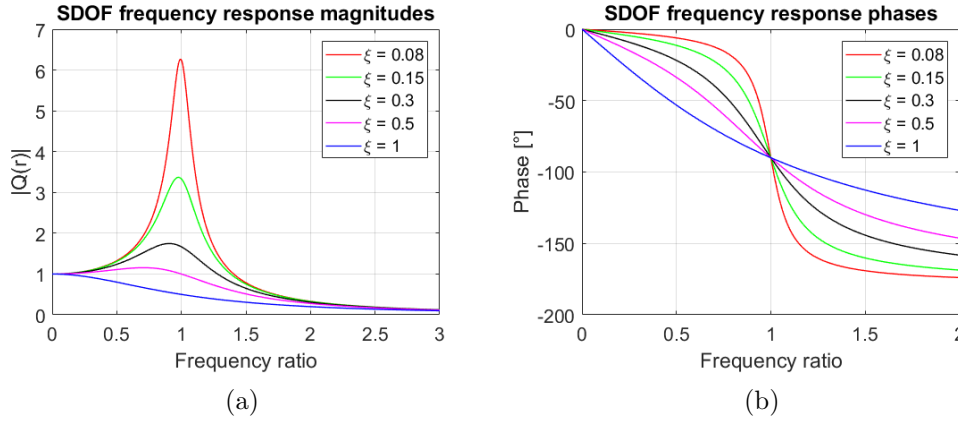


Figure 2.15: Modulus and phase of the dynamic amplification factor for a single degree of freedom system for different values of  $\xi$ .

where  $r = \omega/\omega_n$  is the frequency ratio and  $y_{st} = F_0/K$  is the modal static displacement. We can define  $Q(r) = Y_0/y_{st}$ , so that

$$Q(r) = \frac{1}{1 - r^2 + i2\xi r} \quad (2.35)$$

which is a complex quantity.  $Q(r)$  is called dynamic amplification factor, and it is the factor by which displacement responses are amplified. Since  $Q(r) \in \mathbb{C}$  we can write  $Q(r) = |Q(r)|e^{i\varphi}$ . The modulus  $|Q(r)|$  and the phase  $\varphi$  can be obtained from Eq.(2.35), and are given by

$$|Q(r)| = \frac{1}{\sqrt{(1 - r^2)^2 + (2\xi r)^2}}$$

$$\tan \varphi = -\frac{2\xi r}{1 - r^2}.$$

In Fig.(2.15) the modulus of  $Q(r)$  and its phase  $\varphi$  are plotted. It is possible to notice that when  $r = 1$ , so when we excite the system with a frequency  $\omega$  equal to its natural frequency  $\omega_n$ , the phenomenon of resonance for our mode of interest takes place. Indeed if  $\xi = 0$ , in  $r = 1$  the modulus of  $Q$  has a vertical asymptote, which means that  $Y_0/y_{st} \rightarrow \infty$ , or in other words that the system collapses. As  $\xi$  increases, the maximum value assumed by  $|Q(r)|$  decreases and moves toward left, as visible in graph (a).

It would be interesting to evaluate which is the frequency that would generate a resonance phenomenon if used for exciting the system. For deriving

it, it is enough to evaluate the value of  $r$  in correspondence to the point in which  $|Q(r)|$  has a maximum, which is

$$\frac{d}{dr}((1 - r^2)^2 + (2\xi r)^2) = 0 \quad \implies \quad r = \sqrt{1 - 2\xi^2}$$

so

$$\omega_{res} = \omega_n \sqrt{1 - 2\xi^2}$$

that is the so-called resonance frequency.

Once that the dynamic amplification factor  $Q(r)$  is known, we can easily derive  $Y_0$ , and so Eq.(2.32) is solved. In case  $F(t)$  has a simple expression the solution can be obtained analytically, otherwise the equation must be solved by using a numerical method, as shown in chapter 4.

---

# Chapter 3

## Description of the modelling framework

In this chapter a detailed description of the modelling framework will be given. The flow chart in Fig.(3.1) outlines the way in which topics are presented. It involves two different physical systems, the pedestrians and the structure one, linked through a force model. The description will be made from two distinct points of view, the microscopic and the macroscopic one; it will be shown also the scale passage between the two representations. The structure considered is a footbridge. All models and simulations will be presented in a one-dimensional domain.

In section 3.1 the microscopic crowd model will be introduced; then in section 3.2, by using a statistical representation of the crowd, the mesoscopic crowd model is derived. This allow to pass at a macroscopic description, described in section 3.3. In section 3.4 it will be shown that the macroscopic model is actually a generalization of the microscopic one, and so we will denote them as equivalent. In section 3.5 the structure model will be analysed; finally, in section 3.6 the microscopic and macroscopic force models will be described in details.

### 3.1 The microscopic crowd model

A microscopic crowd model is interested in the behaviour, actions and decisions of each pedestrian as well as interactions among them. Consequently it

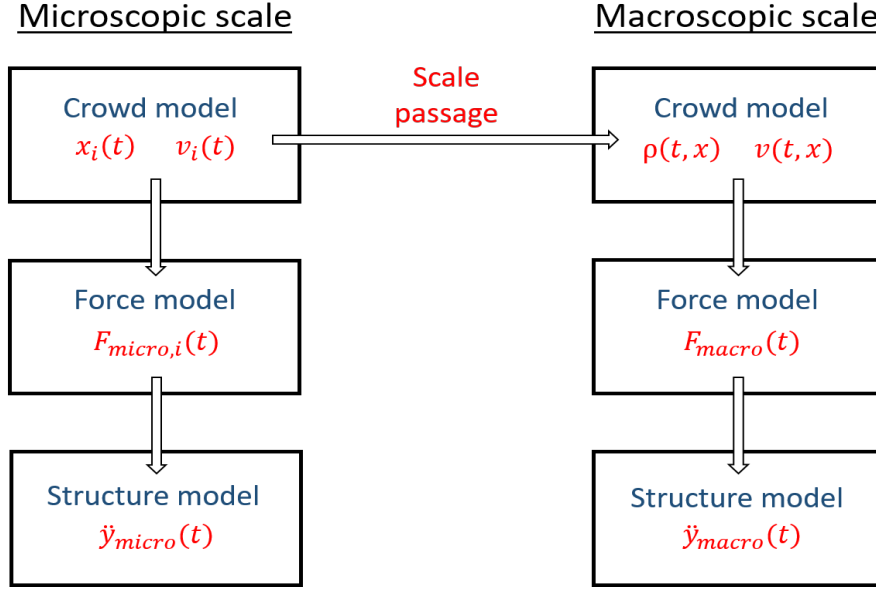


Figure 3.1: Schematic description of the modelling framework.

is based on the assumption that every single agent can be tracked individually. Among all microscopic crowd models shown in chapter 2, the one used in the following is a first-order model expressed as

$$\frac{dx_i}{dt} = v_{d,i} - \frac{1}{N} \sum_{\substack{j=1 \\ j \neq i}}^N K(x_i, x_j) \quad (3.1)$$

where  $N$  is the total number of pedestrians on the footbridge,  $x_i$  is the position of the  $i$ -th pedestrian,  $v_{d,i}$  is the desired velocity of the  $i$ -th pedestrian and  $K$  represents the interaction kernel. Since we assume that the desired velocity is common for each pedestrian, in the following the index  $i$  will be omitted from  $v_{d,i}$ .

Model (3.1) is able to capture the main features of pedestrians walking on footbridges. Indeed, each pedestrian enters the bridge at a preferred speed, which is  $v_d$ ; this velocity would be unchanged in the absence of other pedestrians or obstacles. Since interactions usually take place, the desired velocity is modified and the interaction kernel  $K$  plays the role to do it. The desired velocity is supposed to be a positive constant, hence  $v_d > 0$ ; consequently, the dynamics of the system depend on the choice of  $K$ . In

order to guarantee that model (3.1) is well posed, the following assumptions on the interaction kernel are made:

1. Compactness of the support and frontal orientation of the sensory region. This means that the  $i$ -th pedestrian in position  $x_i$  interacts only with others in front of him/her, within a limited region. This limited space is the so-called sensory region, defined as

$$R_s(x_i) = [x_i, x_i + R]$$

with  $R > 0$ .

2. Boundedness and regularity in  $(x_i, x_i + R)$ . The interaction intensity is proportional to the mutual distance between interacting pedestrians, and varies smoothly with it; a finite maximum value must be provided. Thus

$$K \in C^2(x_i, x_i + R), \quad K, K'' \in L^\infty(x_i, x_i + R), \quad \text{for } i = 1, \dots, N. \quad (3.2)$$

Assumptions (3.2) guarantee that repulsion forces have physical value, so that pedestrians tend to gradually move far from others.

3. Monotonicity in  $(x_i, x_i + R)$ , so

$$K(\xi) > 0, \quad K'(\xi) < 0, \quad \text{for } \xi \in (x_i, x_i + R), \quad \text{for } i = 1, \dots, N$$

and

$$K(x_i) = K(x_i + R) = 0, \quad K(x_i^+) = \lim_{\xi \rightarrow 0^+} K(\xi) > 0, \quad \text{for } i = 1, \dots, N.$$

Thus pedestrian interactions decay within the sensory region as the mutual distance increases and they do not self-interact.

A possible choice of the interaction kernel  $K$  which satisfies all properties above mentioned is

$$K(x_i, x_j) = \eta(R - |x_i - x_j|) \mathbb{1}_{[x_i, x_i + R]}(x_j - x_i) \quad (3.3)$$

where  $R$  is the length of the sensory region and  $\eta$  is the repulsion coefficient. Hence, the microscopic crowd model used in the following is

$$\frac{dx_i}{dt} = v_{d,i} - \frac{1}{N} \sum_{\substack{j=1 \\ j \neq i}}^N \eta(R - |x_i - x_j|) \mathbb{1}_{[x_i, x_i + R]}(x_j - x_i). \quad (3.4)$$

As shown in Fig.(3.2), interactions take place only within the sensory region. Moreover, the argument of the indicator function in Eq.(3.3) specifies that the  $i$ -th pedestrian interacts only with the  $j$ -th pedestrian in position  $x_j > x_i$ , so that the first property is satisfied. Furthermore, the factor  $1/N$  is added in Eq.(3.4) because we are considering a mean interaction. Since the domain is one-dimensional, it is not necessary to introduce a wall-repulsive term.

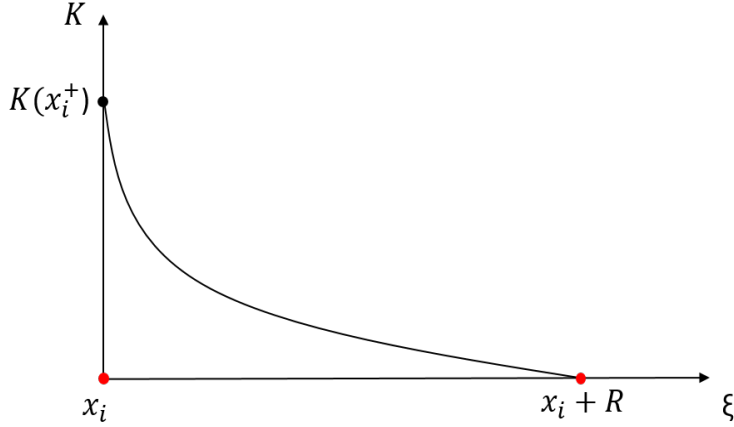


Figure 3.2: Example of a suitable interaction kernel.

The repulsion coefficient  $\eta$  is assumed to take the same value for all pedestrians. It would be preferable to choose  $\eta$  in order to satisfy the constraint  $|v_i| \leq v_{max}$ , where  $v_{max}$  represents the maximum velocity at which pedestrians can walk. By using inequality  $|x - y| \leq |x| + |y|$ , we have

$$\begin{aligned}
 |v_i| &= \left| v_d - \frac{1}{N} \sum_{\substack{j=1 \\ j \neq i}}^N \eta(R - |x_i - x_j|) \mathbf{1}_{[x_i, x_i+R]}(x_j - x_i) \right| \\
 &\leq |v_d| + \frac{\eta}{N} \sum_{\substack{j=1 \\ j \neq i}}^N |R - |x_i - x_j|| \mathbf{1}_{[x_i, x_i+R]}(x_j - x_i) \\
 &\leq |v_d| + \frac{\eta}{N} \sum_{\substack{j=1 \\ j \neq i}}^N R \\
 &= |v_d| + \eta R
 \end{aligned}$$

so

$$\eta \leq \frac{v_{max} - |v_d|}{R} = \eta^* \tag{3.5}$$

Hence, if  $\eta \in (0, \eta^*)$  then  $|v_i| \leq v_{max}$ . We will show in chapter 4 that inequality (3.5) is sufficient but not necessary. Indeed, if it is set a finite value of  $\eta$  such that  $\eta > \eta^*$ , the velocity still remains limited, but the system will reach a steady state in faster time.

In the next section the passage at the mesoscopic scale will be shown, starting from the model presented above.

## 3.2 The mesoscopic crowd model

A mesoscopic crowd model does not track the movement of each pedestrian, but instead studies how an agent interacts with others nearby. A statistical representation of the crowd is used, therefore the time evolution of the whole system is provided by a suitable probability distribution function. Moreover, since we use a statistical point of view, we are automatically assuming that the number of pedestrians  $N$  is huge enough, theoretically  $N \rightarrow \infty$ .

Like in section 2.3, it is assumed that after each interaction pedestrians change their state. In this model the microscopic state of each pedestrian is given only by the position  $x \in \mathbb{R}$ , which is seen as an independent variable. Thus, the distribution function  $f$  is written as  $f = f(t, x)$ . Since we are in a one-dimensional domain, the quantity  $f(t, x)dx$  at time  $t$  represents the infinitesimal average number of pedestrians located between  $x - \frac{1}{2}dx$  and  $x + \frac{1}{2}dx$ . Moreover, the desired velocity is assumed constant in the following, hence  $v_d(x) = v_d$ .

In the following we will see how derive an equation which governs the time evolution of the distribution function.

### 3.2.1 Weak form of a Boltzmann-type equation

We would like to determine how the pedestrian state  $x$  changes due to collisions among other members. Once that this process is defined, it will be easy to derive a time evolution equation for the distribution function  $f(t, x)$ .

In this framework, only pairwise interaction are considered. Therefore, it is like if we extract two generic pedestrians in positions  $x_i$  and  $x_j$  from the crowd, and we assume that only them exist. Hence, in order to study how their microscopic state evolves, we need to define how they interact. For this

---

generic couple, Eq.(3.4) can be written as

$$\begin{cases} \frac{dx_i}{dt} &= v_d - \eta(R - |x_i - x_j|)\mathbb{1}_{[x_i, x_i+R]}(x_j - x_i) \\ \frac{dx_j}{dt} &= v_d \end{cases} \quad (3.6)$$

with the assumption that  $x_j > x_i$ . In Eq.(3.4) the sum is made over all pedestrians beside the  $i$ -th one of which we are studying the behaviour, because self-interactions are not considered. Since we are currently treating only a generic couple of pedestrians, the  $i$ -th pedestrian interacts only with the  $j$ -th one, consequently we set  $N = 1$  in (3.6).

Then we compute a time discretization of the binary interaction (3.6) by using an explicit Euler scheme, and we obtain

$$\begin{cases} x_i(t + \Delta t) &= x_i(t) + \Delta t[v_d - \eta(R - |x_i(t) - x_j(t)|)]\mathbb{1}_{[x_i, x_i+R]}(x_j(t) - x_i(t)) \\ x_j(t + \Delta t) &= x_j(t) + \Delta t v_d \end{cases} \quad (3.7)$$

where  $\Delta t$  is the time step. The interaction assumes this form because the  $i$ -th pedestrian has the  $j$ -th pedestrian within his/her sensory region, while the latter is undisturbed, since the  $i$ -th pedestrian is behind him/her. The configuration is well represented in Fig.(3.3). Interactions of type (3.7) are defined as asymmetric binary interactions.

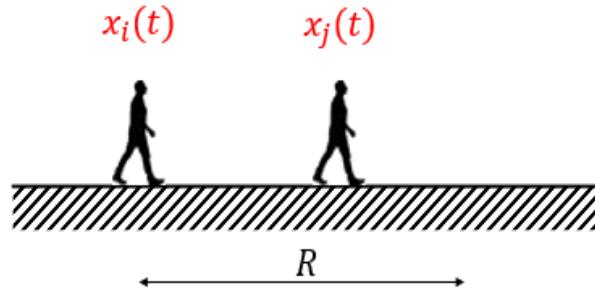


Figure 3.3: Pedestrian in position  $x_j(t)$  is within the sensory region  $R_s(x_i)$  of pedestrian in position  $x_i(t)$ ;  $R$  is the length of the sensory region.

Since we are considering a generic pair of pedestrians, indices can be omitted. While identifying  $x_i = x$  and  $x_j = y$ , the binary interaction (3.7)

can be written as

$$\begin{cases} x(t + \Delta t) &= x(t) + \Delta t [v_d - \eta(R - |x(t) - y(t)|)] \mathbb{1}_{[x, x+R]}(y(t) - x(t)) \\ y(t + \Delta t) &= y(t) + \Delta t v_d. \end{cases} \quad (3.8)$$

This rule defines the time variation of the states  $x(t)$  and  $y(t)$  due to interactions. Then we assume that in a short time interval  $\Delta t$ , a pair of pedestrians interacts with probability proportional to  $\Delta t$ . This mechanism can be described by the introduction of a random variable  $\Lambda$  such that

$$\Lambda \sim \text{Bernoulli}(\Delta t)$$

with  $\Delta t < 1$ . Consequently

$$\begin{aligned} P(\Lambda = 0) &= 1 - \Delta t \\ P(\Lambda = 1) &= \Delta t \end{aligned}$$

where

- $\Lambda = 0$  means that there are no interactions in the time interval  $\Delta t$ ;
- $\Lambda = 1$  means that there are interactions in the time interval  $\Delta t$ .

Thus, we can write relations (3.8) as

$$\begin{cases} x(t + \Delta t) &= x(t) + \Lambda \mathcal{K}(x(t), y(t)) \\ y(t + \Delta t) &= y(t) + \Lambda \mathcal{H}(y(t), x(t)) \end{cases} \quad (3.9)$$

with

$$\begin{aligned} \mathcal{K}(x(t), y(t)) &= v_d - \eta(R - |x(t) - y(t)|) \mathbb{1}_{[x, x+R]}(y(t) - x(t)) \\ &= v_d - K(x(t), t(t)) \\ \mathcal{H}(y(t), x(t)) &= v_d. \end{aligned} \quad (3.10)$$

In (3.10) it is obvious that  $\mathcal{K}(x(t), y(t)) \neq \mathcal{H}(y(t), x(t))$ , which confirm the asymmetry of the binary interactions.

Now we introduce a test function  $\varphi$  such that  $\varphi = \varphi(x) \in \mathbb{R}$ ; the quantity  $\varphi(\cdot)$  is also called observable quantity. The natural use of a probability density relies on the computation of averages. Indeed, once that the probability

density  $f(t, x)$  is given, we can compute the average value of any function  $\varphi(x)$ . We define averages as

$$\langle \varphi(x) \rangle = \int_{\mathbb{R}} \varphi(x) f(t, x) dx. \quad (3.11)$$

Then we apply the function  $\varphi$  at relations (3.9) and we obtain

$$\begin{cases} \varphi(x(t + \Delta t)) &= \varphi(x(t) + \Lambda \mathcal{K}x(t), y(t)) \\ \varphi(y(t + \Delta t)) &= \varphi(y(t) + \Lambda \mathcal{H}(y(t), x(t))) \end{cases} \quad (3.12)$$

and while adding up term by term we have

$$\begin{aligned} \langle \varphi(x(t + \Delta t)) + \varphi(y(t + \Delta t)) \rangle &= \langle \varphi(x(t) + \Lambda \mathcal{K}(x(t), y(t))) + \varphi(y(t) + \\ &\quad + \Lambda \mathcal{H}(y(t), x(t))) \rangle. \end{aligned}$$

Finally, by computing the mean value with respect to  $\Lambda$ , we obtain

$$\begin{aligned} \langle \varphi(x(t + \Delta t)) + \varphi(y(t + \Delta t)) \rangle &= \langle \varphi(x(t + \Delta t)) + \varphi(y(t + \Delta t)) \rangle \Delta t + \\ &\quad + \langle \varphi(x(t)) + \varphi(y(t)) \rangle (1 - \Delta t) \end{aligned}$$

that can be written as

$$\begin{aligned} \frac{\langle \varphi(x(t + \Delta t)) + \varphi(y(t + \Delta t)) \rangle - \langle \varphi(x(t)) + \varphi(y(t)) \rangle}{\Delta t} &= [\langle \varphi(x(t) + \mathcal{K}(x(t), y(t))) + \\ &\quad + \varphi(y(t) + \mathcal{H}(y(t), x(t))) \rangle - \langle \varphi(x(t)) + \varphi(y(t)) \rangle]. \end{aligned}$$

Consequently, if we consider  $\Delta t \rightarrow 0^+$  we obtain the differential equation

$$\frac{d}{dt} [\langle \varphi(x(t)) + \varphi(y(t)) \rangle] = [\langle \varphi(x'(t)) + \varphi(y'(t)) \rangle - \langle \varphi(x(t)) + \varphi(y(t)) \rangle] \quad (3.13)$$

where

$$\begin{cases} x'(t) &:= x(t) + \mathcal{K}(x(t), y(t)) \\ y'(t) &:= y(t) + \mathcal{H}(y(t), x(t)) \end{cases} \quad (3.14)$$

which are the post-interaction states of the interacting pedestrian couple. For the sake of simplicity, the time dependence will be omitted in the following.

The average definition (3.11) holds also for  $x'$ , indeed

$$\langle \varphi(x') \rangle = \int_{\mathbb{R}} \varphi(x') f(t, x') dx$$


---

where  $f$  is the so-called kinetic distribution function; in the following we will also prove that

$$\begin{aligned}\int_{\mathbb{R}} f(t, x) dx &= 1, & \forall t \geq 0 \\ f(t, x) &\geq 0, & \forall x, \forall t\end{aligned}\quad (3.15)$$

which ensure that  $f$  is a probability density function.

In relations (3.14) it is evident that the post-interaction state  $x'$  is function of both the pre-interaction states  $x$  and  $y$ . For avoiding the insertion of another unknown quantity, we use the Boltzmann's ansatz which states that

$$f(t, x') = f(t, x)f(t, y)$$

like if the two states would be independent during the interactions. Under this assumption, we can write

$$\langle \varphi(x') \rangle = \int_{\mathbb{R}} \varphi(x') f(t, x') dx = \int_{\mathbb{R}} \int_{\mathbb{R}} \varphi(x') f(t, x) f(t, y) dx dy \quad (3.16)$$

and also

$$\begin{aligned}\langle \varphi(x) \rangle &= \int_{\mathbb{R}} \varphi(x) f(t, x) dx = \int_{\mathbb{R}} \varphi(x) f(t, x) dx \int_{\mathbb{R}} f(t, y) dy \\ &= \int_{\mathbb{R}} \int_{\mathbb{R}} \varphi(x) f(t, x) f(t, y) dx dy.\end{aligned}\quad (3.17)$$

Definitions (3.16) and (3.17) are valid also for state  $y'$ . Therefore, by substituting (3.11), (3.16) and (3.17) in Eq.(3.13) we obtain

$$\begin{aligned}\frac{d}{dt} \left[ \int_{\mathbb{R}} \varphi(x) f(t, x) dx + \int_{\mathbb{R}} \varphi(y) f(t, y) dy \right] &= \int_{\mathbb{R}} \int_{\mathbb{R}} [\varphi(x') + \varphi(y')] f(t, x) f(t, y) dx dy + \\ &\quad - \int_{\mathbb{R}} \int_{\mathbb{R}} [\varphi(x) + \varphi(y)] f(t, x) f(t, y) dx dy.\end{aligned}\quad (3.18)$$

Since the integration variable is dummy

$$\int_{\mathbb{R}} \varphi(x) f(t, x) dx + \int_{\mathbb{R}} \varphi(y) f(t, y) dy = 2 \int_{\mathbb{R}} \varphi(x) f(t, x) dx$$

Eq.(3.18) becomes

$$\frac{d}{dt} \left[ \int_{\mathbb{R}} \varphi(x) f(t, x) dx \right] = \frac{1}{2} \int_{\mathbb{R}} \int_{\mathbb{R}} [\varphi(x') + \varphi(y') - \varphi(x) - \varphi(y)] f(t, x) f(t, y) dx dy \quad (3.19)$$

which is the weak form of a Boltzmann-type equation, valid for the asymmetrical binary interactions (3.9). It defines the time evolution of the distribution function  $f$  and consequently the statistical evolution of the pedestrian positions.

### 3.2.2 Statistical moments

We can use Eq.(3.19) for computing the time evolution of the statistical moments of  $f$ ; this also allows us also to formally prove that  $f$  is a probability density function. The statistical moments of  $f$  will be studied one by one in the following:

1.  $\varphi(x) = 1$ :

In this case

$$\begin{aligned}\varphi(x') - \varphi(x) &= 0 \\ \varphi(y') - \varphi(y) &= 0\end{aligned}$$

hence, from Eq.(3.19)

$$\frac{d}{dt} \left[ \int_{\mathbb{R}} f(t, x) dx \right] = 0 \quad \Rightarrow \quad \int_{\mathbb{R}} f(t, x) dx = \text{const.}$$

We can conclude that the zero moment is conserved, thus the pedestrian number conservation is ensured. Moreover, if we choose  $f(0, x)$  such that

$$\int_{\mathbb{R}} f(0, x) dx = 1$$

then

$$\int_{\mathbb{R}} f(t, x) dx = 1, \quad \forall t$$

which proves the first property of (3.15).

2.  $\varphi(x) = x$ :

In this case we are going to study the evolution of the mean state of the system. We define

$$Z(t) = \int_{\mathbb{R}} x f(t, x) dx$$

and Eq.(3.19) results as

$$\frac{dZ(t)}{dt} = \frac{1}{2} \int_{\mathbb{R}} \int_{\mathbb{R}} [x' + y' - x - y] f(t, x) f(t, y) dx dy \quad (3.20)$$

but  $x' - x = \mathcal{K}(x, y)$  and  $y' - y = \mathcal{H}(y, x)$ ; hence, by substituting relations (3.10) in Eq.(3.20) we obtain

$$\frac{dZ(t)}{dt} = \int_0^\infty \int_x^{x+R} [2v_d(x) - \eta(R - |x - y|)] f(t, x) f(t, y) dx dy$$

which clearly shows that the first moment is in general not conserved.

3.  $\varphi(x) = x^2$ :

In this case we are going to study the evolution of the second order moment. We define

$$\Sigma(t) = \int_{\mathbb{R}} x^2 f(t, x) dx$$

so Eq.(3.19) becomes

$$\begin{aligned} \frac{d\Sigma(t)}{dt} &= \frac{1}{2} \int_{\mathbb{R}} \int_{\mathbb{R}} [(x')^2 + (y')^2 - x^2 - y^2] f(t, x) f(t, y) dx dy \\ &= \frac{1}{2} \int_{\mathbb{R}} \int_{\mathbb{R}} (x')^2 f(t, x) f(t, y) dx dy - \frac{1}{2} \int_{\mathbb{R}} x^2 f(t, x) dx \int_{\mathbb{R}} f(t, y) dy + \\ &\quad + \frac{1}{2} \int_{\mathbb{R}} \int_{\mathbb{R}} (y')^2 f(t, x) f(t, y) dx dy - \frac{1}{2} \int_{\mathbb{R}} y^2 f(t, y) dy \int_{\mathbb{R}} f(t, x) dx \\ &= \frac{1}{2} \int_{\mathbb{R}} \int_{\mathbb{R}} (x')^2 f(t, x) f(t, y) dx dy - \frac{1}{2} \Sigma(t) + \\ &\quad + \frac{1}{2} \int_{\mathbb{R}} \int_{\mathbb{R}} (y')^2 f(t, x) f(t, y) dx dy - \frac{1}{2} \Sigma(t) \end{aligned}$$

that can be written as

$$\frac{d\Sigma(t)}{dt} + \Sigma(t) = \frac{1}{2} \int_{\mathbb{R}} \int_{\mathbb{R}} [(x')^2 + (y')^2] f(t, x) f(t, y) dx dy. \quad (3.21)$$

By solving Eq.(3.21) we obtain

$$\Sigma(t) = e^{-t} \Sigma(0) + \frac{1}{2} \int_0^t e^{-(t-s)} \int_{\mathbb{R}} \int_{\mathbb{R}} [(x')^2 + (y')^2] f(s, x) f(s, y) dx dy ds$$

which states that the evolution of the second order moment is not conserved. Finally, by combining the results obtained from the first and second order moments, it is possible to derive the time evolution of the variance of the state  $x$ , which is

$$\begin{aligned} Var(x) &= \int_{\mathbb{R}} x^2 f(t, x) dx - \left[ \int_{\mathbb{R}} x f(t, x) \right]^2 \\ &= \Sigma(t) - Z(t)^2. \end{aligned}$$

4.  $\varphi(x) = x^p$ ,  $p > 2$ ,  $p \in \mathbb{N}$ :

In case we are interested in the evolution of higher order moments of  $f$ , we have to study how

$$\frac{d}{dt} \left[ \int_{\mathbb{R}} x^p f(t, x) dx \right]$$

evolves, but this is out of the purpose of the thesis.

### 3.2.3 Fokker-Planck equation

The derivation of the Fokker-Planck equation is needed in order to compute the passage at the macroscopic scale; this is what we are going to discuss in this section.

The previous analysis shows that in general it is difficult to study in detail the asymptotic behaviour of the distribution function  $f(t, x)$  just by considering the evolution of its statistical moments. Another way would be to study directly the asymptotic behaviour of Eq.(3.19) by computing the limit for  $t \rightarrow \infty$ , but if we use this method we would have several technical difficulties and it is not guaranteed that relevant results can be derived. Therefore, in order to gain more detailed insights into the asymptotic distribution we have to use a suitable scaling technique. This will lead us to compute the quasi-invariant interaction limit, which allows the derivation of the Fokker-Planck equation.

The Boltzmann equation obtained in the previous sections is based on a time scale relative to a single binary interaction. While studying the asymptotic behaviour of the system, we have to consider the regime of weak but frequent interactions. Thus, the idea is to scale all terms inherent at the state variations in a way that

$$\begin{cases} x' &= x + \epsilon \mathcal{K}(x, y) \\ y' &= y + \epsilon \mathcal{H}(y, x) \end{cases}$$

where  $\epsilon$  is a small positive number. The smaller  $\epsilon$  is, the less interactions change the post-interaction states; consequently the smaller  $\epsilon$  is, the larger the time scale will be. Indeed, we need to scale the time as  $\tau := \frac{\epsilon}{2}t$ . In this way we pass from the characteristic  $t$ -scale of single microscopic interactions to a larger time scale defined by the variable  $\tau$ . Moreover, we define  $g(\tau, x) :=$

---

$f(2\tau/\epsilon, x)$ ; hence, while doing the limit for  $\epsilon \rightarrow 0^+$ , which is called quasi-invariant interaction limit, we will study the asymptotic behaviour of the distribution function  $f(t, x)$ .

As a consequence of the scaling, the weak form of the Boltzmann equation results

$$\frac{d}{d\tau} \left[ \int_{\mathbb{R}} \varphi(x) g(\tau, x) dx \right] = \frac{1}{\epsilon} \int_{\mathbb{R}} \int_{\mathbb{R}} [\varphi(x') + \varphi(y') - \varphi(x) - \varphi(y)] g(\tau, x) g(\tau, y) dx dy \quad (3.22)$$

and

$$\begin{cases} x' - x = \epsilon \mathcal{K}(x, y) \\ y' - y = \epsilon \mathcal{H}(y, x) \end{cases} \xrightarrow{\epsilon \rightarrow 0^+} \begin{cases} x' - x \rightarrow 0^+ \\ y' - y \rightarrow 0^+. \end{cases}$$

Since  $x' - x$  and  $y' - y$  are infinitesimal quantities, if the function  $\varphi$  is sufficiently regular then also

$$\begin{cases} \varphi(x') - \varphi(x) \rightarrow 0^+ \\ \varphi(y') - \varphi(y) \rightarrow 0^+. \end{cases}$$

Hence, we require that  $\varphi \in C^\infty(\mathbb{R})$  and  $\varphi(x) \rightarrow 0$  when  $|x| \rightarrow \infty$ , so that  $\varphi \in C_c^\infty(\mathbb{R}) = D(\mathbb{R})$ . Under these hypothesis we can compute a third-order Taylor expansion of  $\varphi$  around  $x$

$$\begin{aligned} \varphi(x') - \varphi(x) &= \varphi'(x)(x' - x) + \frac{1}{2}\varphi''(x)(x' - x)^2 + \frac{1}{6}\varphi'''(\bar{x})(x' - x)^3 \\ \varphi(y') - \varphi(y) &= \varphi'(y)(y' - y) + \frac{1}{2}\varphi''(y)(y' - y)^2 + \frac{1}{6}\varphi'''(\bar{y})(y' - y)^3 \end{aligned} \quad (3.23)$$

with

$$\begin{aligned} \bar{x} &\in (\min(x, x'), \max(x, x')) \\ \bar{y} &\in (\min(y, y'), \max(y, y')) \end{aligned}$$

where  $\varphi'(x)$  and  $\varphi'(y)$  denote the space derivatives.

---

Now we substitute (3.23) in Eq.(3.22), and we obtain

$$\begin{aligned}
\frac{d}{d\tau} \left[ \int_{\mathbb{R}} \varphi(x) g(\tau, x) dx \right] &= \underbrace{\frac{1}{\epsilon} \int_{\mathbb{R}} \int_{\mathbb{R}} \varphi'(x) (x' - x) g(\tau, x) g(\tau, y) dx dy}_{\text{I}} + \\
&+ \underbrace{\frac{1}{\epsilon} \int_{\mathbb{R}} \int_{\mathbb{R}} \varphi'(y) (y' - y) g(\tau, x) g(\tau, y) dx dy}_{\text{II}} + \\
&+ \underbrace{\frac{1}{2\epsilon} \int_{\mathbb{R}} \int_{\mathbb{R}} \varphi''(x) (x' - x)^2 g(\tau, x) g(\tau, y) dx dy}_{\text{III}} + \\
&+ \underbrace{\frac{1}{2\epsilon} \int_{\mathbb{R}} \int_{\mathbb{R}} \varphi''(y) (y' - y)^2 g(\tau, x) g(\tau, y) dx dy}_{\text{IV}} + \\
&+ \underbrace{\frac{1}{6\epsilon} \int_{\mathbb{R}} \int_{\mathbb{R}} \varphi'''(\bar{x}) (x' - x)^3 g(\tau, x) g(\tau, y) dx dy}_{\text{V}} + \\
&+ \underbrace{\frac{1}{6\epsilon} \int_{\mathbb{R}} \int_{\mathbb{R}} \varphi'''(\bar{y}) (y' - y)^3 g(\tau, x) g(\tau, y) dx dy}_{\text{VI}}
\end{aligned} \tag{3.24}$$

where

$$\begin{aligned}
\text{I} &= \frac{1}{\epsilon} \int_{\mathbb{R}} \int_{\mathbb{R}} \varphi'(x) \epsilon \mathcal{K}(x, y) g(\tau, x) g(\tau, y) dx dy \\
&= \int_{\mathbb{R}} \int_{\mathbb{R}} \varphi'(x) \mathcal{K}(x, y) g(\tau, x) g(\tau, y) dx dy \\
\text{II} &= \frac{1}{\epsilon} \int_{\mathbb{R}} \int_{\mathbb{R}} \varphi'(y) \epsilon \mathcal{H}(y, x) g(\tau, x) g(\tau, y) dx dy \\
&= \int_{\mathbb{R}} \int_{\mathbb{R}} \varphi'(y) \mathcal{H}(y, x) g(\tau, x) g(\tau, y) dx dy \\
\text{III} &= \frac{1}{2\epsilon} \int_{\mathbb{R}} \int_{\mathbb{R}} \varphi''(x) \epsilon^2 \mathcal{K}(x, y)^2 g(\tau, x) g(\tau, y) dx dy \\
&= \frac{\epsilon}{2} \int_{\mathbb{R}} \int_{\mathbb{R}} \varphi''(x) \mathcal{K}(x, y)^2 g(\tau, x) g(\tau, y) dx dy \\
\text{IV} &= \frac{1}{2\epsilon} \int_{\mathbb{R}} \int_{\mathbb{R}} \varphi''(y) \epsilon^2 \mathcal{H}(y, x)^2 g(\tau, x) g(\tau, y) dx dy \\
&= \frac{\epsilon}{2} \int_{\mathbb{R}} \int_{\mathbb{R}} \varphi''(y) \mathcal{H}(y, x)^2 g(\tau, x) g(\tau, y) dx dy
\end{aligned}$$


---

$$\begin{aligned}
V &= \frac{1}{6\epsilon} \int_{\mathbb{R}} \int_{\mathbb{R}} \varphi'''(\bar{x}) \epsilon^3 \mathcal{K}(x, y)^3 g(\tau, x) g(\tau, y) dx dy \\
&= \frac{\epsilon^2}{6} \int_{\mathbb{R}} \int_{\mathbb{R}} \varphi'''(\bar{x}) \mathcal{K}(x, y)^3 g(\tau, x) g(\tau, y) dx dy \\
VI &= \frac{1}{6\epsilon} \int_{\mathbb{R}} \int_{\mathbb{R}} \varphi'''(\bar{y}) \epsilon^3 \mathcal{H}(y, x)^3 g(\tau, x) g(\tau, y) dx dy \\
&= \frac{\epsilon^2}{6} \int_{\mathbb{R}} \int_{\mathbb{R}} \varphi'''(\bar{y}) \mathcal{H}(y, x)^3 g(\tau, x) g(\tau, y) dx dy.
\end{aligned}$$

If we substitute these results in Eq.(3.24), we obtain

$$\begin{aligned}
\frac{d}{d\tau} \left[ \int_{\mathbb{R}} \varphi(x) g(\tau, x) dx \right] &= \int_{\mathbb{R}} \varphi'(x) \left[ \int_{\mathbb{R}} \mathcal{K}(x, y) g(\tau, y) dy \right] g(\tau, x) dx + \\
&\quad + \int_{\mathbb{R}} \varphi'(y) \left[ \int_{\mathbb{R}} \mathcal{H}(y, x) g(\tau, y) dy \right] g(\tau, x) dx + R(\epsilon)
\end{aligned}$$

where

$$\begin{aligned}
R(\epsilon) &= \frac{\epsilon}{2} \int_{\mathbb{R}} \int_{\mathbb{R}} \varphi''(x) \mathcal{K}(x, y)^2 g(\tau, x) g(\tau, y) dx dy + \\
&\quad + \frac{\epsilon}{2} \int_{\mathbb{R}} \int_{\mathbb{R}} \varphi''(y) \mathcal{H}(y, x)^2 g(\tau, x) g(\tau, y) dx dy + \\
&\quad + \frac{\epsilon^2}{6} \int_{\mathbb{R}} \int_{\mathbb{R}} \varphi'''(\bar{x}) \mathcal{K}(x, y)^3 g(\tau, x) g(\tau, y) dx dy + \\
&\quad + \frac{\epsilon^2}{6} \int_{\mathbb{R}} \int_{\mathbb{R}} \varphi'''(\bar{y}) \mathcal{H}(y, x)^3 g(\tau, x) g(\tau, y) dx dy.
\end{aligned}$$

When we compute the quasi-invariant interaction limit, it is easy to notice that  $R(\epsilon) \rightarrow 0$ ; so, Eq.(3.24) becomes

$$\begin{aligned}
\frac{d}{d\tau} \left[ \int_{\mathbb{R}} \varphi(x) g(\tau, x) dx \right] &= \int_{\mathbb{R}} \varphi'(x) \left[ \int_{\mathbb{R}} \mathcal{K}(x, y) g(\tau, y) dy \right] g(\tau, x) dx + \\
&\quad + \int_{\mathbb{R}} \varphi'(y) \left[ \int_{\mathbb{R}} \mathcal{H}(y, x) g(\tau, y) dy \right] g(\tau, x) dx.
\end{aligned} \tag{3.25}$$

It is worth mentioning that it is possible to relax the hypothesis on the test function  $\varphi$ . Indeed, it is necessary to require only that  $\varphi \in C^3(\mathbb{R})$ , with  $\varphi, \varphi' \rightarrow 0$  when  $|x| \rightarrow \infty$ .

The next step consists in deriving the strong form of Eq.(3.25). Thus, we

compute an integration by parts on Eq.(3.25), and we obtain

$$\begin{aligned}
\int_{\mathbb{R}} \varphi(x) \frac{\partial}{\partial t} g(\tau, x) dx &= \varphi(x) \left[ \int_{\mathbb{R}} \mathcal{K}(x, y) g(\tau, y) dy \right] g(\tau, x) \Big|_{-\infty}^{\infty} + \\
&\quad - \varphi(x) \int_{\mathbb{R}} \frac{\partial}{\partial x} \left[ g(\tau, x) \int_{\mathbb{R}} \mathcal{K}(x, y) g(\tau, y) dy \right] dx + \\
&\quad + \varphi(y) \left[ \int_{\mathbb{R}} \mathcal{H}(y, x) g(\tau, y) dy \right] g(\tau, x) \Big|_{-\infty}^{\infty} + \\
&\quad - \varphi(y) \int_{\mathbb{R}} \frac{\partial}{\partial y} \left[ g(\tau, x) \int_{\mathbb{R}} \mathcal{H}(y, x) g(\tau, y) dy \right] dx
\end{aligned} \tag{3.26}$$

but due to the hypothesis on  $\varphi$ , Eq.(3.26) becomes

$$\begin{aligned}
\int_{\mathbb{R}} \varphi(x) \frac{\partial}{\partial t} g(\tau, x) dx &= - \varphi(x) \int_{\mathbb{R}} \frac{\partial}{\partial x} \left[ g(\tau, x) \int_{\mathbb{R}} \mathcal{K}(x, y) g(\tau, y) dy \right] dx + \\
&\quad - \underbrace{\varphi(y) \int_{\mathbb{R}} \frac{\partial}{\partial y} \left[ g(\tau, x) \int_{\mathbb{R}} \mathcal{H}(y, x) g(\tau, y) dy \right] dx}_{\text{I}}.
\end{aligned} \tag{3.27}$$

Moreover

$$\begin{aligned}
\text{I} &= -\varphi(y) \int_{\mathbb{R}} \frac{\partial}{\partial y} \left[ g(\tau, x) \int_{\mathbb{R}} \mathcal{H}(y, x) g(\tau, y) dy \right] dx \\
&= -\varphi(y) \int_{\mathbb{R}} \frac{\partial}{\partial y} \left[ g(\tau, x) \int_{\mathbb{R}} v_d g(\tau, y) dy \right] dx \\
&= -\varphi(y) v_d \int_{\mathbb{R}} g(\tau, x) dx \frac{\partial}{\partial y} \left[ \int_{\mathbb{R}} g(\tau, y) dy \right] \\
&= 0
\end{aligned}$$

hence Eq.(3.27) becomes

$$\int_{\mathbb{R}} \varphi(x) \left[ \frac{\partial}{\partial \tau} g(\tau, x) + \frac{\partial}{\partial x} \left[ g(\tau, x) \int_{\mathbb{R}} \mathcal{K}(x, y) g(\tau, y) dy \right] \right] dx = 0. \tag{3.28}$$

Since Eq.(3.28) holds  $\forall \varphi$ , we get

$$\frac{\partial}{\partial \tau} g(\tau, x) + \frac{\partial}{\partial x} \left[ g(\tau, x) \int_{\mathbb{R}} \mathcal{K}(x, y) g(\tau, y) dy \right] = 0 \tag{3.29}$$

which is the so-called Fokker-Planck equation. Eq.(3.29) holds for large time, thus it allows us to derive the asymptotic distribution of pedestrian positions

---

over the footbridge. It is noteworthy that Eq.(3.29) is a differential equation and not an integro-differential equation like the Boltzmann one; consequently it is more manageable. It is also noticeable that the interaction function  $\mathcal{K}(x, y)$  is still in the equation, confirming that the dependence on the dynamics at the microscopic scale remains also under the assumption of large time.

The term

$$g(\tau, x) \int_{\mathbb{R}} \mathcal{K}(x, y) g(\tau, y) dy$$

takes the name of mean-field interaction term. Therefore, for large time we do not speak anymore of binary interactions, but instead we have a kind of mean interaction among the pedestrian with state  $x$  and all others with which he/she interacts.

If we define

$$\mathcal{P}[g, g](\tau, x) = -\frac{\partial}{\partial x} \left[ g(\tau, x) \int_{\mathbb{R}} \mathcal{K}(x, y) g(\tau, y) dy \right]$$

as the Fokker-Planck operator, we can write Eq.(3.29) in an operatorial form

$$\partial_{\tau} g(\tau, x) = \mathcal{P}[g, g](\tau, x). \quad (3.30)$$

Also in this context, the main advantage of Eq.(3.30) respect to Eq.(3.19) relies in an easier numerical implementation, but on the other hand we need to add more hypothesis on the solution, like the differentiability.

In the next section we will introduce the macroscopic model and we will study in more detail Eq.(3.29).

### 3.3 The macroscopic crowd model

In the microscopic model used, the state of each pedestrian is described by only one variable, which is the pedestrian position. Thus, the macroscopic model is governed by the Fokker-Planck equation (3.29) and therefore there is no necessity to compute the so-called hydrodynamic limit. Indeed, since we use a first-order microscopic model, we expect that also the macroscopic model is a first-order one; hence, it must be composed by only one equation which states the mass conservation, without any additional law regarding the momentum conservation.

---

For the sake of simplicity, in the following we will denote the time again with  $t$  and not  $\tau$ ; therefore we write the Fokker-Planck equation derived in the previous section as

$$\frac{\partial}{\partial t}g(t, x) + \frac{\partial}{\partial x} \left[ g(t, x) \int_{\mathbb{R}} \mathcal{K}(x, y)g(t, y)dy \right] = 0 \quad (3.31)$$

where

$$v[g](t, x) = \int_{\mathbb{R}} \mathcal{K}(x, y)g(t, y)dy$$

$$F[g](t, x) = g(t, x)v[g](t, x)$$

represent respectively the pedestrian velocity field and the pedestrian flow. Hence, Eq.(3.31) can be written as

$$\frac{\partial}{\partial t}g(t, x) + \frac{\partial}{\partial x}F[g](t, x) = 0$$

which is a transport equation of the quantity  $g$ , with  $v[g]$  as a velocity field.

We would like to identify the distribution function  $g(t, x)$  with the pedestrian density  $\rho(t, x)$ , so that  $g(t, x) = \rho(t, x)$ . By definition, the density of a certain quantity is its mass per unit volume (per unit length in this work), so

$$\int_{\mathbb{R}} \rho(t, x)dx = M(t)$$

where  $M(t)$  is the total mass of the system. In this context  $\rho(t, x)$  is the pedestrian density per unit length, and due to the fact that the property of mass conservation holds, we have

$$\frac{dM(t)}{dt} = 0 \quad \Rightarrow \quad M(t) = M = \text{const}$$

so

$$\int_{\mathbb{R}} \rho(t, x)dx = M$$

thus, the pedestrian density becomes a probability density distribution only if we assume that the total mass of the system is  $M = 1$ . In this case  $\rho(t, x)$  has the same meaning of  $g(t, x)$ , and so  $g(t, x) = \rho(t, x)$ .

---

By recalling Eq.(3.10), the mean-field interaction term can be written as

$$\begin{aligned} \int_{\mathbb{R}} \mathcal{K}(x, y) \rho(t, y) dy &= \int_{\mathbb{R}} \left[ v_d - \eta(R - |x - y|) \mathbb{1}_{[x, x+R]}(y - x) \right] \rho(t, y) dy \\ &= v_d \int_{\mathbb{R}} \rho(t, y) dy - \int_x^{x+R} \eta(R - |x - y|) \rho(t, y) dy \\ &= v_d - \int_{\mathbb{R}} K(x, y) \rho(t, y) dy \end{aligned}$$

where

$$K(x, y) = \eta(R - |x - y|) \mathbb{1}_{[x, x+R]}(y - x)$$

is the interaction kernel. Hence, the macroscopic crowd model becomes

$$\begin{cases} \frac{\partial}{\partial t} \rho(t, x) + \frac{\partial}{\partial x} \left[ \rho(t, x) \left[ v_d - \int_{\mathbb{R}} K(x, y) \rho(t, y) dy \right] \right] = 0 & \text{in } \Omega \times (0, T] \\ \rho(t, 0) = \rho(t, L) & \text{in } \partial\Omega \times (0, T] \\ \rho(0, x) = \rho_0(x) & \text{in } \Omega \end{cases} \quad (3.32)$$

where  $\Omega = [0, L]$  is the domain,  $L > 0$  is the length of the footbridge,  $T > 0$  is a certain final time and  $\rho_0(x)$  is the initial condition. At the boundaries we set periodic conditions, so that a pedestrian who goes out of the footbridge enters immediately again; basically we are assuming that the density in  $x = 0$  and in  $x = L$  takes the same value. Firstly, this choice satisfies the mass conservation, and secondly, it allows us to study the pedestrian motion after a transition phase. In chapter 4 it will be shown how to discretize Eq.(3.32), in order to solve it numerically.

Obviously, Eq.(3.32) is valid only if  $M = 1$ , so if  $\rho(t, x)$  is a probability density function. Otherwise, the equation which describes the motion on a macroscopic scale is different and it will be derived in the following. We define

$$\rho^*(t, x) := M \rho(t, x) \quad (3.33)$$

so that

$$\int_{\Omega} \rho^*(t, x) dx = M \int_{\Omega} \rho(t, x) dx = M.$$


---

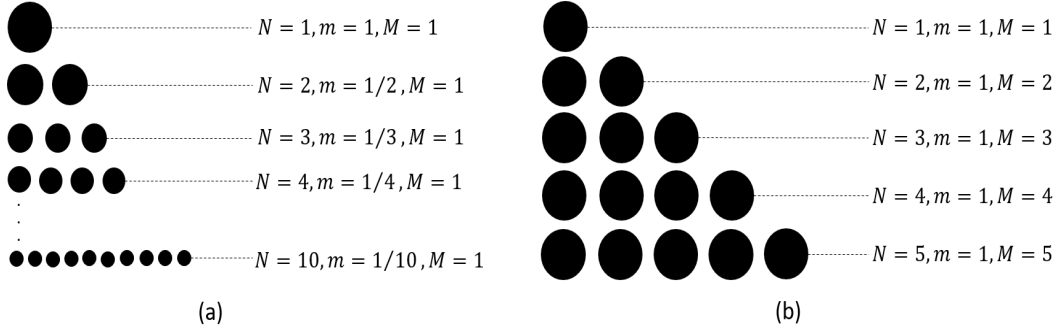


Figure 3.4: In (a) the total mass  $M$  of the system is constant while the mass  $m$  of each pedestrian becomes infinitesimal as  $N$  increases. In (b) the mass  $m$  of each pedestrian is constant while  $M$  grows when  $N$  increases.

By using definition (3.33), Eq.(3.32) becomes

$$\begin{aligned} \frac{1}{M} \frac{\partial}{\partial t} \rho^*(t, x) + \frac{\partial}{\partial x} \left[ \frac{\rho^*(t, x)}{M} v \left[ \frac{\rho^*}{M} \right] (t, x) \right] &= 0 \\ \frac{\partial}{\partial t} \rho^*(t, x) + \frac{\partial}{\partial x} \left[ \rho^*(t, x) v \left[ \frac{\rho^*}{M} \right] (t, x) \right] &= 0 \end{aligned}$$

where

$$\begin{aligned} v \left[ \frac{\rho^*}{M} \right] (t, x) &= \int_{\mathbb{R}} K(x, y) \frac{\rho^*(t, x)}{M} dy \\ &= \frac{1}{M} \int_{\mathbb{R}} K(x, y) \rho^*(t, x) dy \\ &= \frac{1}{M} v[\rho^*](t, x). \end{aligned}$$

Thus, when  $M \neq 1$  and consequently  $\rho(t, x)$  is not a probability density function, the macroscopic model results as

$$\begin{cases} \left[ \frac{\partial}{\partial t} \rho^*(t, x) + \frac{1}{M} \frac{\partial}{\partial x} \left[ \rho^*(t, x) \left[ v_d - \int_{\mathbb{R}} K(x, y) \rho^*(t, y) dy \right] \right] \right] = 0 & \text{in } \Omega \times (0, T] \\ \rho^*(t, 0) = \rho^*(t, L) & \text{in } \partial\Omega \times (0, T] \\ \rho^*(0, x) = \rho_0^*(x) & \text{in } \Omega \end{cases} \quad (3.34)$$

which is equal to (3.32) in case of  $M = 1$ .

The main difference between models (3.32) and (3.34) is well represented in Fig.(3.4). Let's define the total mass of the system  $M$ , the number of pedestrians  $N$  and the mass of each single pedestrian  $m$ ; consequently  $M =$

$mN$ . In model (3.32) we are assuming  $M = 1$ , which implies that the mass of each pedestrian becomes infinitesimal as  $N$  grows; this situation is represented in graph (a). In model (3.34) we are assuming that pedestrians have a certain mass  $m = 1$ , hence  $M = N$ ; this situation is represented in graph (b).

In the following, we will always refer to model (3.32), since it is preferable to work under hypothesis that  $\rho(t, x)$  is a probability density function.

### 3.4 Equivalence of crowd models

We state that there is equivalence between crowd models if the macroscopic crowd model is a generalization of the microscopic one, and if their terms have the same physical meaning. The chosen microscopic crowd model and the derived macroscopic one are respectively

$$\begin{aligned} \frac{d}{dt}x_i(t) &= v_d - \frac{1}{N} \sum_{\substack{j=1 \\ j \neq i}}^N \eta(R - |x_i(t) - x_j(t)|) \mathbb{1}_{[x_i, x_i+R]}(x_j(t) - x_i(t)) \\ \frac{\partial}{\partial t} \rho(t, x) &= -\frac{\partial}{\partial x} \left[ \rho(t, x) \left[ v_d - \int_x^{x+R} \eta(R - |x - y|) \rho(t, y) dy \right] \right] \end{aligned}$$

and we can immediately see the similarity. Indeed, in both cases there is a time derivative and a term which expresses the will of pedestrians to walk at a desired velocity  $v_d$ . Moreover, also the interaction term takes a similar form. In fact, if we assume that  $\rho(t, x)$  is a discrete distribution given by a sum of Dirac delta functions

$$\rho(t, x) = \frac{1}{N} \sum_{i=1}^N \delta(x - x_i)$$

and we substitute it in the mean-field interaction term, we obtain

$$\begin{aligned} \int_x^{x+R} \eta(R - |x - y|) \rho(t, y) dy &= \int_x^{x+R} \eta(R - |x - y|) \frac{1}{N} \sum_{i=1}^N \delta(y - x_i) dy \\ &= \frac{1}{N} \sum_{i=1}^N \eta \int_x^{x+R} (R - |x - y|) \delta(y - x_i) dy \\ &= \frac{1}{N} \sum_{\substack{j=1 \\ j \neq i}}^N \eta(R - |x_i - x_j|) \mathbb{1}_{[x_i, x_i+R]}(x_j - x_i) \end{aligned}$$


---

which is the interaction term of the microscopic crowd model. A further confirmation of the congruence between these two models is given by the following fact: in the macroscopic context the velocity  $v[\rho](t, x)$  is given only when the density  $\rho(t, x)$  is known; in the microscopic context the velocities  $v_i(t), i = 1, \dots, N$  are given only when the pedestrian positions  $x_i(t), i = 1, \dots, N$  are known. Therefore, the pedestrian density at the macroscopic scale plays the role of an equivalent pedestrian position descriptor.

Thanks to these considerations, we can state that the two models describe the same dynamics and consequently they may be considered as equivalent models. Indeed, we can mathematically define the microscopic and macroscopic crowd models above discussed as equivalent only when the solution of the microscopic model converges for  $N \rightarrow \infty$  to the solution of the macroscopic one in  $W_1$  sense, where  $W_1$  represents the Wasserstein metric.

In chapter 4 both models will be solved numerically, by looking for an equivalence in the solutions provided. Moreover, also the Wasserstein metric, which is introduced in the next paragraph, will be numerically evaluated.

### 3.4.1 Wasserstein metric

In the previous section we discussed about a possible equivalence between the microscopic and macroscopic crowd models, but we do not prove it yet. Indeed, we would expect that if we use the microscopic model with large  $N$ , its solution will have the same trend of the macroscopic one. But the hypothesis of large  $N$  is not physically correct in a footbridge vertical vibrations problem. Thus, we would like to derive a number  $N^*$  of pedestrians such that the distance between the discrete and continuous solution is under a certain tolerance  $\epsilon > 0$ . We will now analyse how to evaluate such a distance.

We suppose to have two probability density functions  $h(t, x)$  and  $s(t, x)$ , so

$$\int_{\Omega} h(t, x) dx = \int_{\Omega} s(t, x) dx = 1, \quad \forall t$$

$$h(t, x), s(t, x) \geq 0 \quad \forall x \in \Omega, \forall t$$

represented in graph (a) of Fig.(3.5);  $\Omega \subseteq \mathbb{R}$  is the domain over which  $h(t, x)$  and  $s(t, x)$  are distributed. For the sake of simplicity, we will consider time independent probability density functions, thus  $h(t, x) = h(x)$

---

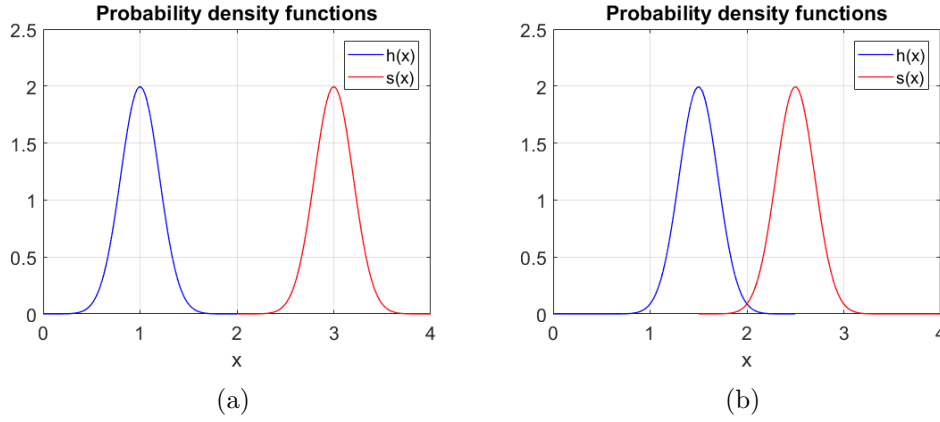


Figure 3.5:  $h(x)$  and  $s(x)$  are two normal probability distributions with  $\sigma = 0.2$ ,  $\mu_h = 1$  and  $\mu_s = 3$  in (a), and with  $\sigma = 0.2$ ,  $\mu_h = 1.5$  and  $\mu_s = 2.5$  in (b).

and  $s(t, x) = s(x)$ ; by the way, the following calculus hold also for time dependent probability density functions.

We would like to evaluate the distance between this two distributions. For instance, we can select the  $L^1(\Omega)$  norm, so that

$$\|h(x) - s(x)\|_{L^1(\Omega)} = \int_{\Omega} |h(x) - s(x)| dx$$

but it has a problem. Indeed, if we have two probability density functions as  $h(x)$  and  $s(x)$ , which are sharp peaked functions, then

$$\|h(x) - s(x)\|_{L^1(\Omega)} \simeq 2$$

because the supports mostly do not intersect. In graph (b) of Fig.(3.5) the distributions  $h(x)$  and  $s(x)$  are represented again, but now their supports are nearer. Since  $h(x)$  and  $s(x)$  are very sharp peaked functions, their supports continue to be only weakly intersected and therefore  $\|h(x) - s(x)\|_{L^1(\Omega)} \simeq 2$ . Hence, the  $L^1$  norm is not able to catch the difference between configuration (a) and (b) in Fig.(3.5) and consequently we cannot use it in a transport-governed problem.

Instead, we have to introduce a new concept of distance able to capture the difference between the two configurations previously showed. For this reason we introduce the Wasserstein metric, amply explained in [3]. It is worth mentioning that this is a metric and not a norm. This metric is

defined as

$$W_p(h, s) = \left( \inf_{\pi \in \Pi(h, s)} \int_{\Omega} \int_{\Omega} |x - y|^p d\pi(x, y) \right)^{\frac{1}{p}} \quad (3.35)$$

where  $p \geq 1$ ,  $x, y \in \Omega$  and  $\Pi(h, s)$  denotes the collection of all measures on the product space  $\Omega \times \Omega$ , with marginals  $h(x)$  and  $s(y)$  on the first and second factors respectively. Therefore,  $\pi \in \Pi(h, s)$  is a generic probability measure on  $\Omega \times \Omega$  with  $h(x)$  as marginal in  $x$  and with  $s(y)$  as marginal in  $y$ , so

$$\begin{aligned} h(x) &= \int_{\Omega} \pi(x, y) dy \\ s(y) &= \int_{\Omega} \pi(x, y) dx. \end{aligned}$$

Of course it does not exist only one probability measure  $\pi$  which satisfies the properties above mentioned; among all measures  $\pi \in \Pi$ , it will be selected one that minimizes the quantity (3.35).

In Fig.(3.6) the product space  $\Omega \times \Omega$  is shown, and we assume to take a generic point  $(\bar{x}, \bar{y})$  in it. Since  $\pi \in \Pi$ , the marginal on  $x$  is  $h(x)$ , while the marginal on  $y$  is  $s(y)$ . Then we fix an infinitesimal mass  $h(x)dx$ , where  $dx$  is an infinitesimal interval with center  $\bar{x}$ . We would like to transport this infinitesimal mass in the interval  $dy$  centred in  $\bar{y}$ , and attributing it to the distribution  $d(y)$ . But this transport has a cost: the more  $\bar{x}$  is distant from  $\bar{y}$ , the higher the cost is. Therefore, the cost is strictly related to the distance. Basically, the distance between the distributions  $h(x)$  and  $s(y)$  corresponds to the minimum cost that it is necessary to pay for transferring the mass from  $h(x)$  to  $s(y)$ . This is how the Wasserstein metric works.

Thus, intuitively the Wasserstein metric  $W_p(h, s)$  will assume higher value in case (a) of Fig.(3.5) than in case (b), because when  $h(x)$  is nearer to  $s(y)$ , it costs less to make a mass transfer. Hence, this metric is able to capture the difference between configurations (a) and (b), and for this reason we will adopt it.

Now we have to understand how to compute it. It is possible to prove that this metric is a minimum more than an infimum. Therefore, if we choose  $p = 1$ , we have

$$W_1(h, s) = \min_{\pi \in \Pi(h, s)} \int_{\Omega} \int_{\Omega} |x - y| d\pi(x, y). \quad (3.36)$$

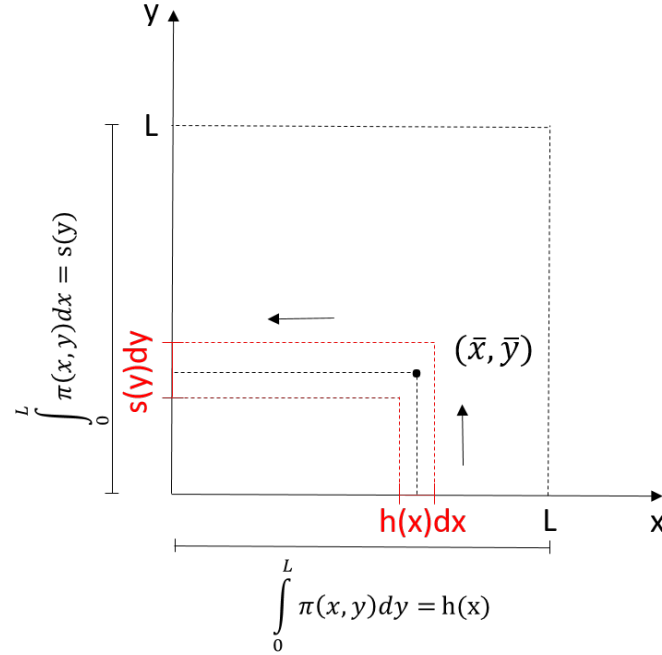


Figure 3.6: Graphical representation of how the Wasserstein metric operate.

In general, an exact value of  $W_1(h, s)$  can be obtained from (3.36) only if we use notions of linear programming. In case of we are working on a metric space  $X = \mathbb{R}$ , it is proved in [94] that the Wasserstein metric can be expressed as

$$W_1(h, s) = \int_{-\infty}^{\infty} |H(x) - S(x)| dx \quad (3.37)$$

where  $H(x)$  and  $S(x)$  are the distribution functions of the probability density distribution  $h(x)$  and  $s(x)$ , respectively. Hence, we can use Eq.(3.37) for measuring the distance between the two probability density distribution above-mentioned.

In the following, we will derive the expression of  $W_1(h, s)$  by assuming that  $h(x)$  is distributed accordingly to a uniform, and  $s(x)$  is a sum of Dirac delta functions, so

$$h(x) = \frac{1}{L} \mathbf{1}_{[0, L]}(x)$$

$$s(x) = \frac{1}{N} \sum_{i=1}^N \delta(x - x_i).$$

First of all, we have to derive the distribution functions, which are given by

$$H(x) = \int_{-\infty}^x h(y)dy, \quad S(x) = \int_{-\infty}^x s(y)dy$$

therefore

$$\begin{aligned} H(x) &= \int_{-\infty}^x \frac{1}{L} \mathbb{1}_{[0,L]}(y)dy \\ &= \begin{cases} 0 & \text{if } x \leq 0 \\ \frac{x}{L} & \text{if } 0 < x \leq L \\ 1 & \text{if } x > L \end{cases} \\ &= \frac{x}{L} \mathbb{1}_{[0,L]}(x) + \mathbb{1}_{[L,\infty]}(x) \end{aligned} \quad (3.38)$$

and

$$\begin{aligned} S(x) &= \int_{-\infty}^x \frac{1}{N} \sum_{i=1}^N \delta(y - x_i)dy \\ &= \frac{1}{N} \sum_{i=1}^N \int_{-\infty}^x \delta(y - x_i) \\ &= \frac{1}{N} \sum_{i=1}^N \mathbb{1}_{[x_i,\infty]}(x). \end{aligned} \quad (3.39)$$

By substituting relations (3.38) and (3.39) into Eq.(3.37), we obtain

$$W_1(h, s) = \int_{-\infty}^{\infty} \left| \frac{x}{L} \mathbb{1}_{[0,L]}(x) + \mathbb{1}_{[L,\infty]}(x) - \frac{1}{N} \sum_{i=1}^N \mathbb{1}_{[x_i,\infty]}(x) \right| dx \quad (3.40)$$

but

$$\begin{aligned} \mathbb{1}_{[L,\infty]}(x) - \frac{1}{N} \sum_{i=1}^N \mathbb{1}_{[x_i,\infty]}(x) &= \frac{1}{N} \sum_{i=1}^N \left( \mathbb{1}_{[L,\infty]}(x) - \mathbb{1}_{[x_i,\infty]}(x) \right) \\ &= -\frac{1}{N} \sum_{i=1}^N \mathbb{1}_{[x_i,L]}(x) \end{aligned} \quad (3.41)$$

hence, by replacing (3.41) into Eq.(3.40), we get

$$W_1(h, s) = \int_0^L \left| \frac{x}{L} - \frac{1}{N} \sum_{i=1}^N \mathbb{1}_{[x_i,L]}(x) \right| dx \quad (3.42)$$

but

$$\sum_{i=1}^N \mathbb{1}_{[x_i, L]}(x) = \begin{cases} 0 & \text{if } 0 \leq x < x_1 \\ 1 & \text{if } x_1 \leq x < x_2 \\ 2 & \text{if } x_2 \leq x < x_3 \\ \vdots & \\ N & \text{if } x_N \leq x < L \\ i & \text{if } x_i \leq x < x_{i+1} \\ 0 & \text{otherwise} \end{cases}$$

consequently Eq.(3.42) becomes

$$\begin{aligned} W_1(h, s) &= \int_0^{x_1} \left| \frac{x}{L} \right| dx + \sum_{i=1}^{N-1} \int_{x_i}^{x_{i+1}} \left| \frac{x}{L} - \frac{i}{N} \right| dx + \int_{x_N}^L \left| \frac{x}{L} - 1 \right| dx \\ &= \frac{x^2}{2L} \Big|_0^{x_1} + \sum_{i=1}^{N-1} \int_{x_i}^{x_{i+1}} \left| \frac{x}{L} - \frac{i}{N} \right| dx + x - \frac{x^2}{2L} \Big|_{x_N}^L \\ &= \frac{L}{2} + \frac{x_1^2}{2L} - x_N + \frac{x_N^2}{2L} + \sum_{i=1}^{N-1} \int_{x_i}^{x_{i+1}} \left| \frac{x}{L} - \frac{i}{N} \right| dx. \end{aligned} \quad (3.43)$$

In order to derive an analytical expression of the Wasserstein metric, we still have to compute the integral on the right-hand side of Eq.(3.43), which is given by

$$\begin{aligned} \int_{x_i}^{x_{i+1}} \left| \frac{x}{L} - \frac{i}{N} \right| dx &= \begin{cases} \int_{x_i}^{x_{i+1}} \left( \frac{x}{L} - \frac{i}{N} \right) dx & \text{if } \frac{x_i}{L} \geq \frac{i}{N} \\ \int_{x_i}^{\frac{iL}{N}} \left( \frac{i}{N} - \frac{x}{L} \right) dx + \int_{\frac{iL}{N}}^{x_{i+1}} \left( \frac{x}{L} - \frac{i}{N} \right) dx & \text{if } \frac{x_i}{L} < \frac{i}{N} \leq \frac{x_{i+1}}{L} \\ \int_{x_i}^{x_{i+1}} \left( \frac{i}{N} - \frac{x}{L} \right) dx & \text{if } \frac{i}{N} > \frac{x_{i+1}}{L} \end{cases} \\ &= \begin{cases} \frac{x_{i+1}^2 - x_i^2}{2L} + \frac{i}{N}(x_i - x_{i+1}) & \text{if } x_i \geq \frac{iL}{N} \\ \frac{i^2 L}{N^2} - \frac{i}{N}(x_i + x_{i+1}) + \frac{x_i^2 + x_{i+1}^2}{2L} & \text{if } x_i < \frac{iL}{N} \leq x_{i+1} \\ \frac{i}{N}(x_{i+1} - x_i) + \frac{x_i^2 - x_{i+1}^2}{2L} & \text{if } \frac{iL}{N} > x_{i+1} \end{cases} \end{aligned} \quad (3.44)$$

and by substituting (3.44) into Eq.(3.43) we obtain an analytical formula for computing  $W_1(h, s)$ .

---

Eq.(3.43) allows us to evaluate the distance between the probability density functions  $h(x)$  and  $s(x)$ . This result will be useful in chapter 4; indeed we will use it for evaluating the distance between the macroscopic and microscopic crowd model solutions.

Finally, let us suppose that pedestrians are evenly distributed in such a way

$$x_i = \frac{iL}{N}, \quad \forall i$$

then Eq.(3.43) becomes

$$\begin{aligned} W_1(h, s) &= \int_0^{\frac{L}{N}} \left| \frac{x}{L} \right| dx + \sum_{i=1}^{N-1} \int_{\frac{iL}{N}}^{\frac{(i+1)L}{N}} \left| \frac{x}{L} - \frac{i}{N} \right| dx + \int_L^L \left| \frac{x}{L} - 1 \right| dx \\ &= \frac{L}{2N^2} + \sum_{i=1}^{N-1} \left[ \frac{(i+1)^2 L}{2N^2} - \frac{i(i+1)L}{N^2} - \frac{i^2 L}{2N} + \frac{i^2 L}{N^2} \right] \\ &= \frac{L}{2N^2} + \sum_{i=1}^{N-1} \left[ \frac{L}{2N^2} + \frac{iL}{N^2} - \frac{iL}{N^2} \right] \\ &= \frac{L}{2N^2} + \frac{L(N-1)}{2N^2} \\ &= \frac{L}{2N} \end{aligned}$$

hence

$$W_1(h, s) \rightarrow 0, \quad N \rightarrow \infty.$$

Indeed, since the macroscopic model relies on the assumption that  $N \rightarrow \infty$ , we expect that for large value of  $N$  the microscopic crowd model solutions here denoted by  $s(x)$  tends to the macroscopic one denoted by  $h(x)$ ; consequently, their distance tends to zero

### 3.5 The structure model

For the reasons explained in section 2.5, the footbridge structure can be modelled with sufficient accuracy using a single degree of freedom modal equation for the mode of interest; consequently a second-order differential equation

$$m\ddot{y}(t) + c\dot{y}(t) + ky(t) = F(t) \tag{3.45}$$


---

governs the system. In Eq.(3.45),  $m$ ,  $k$  and  $c$  are respectively the modal mass, stiffness and damping of the footbridge, while  $y(t)$  is the displacement response at the antinode, the overdot indicating differentiation with respect to time. Moreover, the modal force  $F(t)$  takes into account only the pedestrian motion over the footbridge and it is computed with a model presented in the next paragraph. In chapter 4, Eq.(3.45) will be solved numerically.

The structure model is common over each scale. Hence, the vertical acceleration of the structure will be derived with the use of the same structure model, both for the microscopic and macroscopic scale.

## 3.6 The force model

In this section we will show how to evaluate the force exerted on the footbridge by walking pedestrians. Firstly, the force models on the microscopic and macroscopic scale will be deeply analysed; secondly, we will proof analytically that the macroscopic force model is a generalized form of the microscopic one.

### 3.6.1 The microscopic force model

For the scopes of this study, human-structure interaction is neglected. Therefore, pedestrian action is described by a moving force model. Among the several force models proposed in the literature, the same one used in [2] is adopted and described in the following. For the sake of simplicity, time dependence are omitted. The force exerted by the  $i$ -th pedestrian is modelled as a single sine function, and is given by

$$F_{micro,i}(t) = \alpha_i m_i g \sin(2\pi f_i t) \quad (3.46)$$

where the dynamic load factor  $\alpha_i$  is expressed as a function of the pacing frequency  $f_i$

$$\alpha_i = -0.2649 f_i^3 + 1.3206 f_i^2 - 1.7597 f_i + 0.7613 \quad (3.47)$$

and the pacing frequency  $f_i$  is expressed as a function of the pedestrian velocity  $v_i$

$$f_i = 0.35 v_i^3 - 1.59 v_i^2 + 2.93 v_i \quad (3.48)$$


---

Both relations (3.47) and (3.48) are given by data collected in experiments. Moreover, in Eq.(3.46)  $g$  is the acceleration due to gravity and  $m_i$  is the mass of the  $i$ -th pedestrian. Hence, the force exerted at time  $t$  is given by

$$\begin{aligned} F_{micro}(t) &= \frac{1}{N} \sum_{i=1}^N F_{micro,i}(t) \\ &= \frac{1}{N} \sum_{i=1}^N \alpha_i m_i g \sin(2\pi f_i t) \phi(x_i) \end{aligned} \quad (3.49)$$

where

$$\phi(x_i) = \sin\left(\frac{\pi x_i}{L}\right)$$

is the first mode of the footbridge. So,  $F_{micro}(t)$  is a medium force weighted over the first mode; therefore, pedestrians located in the middle span of the bridge excite more the structure than pedestrians located at the entrance or at the exit. Since the position  $x_i$  and the velocity  $v_i$  of each pedestrian are given by the microscopic crowd model, we are able to derive the force  $F_{micro}(t)$  at each time step.

In the macroscopic crowd model we are assuming that  $M = 1$ ; in order to be able to compare the results, also in the microscopic model we have to assume that the mass of each pedestrian becomes infinitesimal as  $N$  grows. Thus, the mass of each pedestrian is given by  $m_i/N$ , and for this reason the factor  $1/N$  is added in (3.49). Therefore, we will not obtain vertical acceleration value with physical meaning. In case of we are interested in the total force exerted on the footbridge by pedestrians with mass  $m_i$ , it is enough to compute  $\tilde{F}_{micro}(t) = N F_{micro}(t)$ .

### 3.6.2 The macroscopic force model

The macroscopic force model is derived from the microscopic one; therefore, the force exerted by pedestrians at time  $t$  is defined as

$$F_{macro}(t) = \int_{\Omega} h(t, x) \phi(x) \rho(t, x) dx \quad (3.50)$$

where  $\phi(x)$  is the first mode of the system and  $\rho(t, x)$  is the pedestrian density distribution given by the solution of the macroscopic crowd model.

---

The function  $h(t, x)$  is given by

$$h(t, x) = \alpha(t, x)g\sin(2\pi f(t, x)t)$$

where

$$\begin{aligned}\alpha(t, x) &= -0.2649f(t, x)^3 + 1.3206f(t, x)^2 - 1.7597f(t, x) + 0.7613 \\ f(t, x) &= 0.35v[\rho]^3 - 1.59v[\rho]^2 + 2.93v[\rho]\end{aligned}$$

so that everything is only function of the velocity field  $v[\rho](t, x)$ , which is known once that the macroscopic crowd model is solved.

The study is carried out with the assumption that  $\rho(t, x)$  is a probability density function, hence the mass of each pedestrian becomes infinitesimal as  $N$  grows. Consequently, also in this case we will not obtain vertical acceleration value with physical meaning. In the next paragraph we will analyse how to obtain values possibly comparable with experimental data present in literature.

### 3.6.3 Equivalence of force models

We state that there is equivalence between force models if the macroscopic force model is a generalization of the microscopic one and if the solution of the latter converges to the solution of the former for large  $N$ . In the following we will proof analytically and in chapter 4 numerically that the two models previously described are effectively equivalent.

In general  $\rho(t, x)$  can be whatever distribution, but if it becomes a discrete one, then the macroscopic force model should assume the same form of the microscopic one. Indeed, if we express  $\rho(t, x)$  as a sum of Dirac delta functions

$$\rho(t, x) = \frac{1}{N} \sum_{i=1}^N \delta(x - x_i)m_i$$


---

and we substitute it in the macroscopic force model (3.50), we obtain

$$\begin{aligned}
F_{macro}(t) &= \int_{\Omega} h(t, x) \phi(x) \frac{1}{N} \sum_{i=1}^N \delta(x - x_i) m_i dx \\
&= \frac{1}{N} \sum_{i=1}^N m_i g \int_{\Omega} \alpha(t, x) \sin(2\pi f(t, x)t) \phi(x) \delta(x - x_i) dx \\
&= \frac{1}{N} \sum_{i=1}^N \alpha(x_i) m_i g \sin(2\pi f(x_i)t) \phi(x_i) \\
&= \frac{1}{N} \sum_{i=1}^N \alpha_i m_i g \sin(2\pi f_i t) \phi(x_i) \\
&= F_{micro}(t)
\end{aligned}$$

hence  $F_{macro}(t) = F_{micro}(t)$ . Thus, we can state that the macroscopic force model is a generalization of the microscopic one, and therefore they may be equivalent. Of course, in order to mathematically prove the equivalence, we have to see if the solution provided by the microscopic force model converges to the one provided by the macroscopic model for large  $N$ . This analysis will be carried out in a numerical way in chapter 4.

Previously, we pointed out that the decision to perform the studies under the assumption that  $\rho(t, x)$  is a probability density function affects the vertical acceleration results. In both cases, if we want to obtain values comparable with data in literature, we have to operate in the following manner. We denote

$$\tilde{F}_{micro}(t) = \sum_{i=1}^N \alpha_i m_i g \sin(2\pi f_i t) \phi(x_i)$$

so that

$$\begin{aligned}
m\ddot{y}(t) + c\dot{y}(t) + ky(t) &= F_{micro}(t) \\
m\ddot{y}(t) + c\dot{y}(t) + ky(t) &= \frac{1}{N} \tilde{F}_{micro}(t) \\
m(N\ddot{y}(t)) + c(N\dot{y}(t)) + k(Ny(t)) &= \tilde{F}_{micro}(t)
\end{aligned}$$

and by defining  $z(t) = Ny(t)$ , we obtain

$$m\ddot{z}(t) + c\dot{z}(t) + kz(t) = \tilde{F}_{micro}(t). \quad (3.51)$$

Obviously, Eq.(3.51) holds also for  $F_{macro}(t)$ . So, if we would like to obtain vertical acceleration values possibly comparable with data in literature, we

---

have to display  $z(t)$ . As shown in Eq.(3.51), it is enough to multiply the vertical acceleration  $y(t)$  for the number of pedestrians  $N$  on the footbridge.



# Chapter 4

## Numerical results

In this chapter the numerical approach used for implementing all models studied in chapter 3 will be analysed. Moreover, numerical results are discussed.

In particular, in section 4.1 the method used for discretizing the macroscopic crowd model will be presented; the given solution and the results regarding the footbridge vertical acceleration will be discussed. In section 4.2 we will do a similar analysis concerning the microscopic scale. Finally, in section 4.3 the results will be compared.

### 4.1 Macroscopic model results

In chapter 3 we derived the macroscopic crowd model, that for simplicity is here reported

$$\begin{cases} \frac{\partial}{\partial t}\rho(t, x) + \frac{\partial}{\partial x} \left[ \rho(t, x) \left[ v_d - \int_{\mathbb{R}} K(x, y)\rho(t, y)dy \right] \right] = 0 & \text{in } \Omega \times (0, T] \\ \rho(t, 0) = \rho(t, L) & \text{in } \partial\Omega \times (0, T] \\ \rho(0, x) = \rho_0(x). & \text{in } \Omega \end{cases} \quad (4.1)$$

In this section we will provide a numerical solution of Eq.(4.1). This equation can be also written as

$$\begin{cases} \frac{\partial}{\partial t}\rho(t, x) + \frac{\partial}{\partial x}F[\rho](t, x) = 0 & \text{in } \Omega \times (0, T] \\ \rho(t, 0) = \rho(t, L) & \text{in } \partial\Omega \times (0, T] \\ \rho(0, x) = \rho_0(x) & \text{in } \Omega \end{cases} \quad (4.2)$$

where  $F[\rho] = \rho v[\rho]$ . It is evident that Eq.(4.2) is a conservation law, therefore the numeric implementation will be done with a finite volume method. As discussed in chapter 2, the choice of the numerical flux strongly affects the efficiency of this method. By using an example in which the exact solution is known, in the next paragraph we will compare different choices of numerical flux, and we will select a suitable one for our purposes.

#### 4.1.1 Burger's equation

In order to choose the most suitable numerical scheme for solving partial differential equation (4.1), some choice of numerical fluxes are tested on a non-linear hyperbolic model equation

$$\frac{\partial}{\partial t}\rho(t, x) + \frac{\partial}{\partial x}F[\rho](t, x) = 0 \quad (4.3)$$

with  $F[\rho] = \frac{1}{2}\rho^2$ . Eq.(4.3) is the so-called Burger's equation. Regarding the initial conditions, we will use a Heaviside function

$$\rho(x, 0) = \begin{cases} \rho_L & \text{if } x < 0.2 \\ \rho_R & \text{if } x > 0.2 \end{cases} \quad (4.4)$$

The analytical solution of Eq.(4.3) with initial condition (4.4) is known in two cases:  $\rho_L > \rho_R$  and  $\rho_L < \rho_R$ . In the first case, the discontinuity evolves as a shock wave, while in the second case we have an expansion fan. Both configurations are represented in Fig.(4.1), where every straight line is a characteristic line. More analytical details can be found in [97].

The one-dimensional domain  $\Omega = [0, L]$ , with  $L = 1$ , is discretized in space with intervals of length  $\Delta x = 1/320$ ; regarding the time step,  $\Delta t = 1/1000$  is used. Fig.(4.2) shows a comparison between the exact and approximate solutions at time  $t = 0.5$  s, obtained with different numerical schemes. The compared ones are the following:

- First-order Upwind scheme

$$\rho_j^{n+1} = \rho_j^n - \lambda \left[ \frac{1}{2} (\rho_j^n)^2 - \frac{1}{2} (\rho_{j-1}^n)^2 \right]$$

- Lax-Friedrichs scheme

$$\rho_j^{n+1} = \frac{1}{2} [\rho_{j+1}^n + \rho_{j-1}^n] - \frac{\lambda}{2} \left[ \frac{1}{2} (\rho_{j+1}^n)^2 - \frac{1}{2} (\rho_{j-1}^n)^2 \right]$$

- Lax-Wendroff scheme

$$\begin{aligned} \rho_j^{n+1} = & \rho_j^n - \frac{\lambda}{2} \left[ \frac{1}{2} (\rho_{j+1}^n)^2 - \frac{1}{2} (\rho_{j-1}^n)^2 \right] + \\ & + \frac{\lambda^2}{2} \left[ \frac{1}{2} (\rho_j^n + \rho_{j+1}^n) \left( \frac{1}{2} (\rho_{j+1}^n)^2 - \frac{1}{2} (\rho_j^n)^2 \right) + \right. \\ & \left. - \frac{1}{2} (\rho_j^n + \rho_{j-1}^n) \left( \frac{1}{2} (\rho_j^n)^2 - \frac{1}{2} (\rho_{j-1}^n)^2 \right) \right] \end{aligned}$$

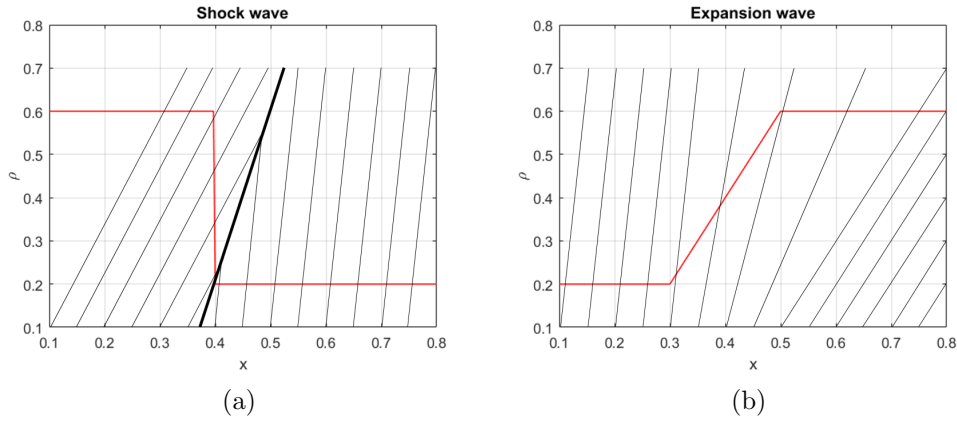


Figure 4.1: Discontinuity evolution with initial condition  $\rho_L = 0.6$ ,  $\rho_R = 0.2$  in (a) and  $\rho_L = 0.2$ ,  $\rho_R = 0.6$  in (b). In both graphs the solution is plotted at time  $t = 0.5$  s.

- MacCormack scheme

$$\begin{aligned} \rho_j^{n+1} = & \rho_j^n - \frac{\lambda}{4} \left[ (\rho_{j+1}^n)^2 - (\rho_j^n)^2 \right] - \frac{\lambda}{4} (\rho_j^n)^2 + \\ & - \frac{\lambda^3}{16} \left[ (\rho_{j+1}^n)^4 + (\rho_j^n)^4 - 2(\rho_{j+1}^n)^2 (\rho_j^n)^2 \right] + \frac{\lambda^2}{4} \rho_j^n \left[ (u_{j+1}^n)^2 - (u_j^n)^2 \right] + \\ & + \frac{\lambda}{4} (\rho_{j-1}^n)^2 + \frac{\lambda^3}{16} \left[ (\rho_j^n)^4 + (\rho_{j-1}^n)^4 - 2(\rho_j^n)^2 (\rho_{j-1}^n)^2 \right] + \\ & - \frac{\lambda^2}{4} \rho_{j-1}^n \left[ (u_j^n)^2 - (u_{j-1}^n)^2 \right] \end{aligned}$$

where  $\lambda = \Delta t / \Delta x$  and  $\rho_j^n$  is the cell average value in cell  $x_j = [x_{j-1/2}, x_{j+1/2}]$  at time  $t^n = n\Delta t$ .

As expected, first-order schemes show the well-known diffusive effect while second-order schemes show unphysical oscillations, especially upstream of the discontinuity. In particular, the Lax-Wendroff and the MacCormack scheme do not even satisfy the maximum principle, which means that if  $\rho(0, x) \in [\rho_{min}, \rho_{max}]$  for all  $x \in \Omega$ , then the numeric solution  $\rho(t, x) \notin [\rho_{min}, \rho_{max}]$ . Therefore, we will not use these schemes. Moreover, the use of an Upwind scheme requires to know which are the downwind and upwind points for each cell; in Eq.(4.1) this is a difficult task, hence we will not use this scheme.

In conclusion, the numerical scheme adopted for discretizing Eq.(4.1) is the Lax-Friedrichs one, even if it is more diffusive than an Upwind scheme.

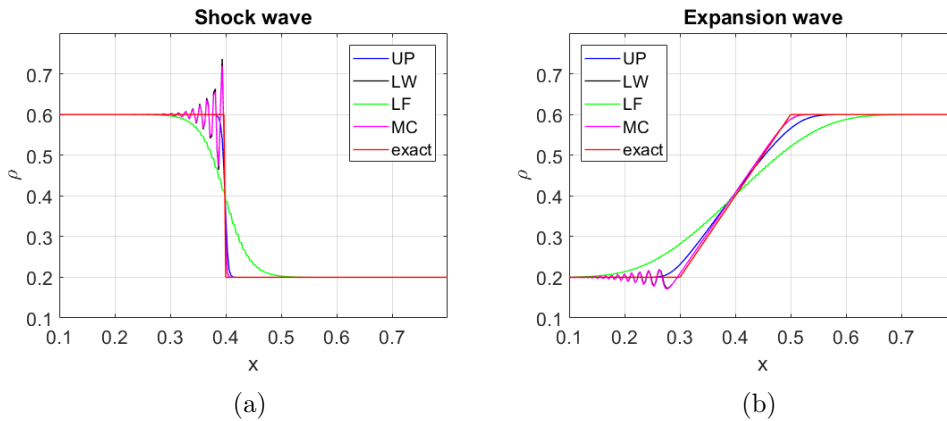


Figure 4.2: Comparison between the exact and approximate solutions of Burger's equation. In both graphs the solution is plotted at time  $t = 0.5$  s.

### 4.1.2 Crowd model

Once that the numerical scheme has been selected, we use it in order to solve numerically Eq.(4.1). In this context, the Lax-Friedrichs scheme can be also written as

$$\rho_j^{n+1} = \frac{1}{2}[\rho_{j+1}^n + \rho_{j-1}^n] - \frac{\lambda}{2} \left[ F[\rho_{j+1}^n] - F[\rho_{j-1}^n] \right] \quad (4.5)$$

hence, we need to evaluate the flux  $F$  in each cell average value. The pedestrian flow is given by

$$\begin{aligned} F[\rho](t, x) &= \rho(t, x)v[\rho](t, x) \\ &= \rho(t, x) \int_{\Omega} \mathcal{K}(x, y)\rho(t, y)dy \\ &= \rho(t, x) \left[ \int_{\Omega} v_d\rho(t, y)dy - \int_{\mathbb{R}} K(x, y)\rho(t, y)dy \right]. \end{aligned} \quad (4.6)$$

For using scheme (4.5), we have to derive the discrete form of flux (4.6). Let  $x_j = j\Delta x$  and  $t^n = n\Delta t$ , we have

$$\begin{aligned} F[\rho](t^n, x_j) &= \rho(t^n, x_j) \left[ \int_{\Omega} v_d\rho(t^n, y)dy - \int_{x_j}^{x_j+R} K(x_j, y)\rho(t^n, y)dy \right] \\ &= \rho(t^n, x_j) \left[ v_d \underbrace{\sum_{\substack{i \text{ s.t.} \\ 0 \leq y_i \leq L}} \rho(t^n, x_j)\Delta x}_{=1} - \sum_{\substack{i \text{ s.t.} \\ |y_i - x_j| \leq R}} K(x_j, y_i)\rho(t^n, y_i)\Delta x \right] \\ &= \rho(t^n, x_j) \left[ v_d - \sum_{\substack{i \text{ s.t.} \\ |y_i - x_j| \leq R}} \eta(R - |x_j - y_i|)\rho(t^n, x_j)\Delta x \right]. \end{aligned}$$

Since  $\rho(t^n, x_j) = \rho_j^n$ , then

$$\begin{aligned} F[\rho](t^n, x_j) &= F[\rho_j^n] \\ &= \rho_j^n \left[ v_d - \sum_{\substack{i \text{ s.t.} \\ |y_i - x_j| \leq R}} \eta(R - |x_j - y_i|)\rho_j^n\Delta x \right] \end{aligned} \quad (4.7)$$


---

and by substituting (4.7) in (4.5), we obtain

$$\begin{aligned} \rho_j^{n+1} = & \frac{1}{2} [\rho_{j+1}^n + \rho_{j-1}^n] - \frac{\lambda}{2} \left[ \rho_{j+1}^n \left[ v_d - \sum_{\substack{i \text{ s.t.} \\ |y_i - x_j| \leq R}} \eta(R - |x_j - y_i|) \rho_{j+1}^n \Delta x \right] + \right. \\ & \left. - \rho_{j-1}^n \left[ v_d - \sum_{\substack{i \text{ s.t.} \\ |y_i - x_j| \leq R}} \eta(R - |x_j - y_i|) \rho_{j-1}^n \Delta x \right] \right]. \end{aligned} \quad (4.8)$$

All quantities on the right-hand side of scheme (4.8) are known, therefore we can derive  $\rho_j^{n+1}$  and advance in time.

As previously mentioned, we use periodic boundary conditions, so that the mass conservation is fulfilled. Regarding the initial condition, we assume that  $\rho(0, x)$  is Beta-distributed over domain  $\Omega = [0, L]$ , so

$$\rho(0, x) = \frac{x^{\alpha-1}(L-x)^{\beta-1}}{B(\alpha, \beta)L^{\alpha+\beta-1}} \quad \text{in } \Omega$$

where we set in particular  $\alpha = \beta = 2$  and

$$B(\alpha, \beta) = \frac{\Gamma(\alpha)\Gamma(\beta)}{\Gamma(\alpha + \beta)} = \frac{\int_0^\infty x^{\alpha-1}e^{-x}dx \int_0^\infty x^{\beta-1}e^{-x}dx}{\int_0^\infty x^{\alpha+\beta-1}e^{-x}dx}.$$

In the mesoscopic model the state of each pedestrian is defined only by his/her position, therefore also in the macroscopic model the unique manner for distinguishing two pedestrians is by looking at their positions; thus, all quantities besides the position must be common for all members.

The desired velocity is assumed to be distributed as  $v_d \sim N(v_m, v_{std})$ ; moreover, we remind that it is assumed that during the whole walking a pedestrian does not change his/her preferred speed, hence  $v_d = \text{const}$ . The values of the other parameters are reported in Table (4.1);  $v_m$  and  $v_{std}$  are taken from experimental data, while  $L$  and  $R$  are inherent to our case study. In section 3.1 we stated that the value of the repulsion coefficient  $\eta$  is chosen such that the inequality

$$\eta \leq \frac{v_{max} - v_d}{R} = \eta^* \quad (4.9)$$

is satisfied, for taking into account the fact that a pedestrian cannot walk faster than a maximum velocity  $v_{max}$ .

---

By the way, we have also stated that inequality (4.9) is sufficient but not necessary. Indeed, for other choices of  $\eta$  such that  $\eta > \eta^*$  the velocity  $v[\rho](t, x)$  does not overcome the maximum value allowed and the dynamics of the model are unchanged; the unique difference is that the pedestrian density  $\rho(t, x)$  requires less time before to reach a steady constant value. The repulsion coefficient value used is reported in Table (4.1); with this choice, repulsion forces assume values with physical meaning and a steady state configuration is reached in reasonable time.

Parameter	$L$ [m]	$R$ [m]	$\eta$ [s <sup>-1</sup> ]	$v_m$ [ms <sup>-1</sup> ]	$v_{std}$ [ms <sup>-1</sup> ]
Value	100	2	20	1.34	0.24

Table 4.1: Parameter values used in numerical simulations.

The total number of cells used is  $J = 5000$ , therefore each cell has a length of  $\Delta x = [x_{j-1/2}, x_{j+1/2}] = 0.02$ , while the time step is  $\Delta t = 0.002$ .

The time evolution of the solution of the macroscopic crowd model is shown in Fig.(4.3). At the initial time, pedestrians in the second half of the footbridge have in front of them a lower pedestrian density with respect to the ones behind, thus they tend to walk faster. On the other hand, pedestrians in the first half of the footbridge have in front of them a higher pedestrian density with respect to the ones behind and so they tend to walk slower. Since periodic boundary conditions are used, pedestrians in the second half of the footbridge suddenly re-enter into it as time passes; therefore, we keep on having pedestrians that tend to walk faster than others, and as a result, a sort of discontinuity in the pedestrian density is formed, which is clearly visible in Fig.(4.3a). This sort of wave spreads over the domain, and it is relaxed over time, as Fig.(4.3d) shows. These dynamics are dictated by the repulsion forces among pedestrians, who constantly try to position themselves at a certain distance from neighbours. When this mechanism takes place, the result is that the pedestrian density  $\rho(t, x)$  becomes uniformly distributed over domain  $\Omega$ , as shown in Fig.(4.3f).

Moreover, in Fig.(4.4) the time evolution of the velocity field is shown. The trend is specular to the one of the density; indeed in regions of high pedestrian density, the velocity is lower while in regions of low pedestrian density, the velocity is higher. Consequently, a sort of discontinuity visible in Fig.(4.4a) is formed again, which is then relaxed over time, as shown in

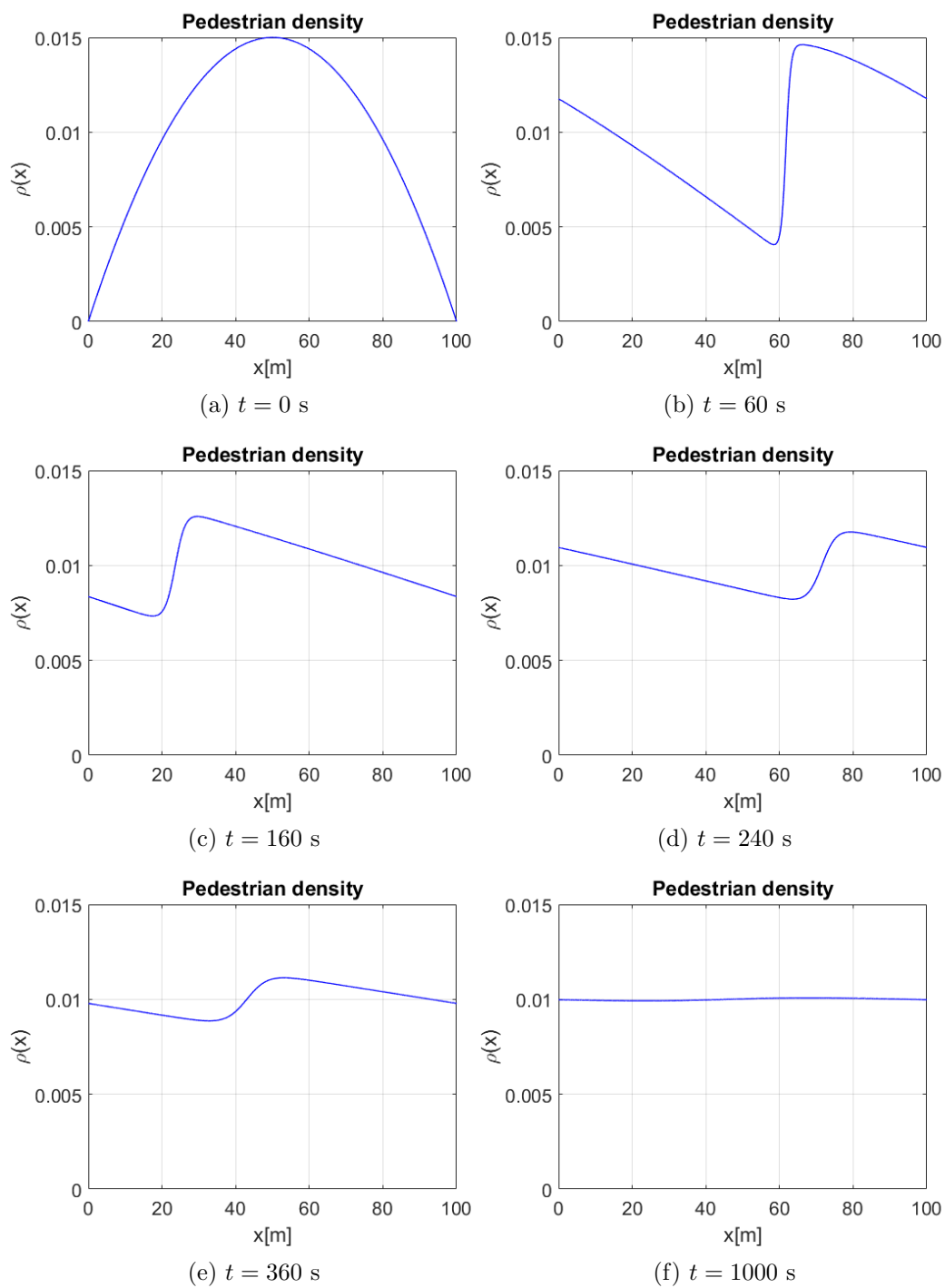


Figure 4.3: Time evolution of the pedestrian density.

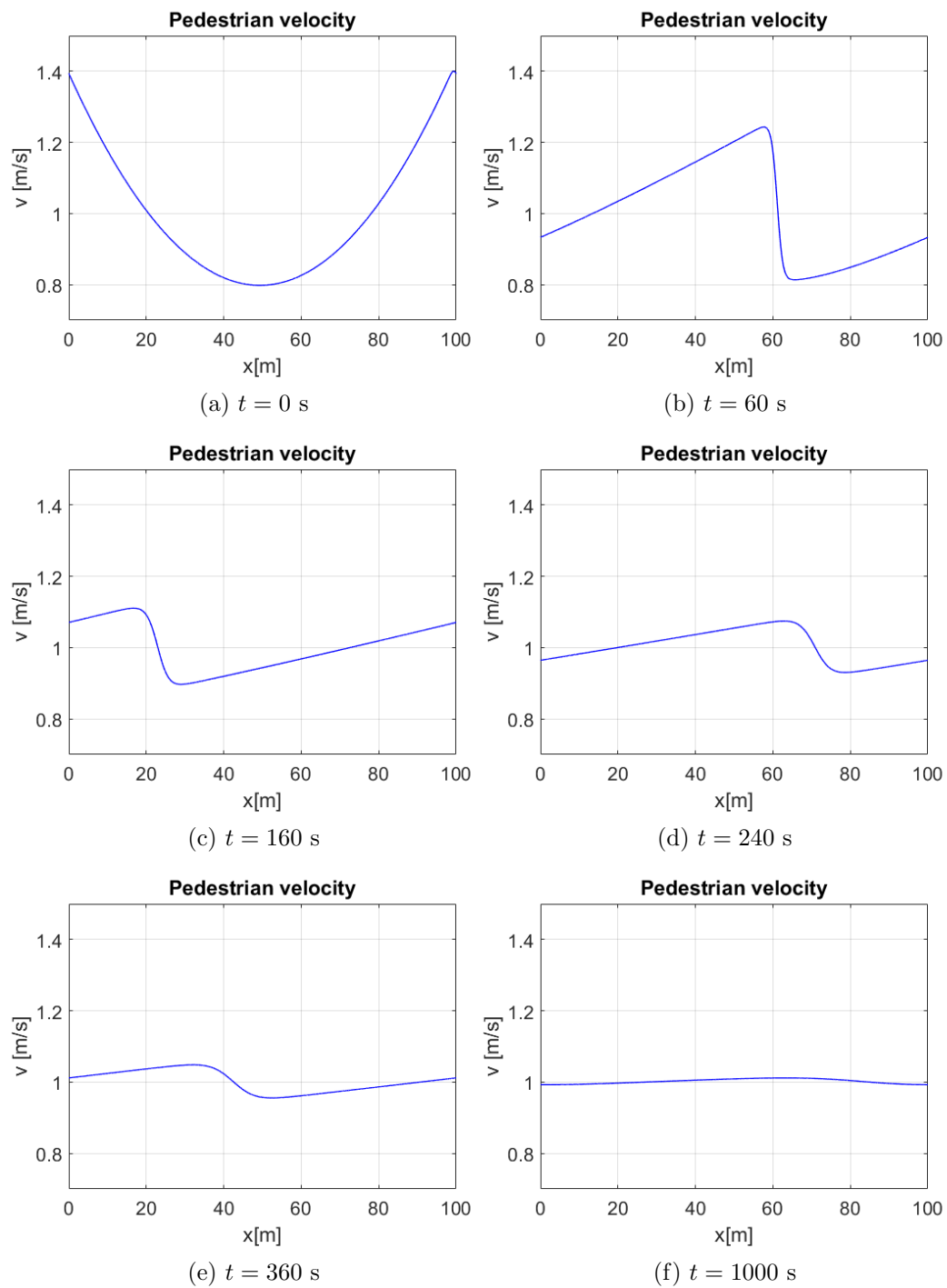


Figure 4.4: Time evolution of the pedestrian velocity.

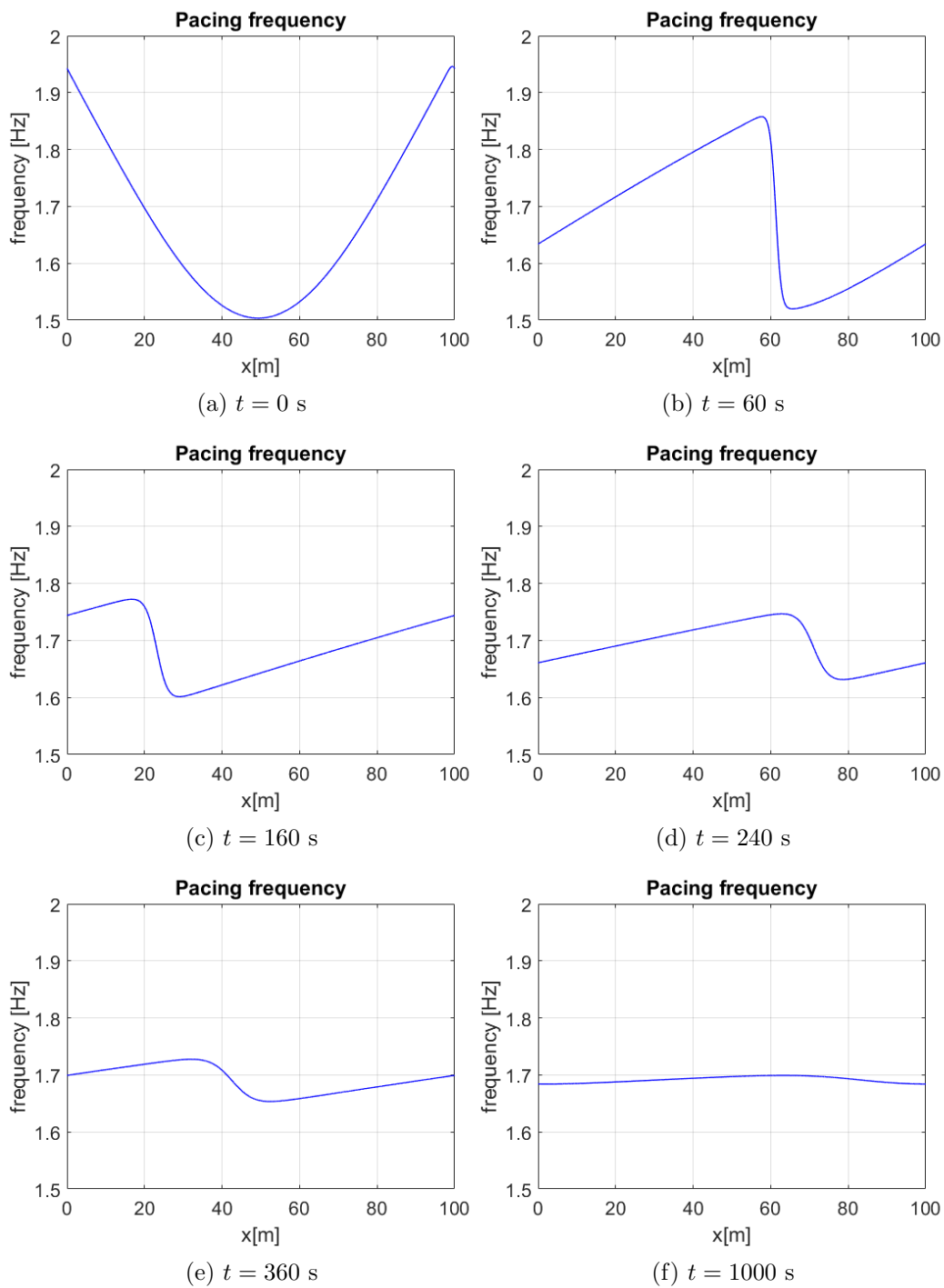


Figure 4.5: Time evolution of the pedestrian pacing frequency.

Fig.(4.4d). Since the density tends to assume a constant value over the footbridge for large time, the velocity tends to become uniform too, as displayed in Fig.(4.4f).

Finally, in Fig.(4.5) we show the time evolution of the pacing frequency. When pedestrians walk faster, they tend to complete more steps per second, hence the pacing frequency increases; on the other hand, when pedestrians walk more slowly, the opposite occurs. This explains why the velocity and the pacing frequency have similar trend.

All graphs above discussed have been derived with desired velocity  $v_d = 1.41$  m/s; in case of other values are chosen, the time evolution of  $\rho(t, x)$ ,  $v[\rho](t, x)$  and  $f(t, x)$  would not change. The unique difference would be that the sort of discontinuity would propagate at a different speed.

In the next paragraph we will analyse the numerical results regarding the dynamic load due to pedestrian motion on the footbridge and the vertical acceleration of the structure.

### 4.1.3 Force model

For deriving the vertical acceleration of the footbridge due to pedestrian motion, firstly we need to obtain the dynamic load  $F_{macro}(t)$ . The pedestrian density is given by the solution shown in Fig.(4.3), therefore we can apply the model described in section 3.6.2, and evaluate

$$F_{macro}(t) = \int_{\Omega} h(t, x) \phi(x) \rho(t, x) dx$$

as

$$F_{macro}(t) = \sum_{j=1}^J \alpha(x_j) g \sin(2\pi f(x_j)t) \sin\left(\frac{\pi x_j}{L}\right) \rho_j(t) \Delta x$$

for each time step. The solution obtained is shown in Fig.(4.6); since the pedestrian density assumes different values along the footbridge as displayed in Fig.(4.3), the force is not constant. Moreover, the values obtained do not have physical meaning because we are working under the assumption that  $M = 1$ , but they are useful for making a comparison with the microscopic model results.

---

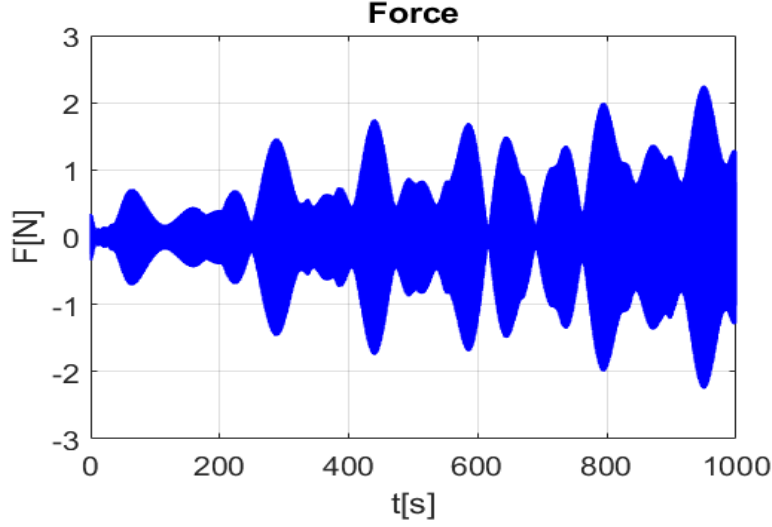


Figure 4.6: Dynamic load exerted by pedestrians on the footbridge.

#### 4.1.4 Structure model

Once that the dynamic load  $F(t)$  is given, it is possible to evaluate the vertical acceleration  $\ddot{y}(t)$ . The chosen parameters are reported in Table (4.2). Therefore

$$\begin{aligned}
 k &= m\omega_n^2 = 7.887 \times 10^6 \frac{N}{m} \\
 c &= 2m\omega_n\xi = 6.280 \times 10^3 \frac{Ns}{m} \\
 \omega_n &= 2\pi f_n = 12.56 \frac{\text{rad}}{s} \\
 f_{res} &= f_n\sqrt{1-2\xi^2} \simeq f_n.
 \end{aligned}$$

As shown in Fig.(4.5), the pacing frequency tends to assume values in between 1.7 Hz and 2.1 Hz; thus, only footbridges with natural frequency that belongs to this frequency interval are subjected to high values of vertical acceleration. This justifies the choice to assume  $f_n = 2$  Hz.

Due to the fact that we are working under the assumption of  $M = 1$ , the pedestrian mass becomes infinitesimal as  $N$  grows; consequently, the total mass is given only by the one of the footbridge. In cases where pedestrians have real mass, it is advisable to add it at the one of the footbridge, because the results can strongly change.

Parameter	$m[\text{Kg}]$	$f_n[\text{Hz}]$	$\xi[-]$
Value	$5 \times 10^4$	2	$5 \times 10^{-3}$

Table 4.2: Dynamic properties of the structure model.

Then, the vertical acceleration is given by

$$\begin{cases} m\ddot{y}(t) + c\dot{y}(t) + ky(t) = F(t) \\ y(0) = 0 \\ \dot{y}(0) = 0 \end{cases} \quad (4.10)$$

Eq.(4.10) is solved with the use of a Beta-Newmark method. Before to show the numerical results, it is explained how this method works.

The subscript  $n$  indicates that the quantity is evaluated at time  $t_n = n\Delta t$ . Since  $y_0$  and  $\dot{y}_0$  are given by the initial conditions, it is possible to derive  $\ddot{y}_0$  as

$$\ddot{y}_0 = \frac{F_0 - ky_0 - c\dot{y}_0}{m}$$

and this provides a starting point for the algorithm.  $F_0$  denotes the quantity  $F_{macro}(0)$ . Then, at a generic time  $t_n$  we have

$$\ddot{y}(t) = a(t) = a_n + \frac{t - t_n}{\delta t} (a_{n+1} - a_n) \quad (4.11)$$

and by integrating Eq.(4.11) we obtain

$$\begin{aligned} \dot{y}(t) = v(t) &= v_n + (t - t_n)a_n + \frac{(t - t_n)^2}{2\Delta t} (a_{n+1} - a_n) \\ y(t) &= y_n + (t - t_n)v_n + \frac{(t - t_n)^2}{2} a_n + \frac{(t - t_n)^3}{6\Delta t} (a_{n+1} - a_n). \end{aligned} \quad (4.12)$$

It is possible to generalize relations (4.12) as

$$\begin{aligned} v_{n+1} &= v_n + \Delta t [(1 - \gamma)a_n + \gamma a_{n+1}] \\ y_{n+1} &= y_n + \Delta t v_n + \frac{\Delta t^2}{2} [(1 - 2\beta)a_n + 2\beta a_{n+1}] \end{aligned} \quad (4.13)$$

where  $\beta$  and  $\gamma$  are two parameters. In both relations (4.13) the unique unknown quantity is  $a_{n+1}$ . The governing equation at time  $t_{n+1}$  is

$$ma_{n+1} + cv_{n+1} + ky_{n+1} = F_{n+1} \quad (4.14)$$

so, by substituting relations (4.13) in (4.14) we obtain

$$a_{n+1} = \frac{1}{m + \Delta t c \gamma + \Delta t^2 k \beta} \left[ -c v_n + \Delta t c (\gamma - 1) - k y_n - \Delta t k v_n + \frac{\Delta t^2}{2} k (2\beta - 1) a_n + F_{n+1} \right]. \quad (4.15)$$

All quantities on the right-hand side of (4.15) are known, therefore we can derive  $a_{n+1}$ ; consequently, from relations (4.13) we obtain  $v_{n+1}$  and  $x_{n+1}$ , so we can advance in time. The final output will be  $a(t) = \ddot{y}(t)$  given for all time  $t \geq 0$ . This method is unconditionally stable only if

$$\frac{1}{2} \leq \gamma \leq 2\beta$$

thus the numerical simulations will be carried out with  $\gamma = \frac{1}{2}$  and  $\beta = \frac{1}{4}$ .

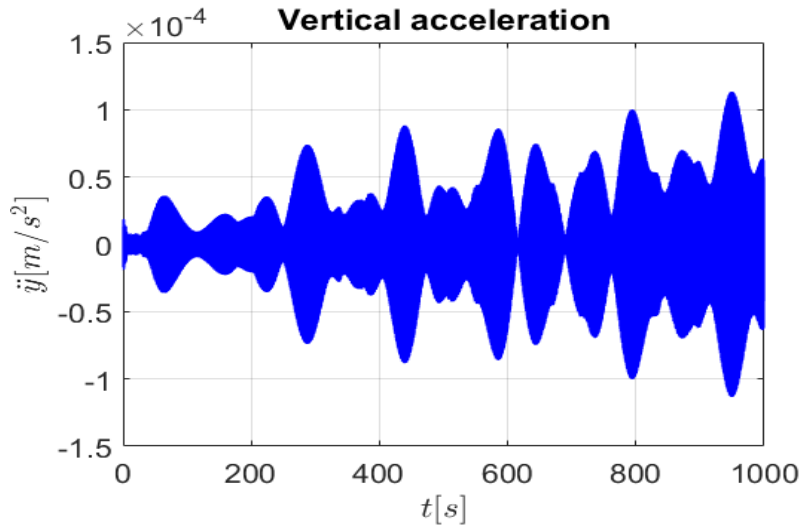


Figure 4.7: Vertical acceleration of the footbridge due to pedestrian motion.

The vertical acceleration of the structure derived with the use of this method is shown in Fig.(4.7). During the first 200 s of simulation, the values of vertical acceleration are smaller in comparison with others given for larger time. This trend can be explained by looking at Fig.(4.5), where it is displayed the time evolution of the pedestrian pacing frequency. Indeed, in graphs (a), (b) and (c) the pacing frequency is far from the natural frequency of the footbridge, especially in the middle span, consequently the structure

oscillates less. On the other hand, for larger time the pacing frequency assumes almost a constant value which is nearer to the natural frequency of the footbridge and therefore its oscillations are more pronounced.

Finally, since we used a finite volume method for discretizing a conservation mass equation, we expect that the algorithm preserves the mass as well during the entire simulation time. In Fig.(4.8) is shown that  $M = 1 \forall t$ , hence the algorithm works correctly, and the results obtained are reliable.

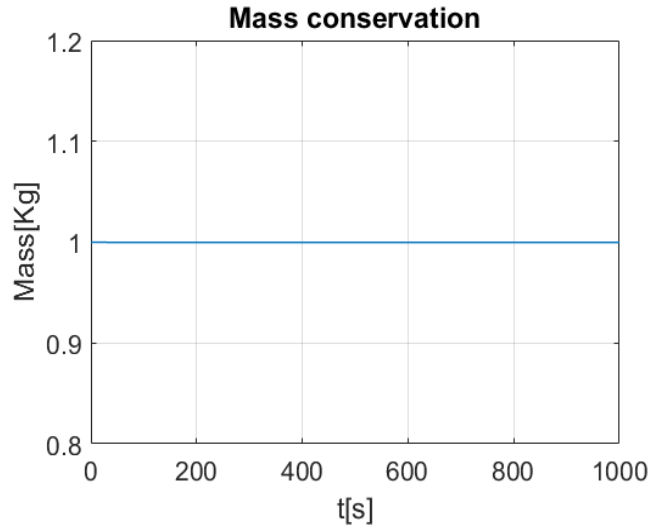


Figure 4.8: Total mass of the system.

## 4.2 Microscopic model results

In chapter 3 we have discussed the microscopic model chosen in this work, which is here reported for simplicity

$$\frac{dx_i}{dt} = v_d - \frac{1}{N} \sum_{\substack{j=1 \\ j \neq i}}^N \eta(R - |x_i - x_j|) \mathbb{1}_{[x_i, x_i+R]}(x_j - x_i) \quad (4.16)$$

accompanied by periodic boundary conditions and initial conditions  $x_i(0) = x_{0,i}$ , for  $i = 1, \dots, N$ . In this section we will provide all numerical results inherent to the simulation of model (4.16). In particular, in paragraph 4.2.1 the attention is given to the crowd model, in paragraph 4.2.2 results inherent

---

to the force model are shown and finally in 4.2.3 the vertical acceleration of the structure is analysed.

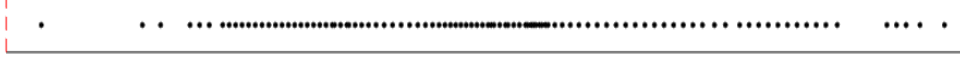


Figure 4.9:  $N = 100$  pedestrians walking along a footbridge with length  $L = 100$  m and width  $B = 2$  m. Due to the assumption of one-dimensional domain, pedestrians can walk only along a straight line.

### 4.2.1 Crowd model

Since we are dealing with an ordinary differential equation, time integration can be simply done by using an explicit Euler scheme, so

$$x_i(t + \Delta t) = x_i(t) + \Delta t v_i(t) \quad \text{for } i = 1, \dots, N$$

where  $\Delta t$  is the time step with which the time discretization is made. In this way we can predict the position of each pedestrian at time  $t + \Delta t$ , once the positions and the velocities at time  $t$  are known. In the following we will use  $\Delta t = 0.005$ .

As in the macroscopic model, all simulations are carried out in a one-dimensional domain. Such an assumption can be considered natural, due to the fact that we are interested only in crowd motion over a footbridge. Indeed, footbridges tend to be long but with a reduced width, therefore pedestrians tend to walk in columns. In Fig.(4.9) an instant time of a simulation over a footbridge with length  $L = 100$  m and width  $B = 2$  m is reported; since the domain has only one dimension, pedestrians can move only along a straight line.

Regarding the initial conditions, it is assumed that at time  $t = 0$  s all pedestrians are already on the footbridge, with positions distributed according to a Beta distribution. An example is given in Fig.(4.10), where in graph (a) the positions of the 100 pedestrians are sampled by a uniform distribution, while in graph (b) they are sampled by a Beta distribution with parameters  $\alpha = \beta = 2$ . For instance, the first configuration takes into account a normal flow condition on the footbridge; the second one is able to simulate the

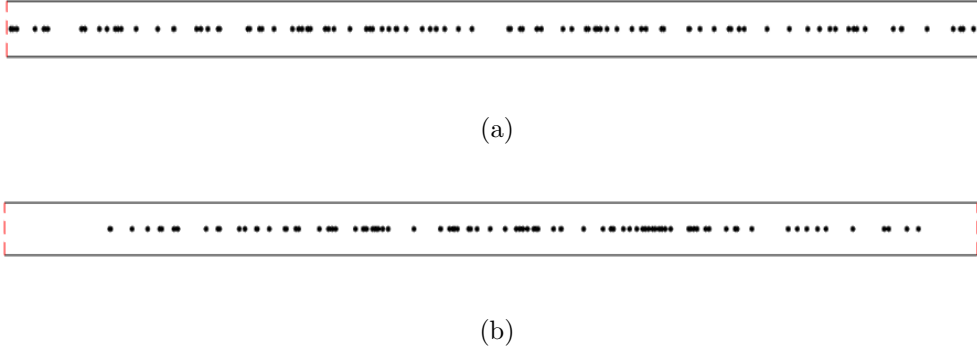


Figure 4.10: In graph (a) the pedestrian positions are distributed according to a uniform distribution; in graph (b) they follow a Beta distribution. In both cases the total number of pedestrians is  $N = 100$ .

evolution of a crowded region in the middle span of the footbridge, caused e.g. by the presence of an event. For keeping valid the assumption of mass conservation, periodic boundary conditions are assigned; thus, pedestrians who go out of the footbridge, immediately re-enter.

The parameter values are assigned like in the macroscopic crowd model, consequently they are reported in Table (4.1). Since the simulations will be carried out mostly with high values of  $N$ , the length of the sensory region is set again to  $R = 2$  m. Indeed, in crowded areas, it is reasonable to assume that pedestrians are influenced only by others nearby.

In Fig.(4.11) the time evolution of the pedestrian positions over a footbridge with length  $L = 100$  m is shown. In order to understand better the behaviour of the crowd, two generic pedestrians are marked with different colours, blue and red, while all others are black. The total number of pedestrians on the footbridge is  $N = 125$ . The desired velocity, equal for each agent, is set to  $v_d = 1.41$  m/s. The initial condition is reported in graph (a); the pedestrian positions are Beta distributed. As time passes, pedestrians tend to keep a certain distance among each others, due to repulsion forces acting within the sensory region. Consequently, in graphs (b),(c) and (d) it is possible to see how they tend to occupy the entire available surface. During this phase, always due to repulsion forces, the distance between the  $i$ -th and  $j$ -th pedestrian varies too. Finally, pedestrian positions tend to be evenly distributed over the footbridge for large time, and this is visible in graph (f).

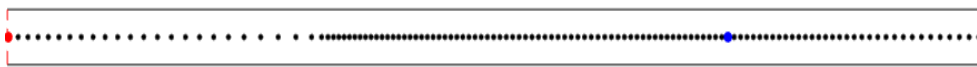
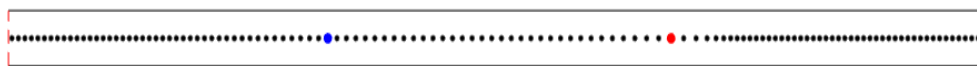
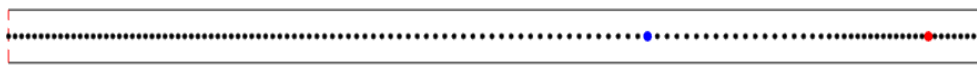
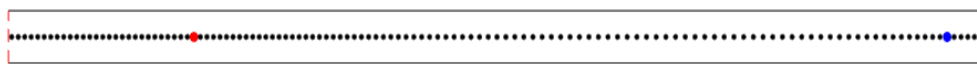
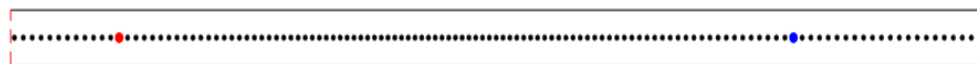
(a)  $t = 0$  s(b)  $t = 100$  s(c)  $t = 200$  s(d)  $t = 300$  s(e)  $t = 400$  s(f)  $t = 1000$  s

Figure 4.11: Time evolution of the pedestrian positions. In blue and red is represented a generic couple of pedestrian  $i$  and  $j$ ; the total number of pedestrians is  $N = 125$ .

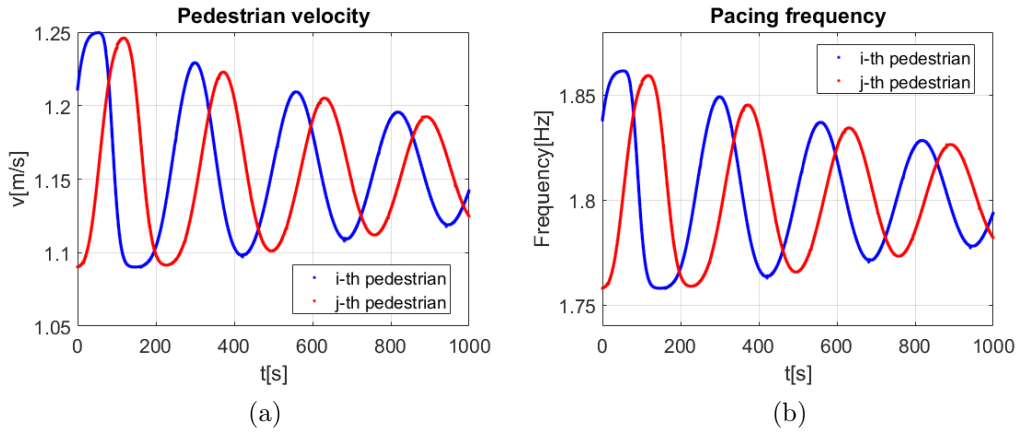


Figure 4.12: Velocities and pacing frequencies of a generic couple of pedestrians  $i$  and  $j$  marked respectively in blue and red in Fig.(4.11); the total number of agents on the footbridge is  $N = 125$  and the desired velocity is  $v_d = 1.41$  m/s.

Therefore we can conclude that from positions distributed as a Beta, after 1000 s we obtain positions which are evenly distributed, and this is consistent with results given by the macroscopic model. Of course, we expect such a dynamics for whatever initial condition.

Moreover, in Fig.(4.12) the velocities and the pacing frequencies of the marked couple of pedestrians  $i$  and  $j$  are reported. Since the pacing frequency depends only on the velocity, there is a huge similarity in the trend of graphs (a) and (b); indeed, when the velocity increases, the number of steps per second increases too, and vice versa. For both pedestrians the desired velocity is never reached during the simulation; in fact, due to interactions among others within the sensory region, the velocity is lower. Moreover, both quantities oscillate more during the first 500 s of simulation than during the last 500 s; indeed, the system tends to a steady configuration for large time, consequently we expect that also the velocity and the pacing frequency reach a steady value, and for this reason the amplitude of the oscillations decreases over time.

Obviously, the total number of pedestrians affects the changes in velocity and pacing frequency. For instance in Fig.(4.13) the above-mentioned quantities are reported for  $N = 70$ , and it is clearly visible that a generic agent is able to hold a velocity much nearer to the desired one, and also the amplitude of the oscillations is reduced in comparison with Fig.(4.12).

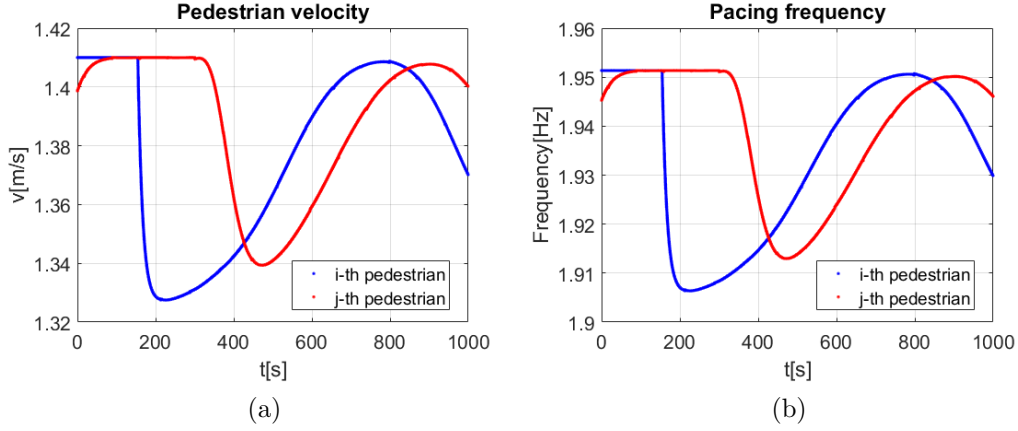


Figure 4.13: Velocities and pacing frequencies of a generic couple of pedestrians; the total number of agents on the footbridge is  $N = 70$  and the desired velocity is  $v_d = 1.41$  m/s.

## 4.2.2 Force model

In order to derive the vertical acceleration of the footbridge, firstly we need to evaluate the dynamic load  $F_{micro}(t)$ . The model we use is the one presented in section 3.6.1, so

$$F_{micro}(t) = \frac{1}{N} \sum_{i=1}^N \alpha_i m_i g \sin(2\pi f_i t) \phi(x_i). \quad (4.17)$$

where it is assumed that  $m_i = m_p$  for  $i = 1, \dots, N$  with  $m_p = const$ , so that all pedestrians weight the same. In literature, the value of  $m_p$  is usually a sample of a normal distribution with mean value  $m_{mean} = 75$  kg and standard deviation  $m_{std} = 15$  kg. In this work, we assume  $m_p = 75$  kg.

Since the pedestrian positions and velocities are known by the crowd model, it is possible to compute the exerted force on the structure. The results obtained by implementing Eq.(4.17) are reported in Fig.(4.14). These values are obtained with the hypothesis that pedestrians have infinitesimal mass as  $N$  grows; hence they are small in comparison to what we expect in reality, but they are useful for making analogies with the macroscopic model.

Results shown in Fig.(4.14) are carried out with desired velocity  $v_d = 1.41$  m/s and they are averaged over 5 simulations. Moreover, since the system reaches a steady configuration in a short time for  $N = 125$ , the amplitude of

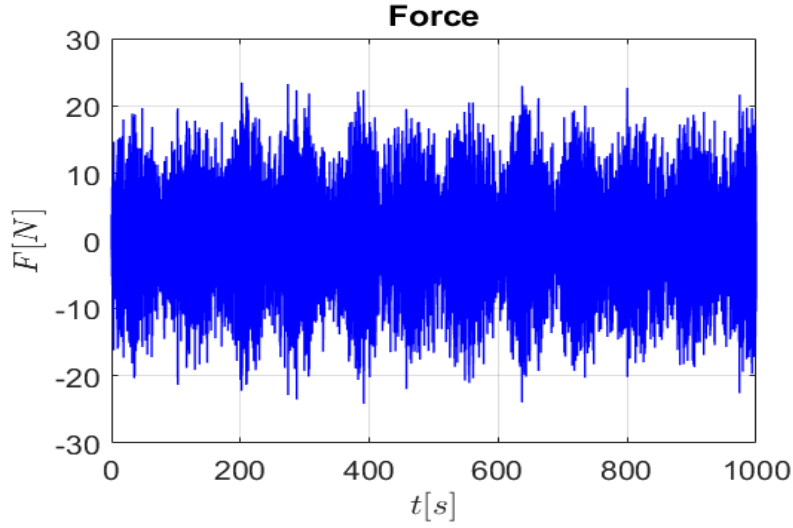


Figure 4.14: Dynamic load exerted by  $N = 125$  pedestrians on the footbridge; the force is obtained with the assumption of  $M = 1$ .

the oscillations remains almost constant during the entire simulation.

### 4.2.3 Structure model

Once that the dynamic load  $F_{micro}(t)$  is given, it is finally possible to evaluate the vertical acceleration of the structure. Therefore, we need to derive  $\ddot{y}(t)$  from

$$\begin{cases} m\ddot{y}(t) + c\dot{y}(t) + ky(t) = F_{micro}(t) \\ y(0) = 0 \\ \dot{y}(0) = 0. \end{cases} \quad (4.18)$$

Eq.(4.18) is solved again by using a Beta-Newmark method with parameters  $\gamma = 1/2$  and  $\beta = 1/4$ , as shown in section (4.1.3). The footbridge is modelled like in the macroscopic model, consequently the chosen parameters are reported in Table (4.2). Again, the pedestrian masses are not added to the footbridge one during the simulations.

The results obtained when the structure is excited by the force  $F_{micro}(t)$  given in Eq.(4.17) are shown in Fig.(4.15); these are the results obtained by doing an average over 5 simulation. Obviously, the values obtained are smaller than what we expect in reality, indeed the vertical acceleration is almost imperceptible, but they will be useful for making a comparison with

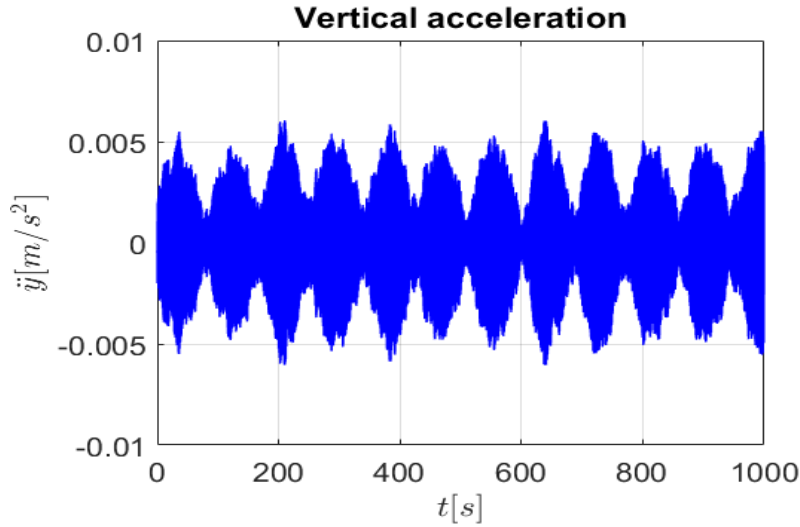


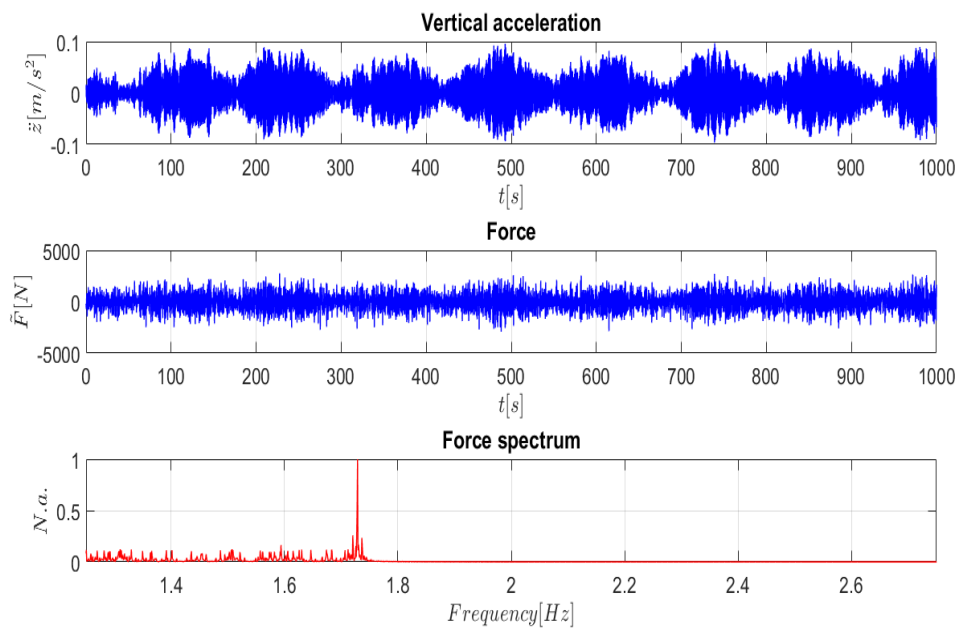
Figure 4.15: Vertical acceleration of the footbridge due to pedestrian motion under the assumption of  $M = 1$ ; the system is exerted by the force  $F(t)$  and the total number of pedestrian is  $N = 125$ .

the macroscopic model. Moreover, since the system reaches a steady configuration in a short time for  $N = 125$ , the amplitude of the oscillations remains almost constant during the entire simulations.

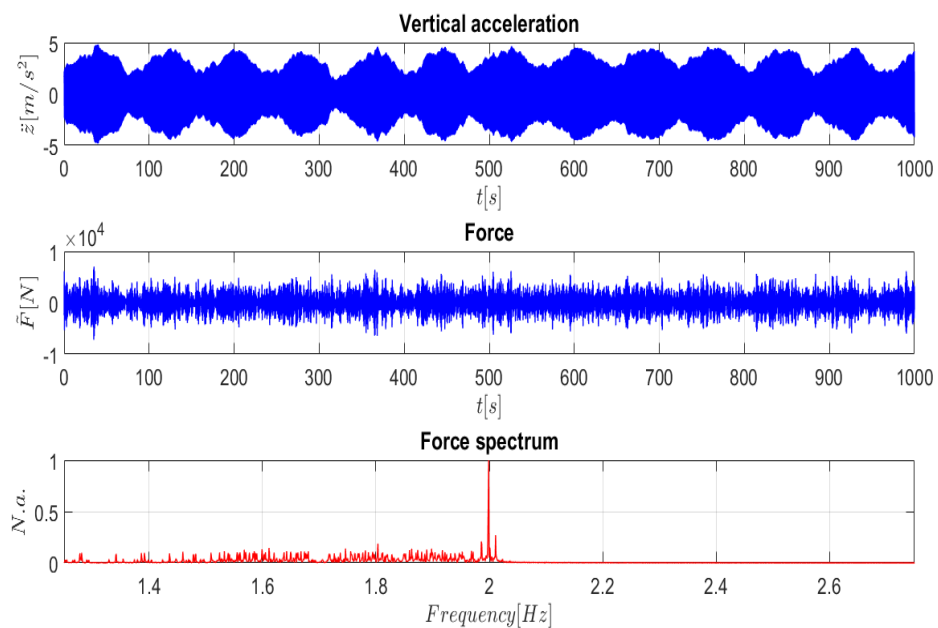
A deeper insight into the vertical acceleration is given by the results shown in Fig.(4.16). In both cases (a) and (b) the structure has been excited by the force  $\tilde{F}_{micro}(t)$ ; hence, we obtain the vertical acceleration  $\ddot{z}(t)$ . The unique parameter that differ is the desired velocity of pedestrians, set to  $v_d = 1.05$  m/s in (a) and to  $v_d = 1.50$  m/s in (b). Therefore, we can state that the vertical acceleration of the footbridge induced by a crossing flow of pedestrians in leisure time is well simulated by the configuration (a), while graph (b) simulates pedestrian motion during a rush hour.

Each vertical acceleration graph is accompanied by the graph of the force which excites the structure and its frequency spectrum, that reveals which are the main frequencies in the force signal.

In case (a) almost all the energy of the force signal is concentrated in  $f = 1.72$  Hz while a small amount is in lower frequencies;  $f$  corresponds to the pacing frequency of pedestrians. Hence, we are far from a resonance phenomenon because the natural frequency of the footbridge is  $f_n = 2$  Hz and consequently the vertical acceleration is limited. The pedestrian comfort



(a)



(b)

Figure 4.16: Vertical accelerations generated by  $N = 125$  pedestrians, and relative force and force spectrum; in (a) the desired velocity is set to  $v_d = 1.05$  m/s while in (b) is set to  $v_d = 1.50$  m/s. N.a. is the acronym of normalized amplitude.

Comfort level	Degree of comfort	Vertical acceleration
CL 1	maximum	$< 0.50m/s^2$
CL 2	medium	$0.50 - 1.00m/s^2$
CL 3	minimum	$1.00 - 2.50m/s^2$
CL 4	unacceptable discomfort	$> 2.50m/s^2$

Table 4.3: Defined comfort classes and related vertical acceleration values [79].

classes and related values of vertical acceleration of the structure are reported in Table (4.3), and they are provided by the "European design guide for footbridge vibration" [79]; in this configuration we would be always in a comfort level CL1, which is the maximum one. Consequently, pedestrians can easily cross the footbridge, with a slight feeling of disturbance or even with any discomfort.

In case (b) things are different. First of all, the energy of the force signal is entirely concentrated in  $f = 2$  Hz; consequently, a resonance phenomenon is triggered. Indeed, by referring again to Table (4.3), we would be in a comfort level CL4, since the acceleration is often over  $2.5 \text{ m/s}^2$ .

The main purpose of Fig.(4.16) is to show how the pedestrian behaviour can determine the stability or instability of a footbridge; indeed, by passing from leisure activities to rush hour periods the comfort of the structure strongly changes and the engineers must consider this phenomenon. Obviously this is only an example, because the results change when, for instance, another number of pedestrians is used or different footbridge lengths or weights are considered. Moreover, it should be kept in mind that, in this study, human-structure interaction has been neglected and that, if considered, lower accelerations are expected.

### 4.3 Comparing results

We will compare the results given by the microscopic and macroscopic models in this section. The macroscopic scale lays on the assumption that the number of pedestrians on the footbridge must be large enough, let us say  $N \rightarrow \infty$ , in order to consider the flow of pedestrians as continuous; we would

---

like to obtain an estimate of the number of pedestrians from which a macroscopic approximation is valid. We have seen in section 4.1 and 4.2 that the models on the two scales have the same dynamics, hence an estimate of  $N$  can be obtained by increasing step by step the number of pedestrians in the microscopic model, and select a certain number  $N^*$  such that the microscopic solution assumes the same behaviour of the macroscopic one, at least in some asymptotic regime. In this manner we have a deeper understanding about the meaning of treating the crowd as a fluid in footbridge problems.

A first comparison between the two scales is done by looking at the results provided by the force models and at the values of vertical accelerations previously discussed.

The values of major interest in structural responses are the maximum reached during the whole time history; indeed the structure must be able to bear such a load. In section 4.1 we have reported the values of force which excite the structure and the corresponding vertical accelerations; we remind that the values obtained do not have physical meaning, because we are working under the assumption that pedestrians have infinitesimal mass.

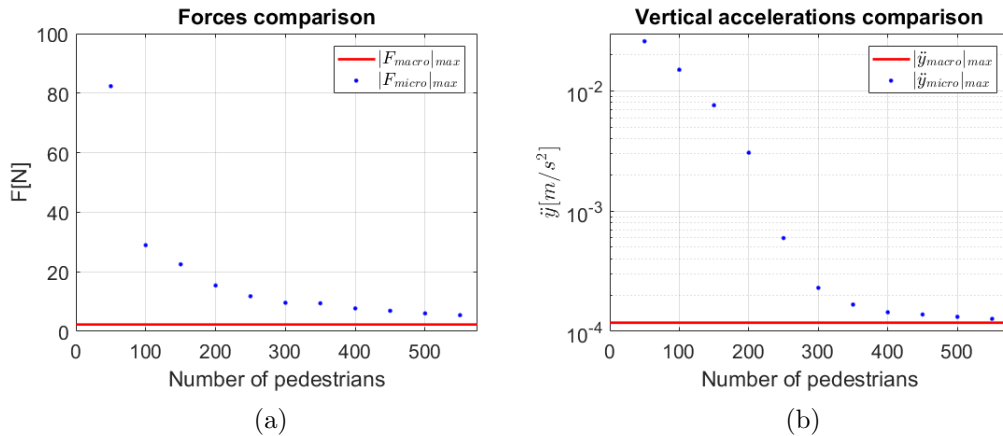


Figure 4.17: In blue are reported the maximum values in modulus of force and vertical acceleration provided by the microscopic force and structural models during a time simulation of 1000 s; In red are reported the maximum values in modulus of force and vertical acceleration provided by the macroscopic force and structural models during a time simulation of 1000 s. A logarithmic scale on the  $y$ -axis is used in graph (b).

In order to compare the results, we evaluate the maximum amplitude of force and vertical acceleration provided by the microscopic force and struc-

ture models when  $N$  varies with the one provided by the respective macroscopic models. The results obtained are summarized in Fig.(4.17). Both the force and the vertical acceleration values given by the microscopic models tend to the one given by the macroscopic models when  $N$  increases. Moreover, Fig.(4.17) proves that the microscopic force and structure models become equivalent to the macroscopic ones for large values of  $N$ ; indeed for  $N = 550$  the maximum values reached during 1000 s of simulation are almost similar. Contrarily to what expected, when the number of pedestrians increases the structure is excited by lower forces and its vertical accelerations become lower too; this is again a consequence of the fact that we consider pedestrians with infinitesimal mass as  $N$  grows.

A second comparison can be made by looking at the results provided by the crowd models. The time evolution of the pedestrian density in the macroscopic framework is reported in Fig.(4.3); while starting from a Beta distribution,  $\rho(t, x)$  tends to a uniform one for large time. The same behaviour is shown by the microscopic crowd model in Fig.(4.11). Just by looking at the two figures above-mentioned we can easily conclude that the two models have the same dynamics, but it is hard to state how far the two solutions are; moreover, the macroscopic crowd model always presents this time evolution, while the microscopic one can change it when  $N$  varies. Therefore, we would like to measure the distance between the two solutions for increasing values of  $N$  and consequently we would like to find a number of pedestrians  $N^*$  such that the microscopic crowd model provides a solution that can be considered as equivalent to the macroscopic one. In conclusion, we will be able to state that a macroscopic approximation is valid if there are at least  $N^*$  pedestrians over the footbridge, instead of generically say  $N \rightarrow \infty$ .

In the following we denote by  $\rho_{macro}(t, x)$  the continuous pedestrian density given by the macroscopic crowd model and by  $\rho_{micro}(t, x)$  the discrete pedestrian density given by the microscopic crowd model. We have proved that  $\rho_{macro}(t, x)$  becomes uniformly distributed for large time; since we are interested in the asymptotic behavior of the systems, we assume that

$$\rho_{macro}(x) = \frac{1}{L} \mathbb{1}_{[0,L]}(x).$$


---

Instead,  $\rho_{micro}(t, x)$  is a sum of Dirac delta functions, hence

$$\rho_{micro}(t, x) = \frac{1}{N} \sum_{i=1}^N \delta(x - x_i(t)).$$

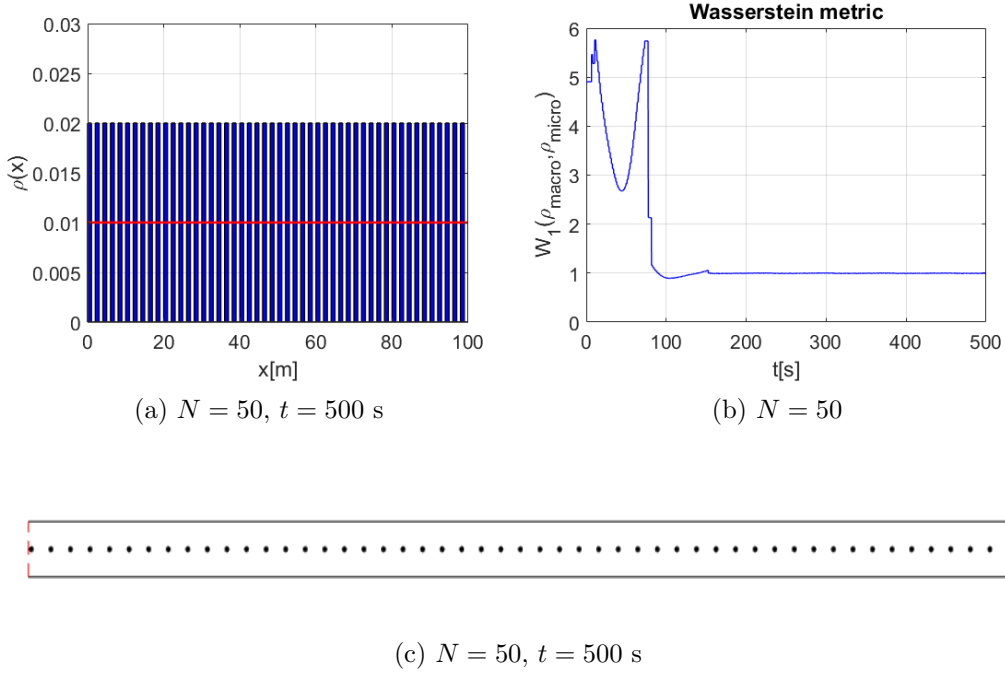


Figure 4.18: In histogram (a) it is reported  $\rho_{micro}(t, x)$  in blue and  $\rho_{macro}(x)$  in red; the time evolution of the Wasserstein metric is shown in (b); the pedestrian positions on the footbridge are shown in (c). All graphs are obtained with  $N = 50$ .

In order to derive an estimate of  $N$  such that the models on the two scales are equivalent, we need to compare the distance between the two density probability functions  $\rho_{macro}(x)$  and  $\rho_{micro}(t, x)$  for large time. For evaluating this distance, we use two methods:

- a histogram which gives information about the spatial distribution of pedestrian positions on the footbridge; in each interval  $I_k$  is evaluated the quantity  $n_k/N$ , which is the fraction of pedestrians in  $I_k$  at a certain time  $t^n$ . All intervals are 1 meter long, hence  $|I_k| = 1, \forall k$ ;
- the Wasserstein metric, which allows us to compute the distance between a continuous and a discrete density probability functions, by

using relation (3.43) shown in paragraph 3.4.1. Moreover, we have proved that

$$W_1(\rho_{macro}(x), \rho_{micro}(t, x)) = \frac{1}{2N}$$

when pedestrians are evenly distributed. Thus, we expect that the Wasserstein metric tends to  $\frac{1}{2N}$  for large time. Furthermore, we fix a threshold of  $10^h$  with  $h = 1$ , so that only when

$$W_1(\rho_{macro}, \rho_{micro}) \leq 10^{-h}$$

we will be able to conclude that the discrete pedestrian density  $\rho_{micro}(t, x)$  assumes the same form of the continuous pedestrian density  $\rho_{macro}(x)$ , and so that the two models are equivalent.

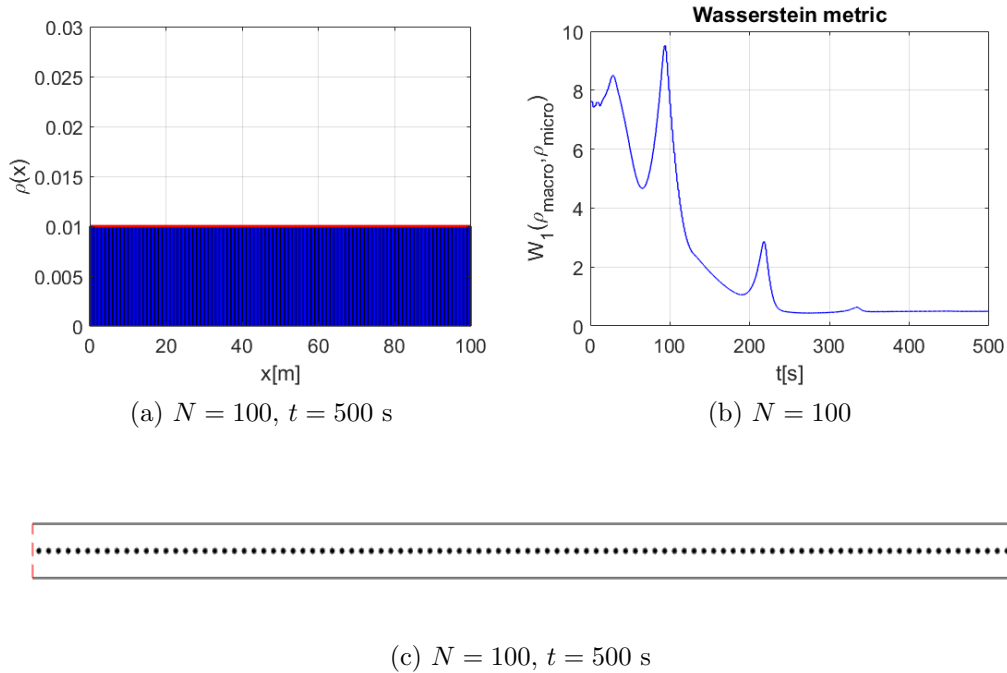


Figure 4.19: In histogram (a) it is reported  $\rho_{micro}(t, x)$  in blue and  $\rho_{macro}(x)$  in red; the time evolution of the Wasserstein metric is shown in (b); the pedestrian positions on the footbridge are shown in (c). All graph are obtained with  $N = 100$ .

The model parameter values used in the microscopic crowd model for carrying out the following results are the ones used in section 4.2, with  $v_d = 1.41$  m/s. Of course,  $N$  varies.

The results obtained with  $N = 50$  are reported in Fig.(4.18). Pedestrians tend to keep their sensory region empty, hence we do not have two agents nearer than 2 m; moreover, since  $N$  is low, a lot of pedestrians are able to walk at their desired velocity and they are not influenced by others. This behaviour explains the pattern of histogram in Fig.(4.18a); the red line represents the value assumed for large time by the continuous pedestrian density. Moreover, the time evolution of the Wasserstein metric is reported in Fig.(4.18b); after a transitional phase, it tends to  $\frac{1}{2N} = 1$ , meaning that pedestrians are evenly distributed, as confirmed in Fig.(4.18c).

The results obtained with  $N = 100$  are shown in Fig.(4.19). Pedestrians try to occupy all the available space in order to let as empty as possible their sensory regions; consequently, each agent is located at 1 m from his/her predecessor for large time. Histogram (4.19a) confirms that pedestrians are evenly distributed, which is also visible in Fig.(4.19c). Moreover, the time evolution of the Wasserstein metric is reported in Fig.(4.19b); as expected, after a transitional phase it tends to  $\frac{1}{2N} = 0.5$ .

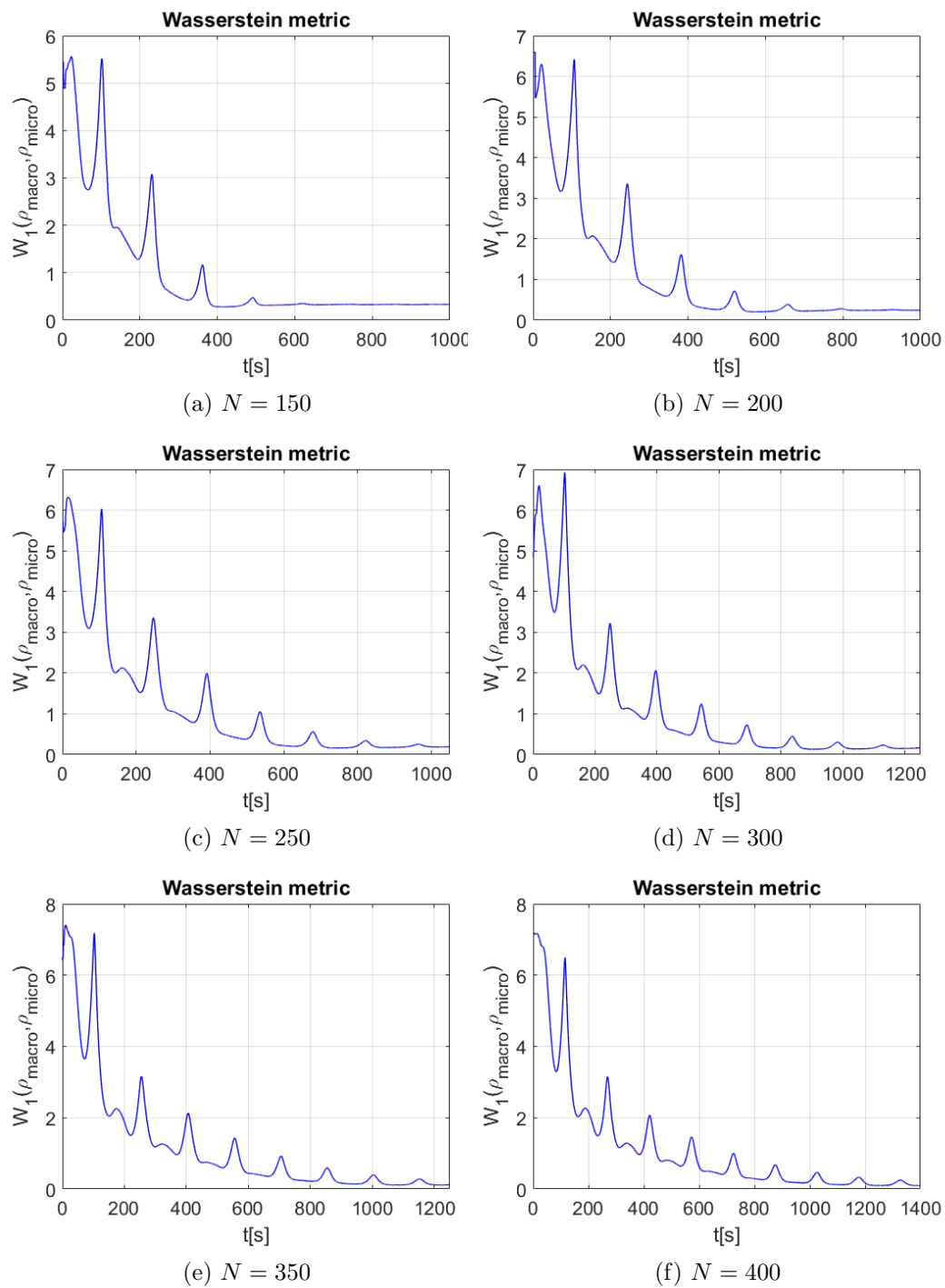
The time evolution of the Wasserstein metric for increasing values of  $N$  is reported in Fig.(4.20). Each graph shows a transitional phase, which becomes longer as  $N$  increases; indeed, when the number of pedestrians is large, the system requires more time for reaching a steady configuration. By the way, in all cases the Wasserstein metric tends to  $\frac{1}{2N}$  for large time, which means that an evenly distribution of pedestrians on the footbridge is always reached independently by the value of  $N$ . Moreover, Fig.(4.20) shows also that

$$W_1(\rho_{macro}, \rho_{micro}) \rightarrow 0, \quad N \rightarrow \infty$$

for large time.

Finally, the results inherent to  $N = 550$  are shown in Fig.(4.21). Due to the large number of pedestrians on the footbridge, the walkers cannot let empty their sensory regions; by the way, they try to stay as far as possible from other members and consequently an evenly distribution is reached again for large time. Indeed, histogram (4.21a) shows that there is always the same number of pedestrians every 2 m - not every 1 m because it would not be possible to have 5.5 pedestrians in each interval. Also the time evolution of the Wasserstein metric in Fig.(4.21b) confirms that an evenly distribution is reached for large time; due to the high number of pedestrians, the transitional

---

Figure 4.20: Time evolution of the Wasserstein metric as  $N$  varies.

phase is longer. The pedestrian positions over the footbridge are reported in Fig.(4.21c); in this case it is almost impossible to recognize single pedestrians, indeed the walking crowd seems more a continuous fluid than a discrete quantity, contrarily to what shown for  $N = 50$  and  $N = 100$ .

As previously said, we are able to conclude that the discrete pedestrian density  $\rho_{micro}(t, x)$  assumes the same form of the continuous pedestrian density  $\rho_{macro}(x)$ , and so that the two models are equivalent, only when

$$W_1(\rho_{macro}, \rho_{micro}) \leq 10^{-h} \quad (4.19)$$

with  $h = 1$ . Since  $\rho_{micro}$  is time dependent, the Wasserstein metric too, therefore we have to decide at which time evaluate it. Obviously, we expect that inequality (4.19) would be satisfied only for large time and for a certain number of pedestrians  $N > N^*$ , which will be derived in the following.

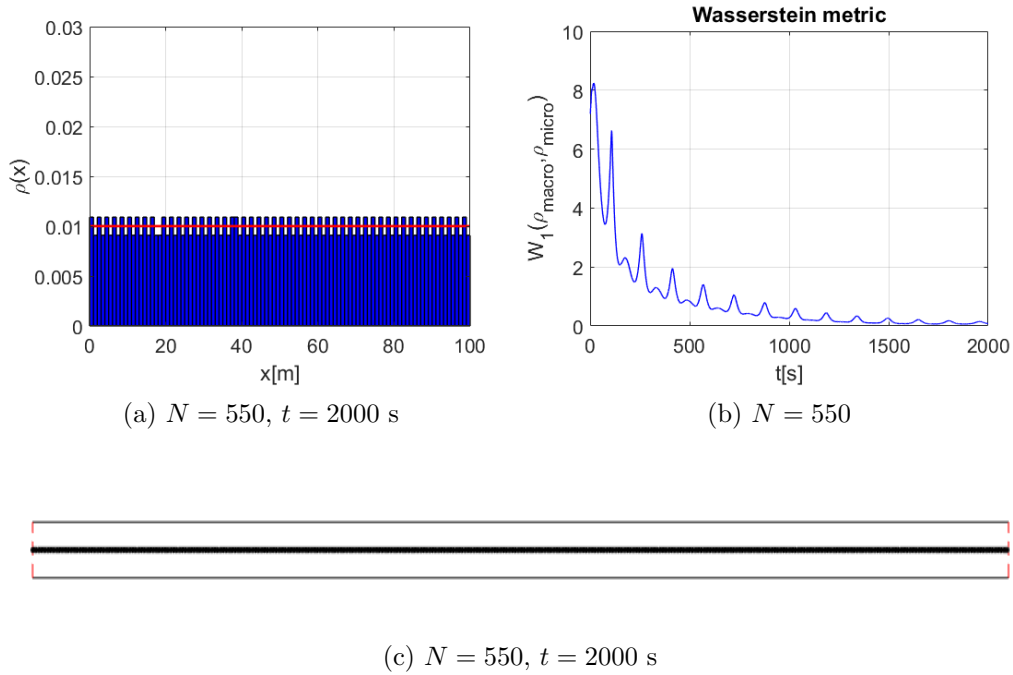


Figure 4.21: In histogram (a) it is reported  $\rho_{micro}(t, x)$  in blue and  $\rho_{macro}(x)$  in red; the time evolution of the Wasserstein metric is shown in (b); the pedestrian positions on the footbridge are shown in (c). All graphs are obtained with  $N = 550$ .

Firstly, we need to compute the mean pedestrian velocity  $\bar{v}(N)$ ; in order to obtain  $\bar{v}(N)$ , the mean velocity of all pedestrians on the footbridge is

$N$	$\bar{v}(N)$	$T(N)$	$t_0(N)$	$W_1(N)$
50	1.397	71.581	1073.715	1
100	1.201	83.263	1248.945	0.5
150	1.134	88.183	1322.745	0.333
200	1.102	90.744	1361.16	0.25
250	1.079	92.678	1390.17	0.2
300	1.066	93.808	1407.12	0.166
350	1.061	94.251	1413.765	0.142
400	1.052	95.057	1425.855	0.125
450	1.035	96.618	1449.27	0.111
500	1.013	98.716	1480.74	0.1
550	0.978	102.249	1533.735	0.09

Table 4.4: Values of mean velocity  $\bar{v}(N)$  in m/s, crossing time  $T(N)$  in seconds, reference time  $t_0(N)$  in seconds and Wasserstein metric  $W_1(N)$  as  $N$  varies.

evaluated for each time step, and consequently the mean value over all time steps is computed. We denote by  $T(N)$  the time needed for crossing the footbridge with velocity  $\bar{v}(N)$ , hence

$$T(N) = \frac{L}{\bar{v}(N)}.$$

As previously stated, we are only interested in the asymptotic behaviour of the system, therefore we fix a time  $t_0(N) = 15T(N)$  and we compute  $W_1(\rho_{macro}(x), \rho_{micro}(t_0(N), x))$ . The results are shown in Table (4.4); for the sake of simplicity, we denoted by

$$W_1(N) := W_1(\rho_{macro}(x), \rho_{micro}(t_0(N), x)).$$

We remind that all values reported in Table (4.4) are obtained with desired velocity  $v_d = 1.41$  m/s.

The mean velocity  $\bar{v}(N)$  decreases as  $N$  increases; indeed, when  $N$  increases the repulsion forces increase too, therefore pedestrians walk slower. Even for high values of  $N$  the velocity  $\bar{v}(N)$  does not tend to zero, because all pedestrians have the same desired velocity; thus, once that an evenly distribution is reached, pedestrians walk at a constant speed, and queue are not formed. Since  $\bar{v}(N)$  decreases when  $N$  increases, the crossing time  $T(N)$

increases; this means that for increasing values of  $N$  a pedestrian needs more time for crossing the footbridge. Finally, the value assumed by the Wasserstein metric at time  $t_0(N)$  is reported; in all cases, pedestrians are evenly distributed at time  $t_0(N)$ , hence

$$W_1(N) = \frac{1}{2N}.$$

For the sake of simplicity, the results inherent to the Wasserstein metric when  $N$  varies are summarized in Fig.(4.22). As expected, the distance between the discrete and continuous pedestrian densities decreases as  $N$  increases. Indeed, it is more appropriate a discrete description of the crowd in Fig.(4.18c) than in Fig.(4.21c), therefore  $\rho_{micro}$  differs from  $\rho_{macro}$  for  $N = 50$ , and consequently  $W_1(50) = 1$ ; on the contrary, it is more appropriate a continuous description of the crowd in Fig.(4.21c) than in Fig.(4.18c), therefore  $\rho_{micro}$  is similar to  $\rho_{macro}$  for  $N = 550$ , and consequently  $W_1(550) = 9 \times 10^{-2}$ .

Moreover, Fig.(4.22) shows that  $W_1(N)$  assumes values under the threshold only for  $N > N^*$  with  $N^* = 500$ ; hence

$$\text{if } N > N^* \implies W_1(N) = W_1(\rho_{macro}(x), \rho_{micro}(t_0(N), x)) < 10^{-1}.$$

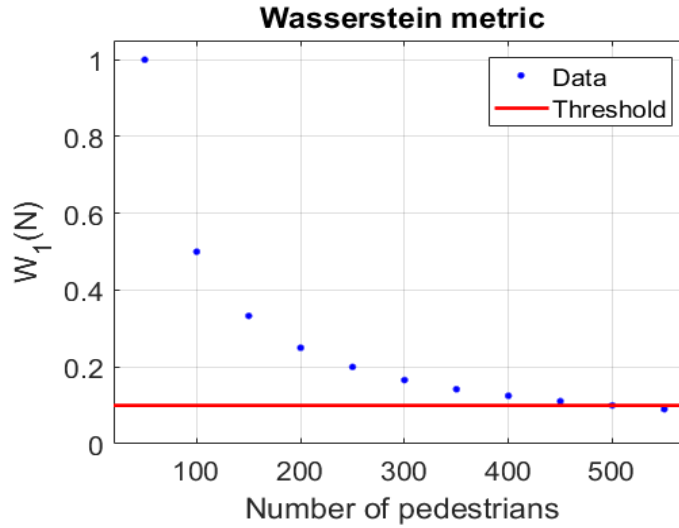


Figure 4.22: Wasserstein metric computed at time  $t_0(N)$  for increasing values of  $N$ .

In chapter 3 we have shown that the passage from a microscopic to a macroscopic scale is basically founded on the assumption that  $N \rightarrow \infty$ ; in

this section we have proved that is enough to take  $N > N^*$ , with  $N^* = 500$ . This means that if we decide to use a macroscopic framework for analysing the vertical acceleration of a footbridge with length  $L = 100$  m, it is automatically assumed that on the structure there are at least 500 pedestrians. Therefore, it is like to assume that there are 5 pedestrians in each meter, and such a condition is rarely verified in real contexts. By the way, we have used a one-dimensional domain because normally footbridges have a reduced width to length ratio; if we consider that, normally, the footbridge width is in the range 2 – 5 m, then we are able to state that the macroscopic approximation is valid when there are at least from 1 to 2.5 pedestrians in each  $\text{m}^2$ . These crowd density values, at least in the range 1 – 1.5 ped/ $\text{m}^2$ , have been often recorded on real footbridges.

In any cases, by using a macroscopic approximation we are assuming that the footbridge is occupied by a number of pedestrians that is seldom reached in service. This is one of the main reasons which explains why in literature almost all models dealing with footbridge vibration problems are based on a microscopic scale, despite the fact that a model based on a macroscopic scale has a reduced computational time.

# Chapter 5

## Conclusions and future works

This study presented a mathematical framework able to simulate vibrations in footbridges that are prone to excessive vertical vibrations due to multiple pedestrians walking. The framework is composed by a cascade of models which are necessary to describe this phenomenon. Firstly, a crowd model was needed for taking into account the pedestrian behaviour, so it describes their way to interact with other members and with the environment, their strategies and their goals. Secondly, a force model was introduced, which uses the pedestrian velocities given by the crowd model for evaluating the dynamic load exerted on the footbridge. Finally, a structure model was proposed, which uses the dynamic load provided by the force model for computing the vertical acceleration of the footbridge. All the analysis has been carried out by keeping a constant parallelism between two different scales, respectively a microscopic and a macroscopic one. Moreover, all results were carried out under the assumption that the pedestrian mass scales with the number of pedestrians  $N$ , so that the total mass of the system remains constant and unitary over time.

### 5.1 Summary of results

The modelling framework used in our work can be subdivided in three consecutive steps.

### 1. Definition of crowd models:

The following microscopic crowd model

$$\frac{dx_i}{dt} = v_{d,i} - \frac{1}{N} \sum_{\substack{j=1 \\ j \neq i}}^N K(x_i, x_j) \quad (5.1)$$

accompanied by suitable initial conditions  $x_i(0) = x_{0,i}$  was selected in order to describe the evolution of pedestrian positions and walking velocities in time and space. Model (5.1) is a first-order one; it takes into account the pedestrian desire to walk at a preferred speed  $v_d$ , but due to interaction with other agents, this desired velocity is modified by the interaction kernel  $K$ . The interactions take place only within the sensory region of each pedestrian, hence the interaction kernel used is

$$K(x_i, x_j) = \eta(R - |x_i - x_j|) \mathbb{1}_{[x_i, x_i+R]}(x_j - x_i).$$

Then a scale passage was made; therefore, a statistical representation of the crowd was used which automatically implies the assumption of  $N \rightarrow \infty$ , and analogies with the kinetic theory of rarefied gases allowed us to derive a weak form of a Boltzmann-type equation, which is

$$\frac{d}{dt} \left[ \int_{\mathbb{R}} \varphi(x) f(t, x) dx \right] = \frac{1}{2} \int_{\mathbb{R}} \int_{\mathbb{R}} [\varphi(x') + \varphi(y') - \varphi(x) - \varphi(y)] f(t, x) f(t, y) dx dy \quad (5.2)$$

valid for asymmetric binary interactions. Finally, Eq.(5.2) was studied in the asymptotic regime, and the quasi-invariant interaction limit allowed us to derive the Fokker-Planck equation.

Since we worked with a first-order crowd model, we did not have to compute the hydrodynamic limit. Indeed, after that the distribution function  $f(t, x)$  was identified with the pedestrian density  $\rho(t, x)$ , we had immediately derived the macroscopic model from the Fokker-Planck equation, which is

$$\begin{cases} \frac{\partial}{\partial t} \rho(t, x) + \frac{\partial}{\partial x} \left[ \rho(t, x) \left[ v_d - \int_{\mathbb{R}} K(x, y) \rho(t, y) dy \right] \right] = 0 & \text{in } \Omega \times (0, T] \\ \rho(t, 0) = \rho(t, L) & \text{in } \partial\Omega \times (0, T] \\ \rho(0, x) = \rho_0(x). & \text{in } \Omega \end{cases} \quad (5.3)$$

This procedure allowed us to obtain a macroscopic model directly from the microscopic one; indeed, model (5.3) contains the same interaction kernel of model (5.1).

Models (5.1) and (5.3) provide respectively the time evolution of the discrete and continuous pedestrian density on the footbridge, which are used by the force model for evaluating the dynamic load exerted on the structure. Moreover, it was analytically proved that the macroscopic crowd model is a generalization of the microscopic one.

## 2. Definition of force models:

Pedestrian action was described by a moving force model. In the microscopic force model, the force exerted by the  $i$ -th pedestrian was modelled by a single sine function and was expressed as

$$F_{micro}(t) = \frac{1}{N} \sum_{i=1}^N \alpha_i m_i g \sin(2\pi f_i t) \phi(x_i) \quad (5.4)$$

while in the macroscopic framework the following relation was used

$$F_{macro}(t) = \int_{\Omega} h(t, x) \phi(x) \rho(t, x) dx. \quad (5.5)$$

It is evident that the discrete and continuous pedestrian density must be known for using relations (5.4) and (5.5). Moreover, it was analytically proved that the macroscopic force model is a generalization of the microscopic one.

## 3. Definition of the structure model:

Since it is usually assumed that only one mode mainly contributes to the structural response in footbridge vibration problems, a dynamic system with a single degree of freedom was used; hence equation

$$m\ddot{y}(t) + c\dot{y}(t) + ky(t) = F(t) \quad (5.6)$$

is used for computing the vertical acceleration. The structure model is common over each scale; depending on the use of  $F_{micro}(t)$  or  $F_{macro}(t)$  in Eq.(5.6) we obtained respectively  $\ddot{y}_{micro}(t)$  or  $\ddot{y}_{macro}(t)$ .

---

Consecutively, all models above-mentioned were solved numerically. Model (5.1) was implemented by using an explicit Euler scheme while we use a finite volume method with a Lax-Friedrichs numerical flux for model (5.3). The spatial grid used in the finite volume method was also used for computing the integral through a rectangle quadrature rule in force models (5.4) and (5.5). Instead, Eq.(5.6) was implemented with the usage of a Beta-Newmark method.

Moreover, numerical results were discussed. The time evolution of the continuous pedestrian density provided by model (5.3) was shown; independently by the initial conditions,  $\rho(t, x)$  always became uniformly distributed over the footbridge. The discrete pedestrian density provided by model (5.1) showed a similar behaviour. In both cases, also the time evolution of the pedestrian velocity and pacing frequency was analysed, and it was shown in the microscopic framework that pedestrians walk slower when  $N$  increases. Also results concerning the forces applied by pedestrians on the structure and the induced vertical accelerations were discussed; in particular, it was shown that on the basis of the pedestrian activity - leisure time or rush hour - the footbridge vertical vibrations strongly change, and different levels of comfort were reached.

Finally, a comparison was made between results provided by models on the two scales. Since the values of major interest in structural responses are the maximum reached during the whole time history, we decided to compare them. We proved that the values provided by the microscopic force and structural models tend to the values provided by the respective macroscopic models when  $N$  increases; indeed a macroscopic approximation is valid in the limit  $N \rightarrow \infty$ , hence we expected that by increasing the number of pedestrians in the microscopic models, the results would tend to be equal, and models equivalent. Also the crowd models were compared by the usage of the Wasserstein metric and histograms; in particular, the distance between the discrete and continuous pedestrian density on the footbridge was computed for increasing values of  $N$ . With this technique we found out an estimate  $N^*$  which ensures the validity of a macroscopic approximation of the crowd.

---

## 5.2 Suggestions for future research

There are several perspectives for future research that would extend and possibly would improve our current work.

All the analysis was carried out on a one-dimensional domain; it could be possible to study footbridge vibration problems by working on a two-dimensional domain. Surely, more difficulties will occur in the crowd model definition, since boundary repulsion forces should be introduced, and also the scale passage will be more challenging; for instance, all integrals will be made over the two space dimensions instead of only one, and also the expression of the binary interaction will be more elaborated, since we will have to define how pedestrians interact in direction  $x$  and  $y$ . Moreover, if a two-dimensional domain is used, obstacles on the footbridge deck could be added, in order to analyse the impact that they have on footbridge vibrations.

Both at the microscopic and macroscopic scales, we have used a first-order differential crowd model. A possible development consists in using second-order differential crowd model. Overall, the crowd model will be more detailed than the one used, because we will have an additional equation which will directly describe the time evolution of pedestrian velocities. On the other hand, the scale passage will become difficult from a mathematical point of view, since we will have to work with a distribution function  $f(t, x, v)$  instead of  $f(t, x)$ . Moreover, since in the mesoscopic model two pedestrians  $i$  and  $j$  are distinguishable only by their positions  $x_i$  and  $x_j$ , we were obligated to assume that in the microscopic model all pedestrians had the same characteristic, such as mass and desired velocity, and therefore the inter-subject variability was neglected. As a further improvement of our work, it could be possible to include the inter-subject variability and try to understand if results would change; of course, mathematical difficulties will arise in the scale passage.

As previously stated, all results obtained and compared in this work were carried out under the assumption that the total mass of the system is time independent and unitary, hence pedestrians have infinitesimal mass as  $N$  increases. The same analysis could be done by using massive pedestrian, in order to evaluate if the obtained estimate  $N^*$  would change or not.

Pedestrian action was described by a moving force model; by the way,

---

other choices could be done. For instance, pedestrian-structure interactions could be modelled by coupling a single degree of freedom system describing the structure with  $N$  single degree of freedom systems describing a crowd of  $N$  pedestrians. This choice would probably provide more accurate force and vertical acceleration values than the one provided by our model but on the other hand the calibration of the force model will be difficult due to parameter uncertainties.

Regarding the structure, we modelled the footbridge with a dynamic system with one degree of freedom; of course other choices can be done, and for instance a finite element method could be used.

Basically, the sub-models describing crowd dynamics, walking forces due to pedestrian motion and vertical accelerations can be updated as soon as better models will be published or new relevant experimental data will be available for calibration and verification.

Finally, in this work an estimate of number of pedestrian  $N^*$  for which a macroscopic approximation is valid was derived for a fixed footbridge length, in particular  $L = 100$  m. Obviously, the same procedure used for deriving  $N^*$  can be done when  $L$  varies, and it would be interesting to understand if exist a formula which expresses  $N^*$  as function of  $L$ .

---

# Appendix A

## Finite Volume Method

The finite volume method is a technique for representing and evaluating partial differential equations in the form of algebraic equations. Extensive introductions of this method can be found in [64–67] accompanied by an amply variety of applications to real world problems. In the following we will give only the main concepts of this technique.

A conservation law is an initial/boundary-value problem of type

$$\begin{cases} \frac{\partial u}{\partial t} + \nabla \cdot \mathbf{F}(u) = 0 & \text{in } \Omega \times (0, T] \\ u(t, \mathbf{x}) = g(t, \mathbf{x}) & \text{in } \partial\Omega \times (0, T] \\ u(0, \mathbf{x}) = u_0(\mathbf{x}) & \text{in } \Omega \end{cases} \quad (\text{A.1})$$

where  $u = u(t, \mathbf{x})$  is an unknown scalar quantity defined for  $t \geq 0$  in a domain  $\Omega \subseteq \mathbb{R}^d$  and it is equal to a given function  $g(t, \mathbf{x})$  on the boundaries domain  $\Gamma = \partial\Omega$ ; moreover,  $T > 0$  is a certain final time,  $u_0(\mathbf{x})$  is the initial condition,  $\mathbf{F}(u) = \mathbf{F}(u, t, \mathbf{x})$  is a function with image in  $\mathbb{R}^d$  called flow of  $u$ , while

$$\nabla \cdot \mathbf{F}(u) = \frac{\partial F_1(u)}{\partial x_1} + \dots + \frac{\partial F_d(u)}{\partial x_d}$$

is the divergence of the vector field  $\mathbf{x} \mapsto \mathbf{F}(u(t, \mathbf{x}), t, \mathbf{x})$  made only on the spatial variables. For the sake of simplicity, even if  $\mathbf{F}$  has functional dependence from  $u$ , round bracket are used.

First of all we show why an equation of type (A.1) is called conservation law. For doing this, we fix a region  $\Sigma \subset \Omega$  with boundary  $\partial\Sigma$  sufficiently regular so that in  $\Sigma$  it holds the divergence theorem. Then, by integrating

Eq.(A.1) on  $\Sigma$  and while applying the divergence theorem, we obtain

$$\begin{aligned} 0 &= \int_{\Sigma} \left( \frac{\partial u}{\partial t} + \nabla \cdot \mathbf{F}(u) \right) d\mathbf{x} \\ &= \frac{d}{dt} \int_{\Sigma} u d\mathbf{x} + \int_{\Sigma} \nabla \cdot \mathbf{F}(u) d\mathbf{x} \\ &= \frac{d}{dt} \int_{\Sigma} u d\mathbf{x} + \int_{\partial\Sigma} \mathbf{F}(u) \cdot \mathbf{n} d\gamma \end{aligned}$$

where  $\mathbf{n}$  is a unit vector normal to the surface  $\partial\Sigma$  and pointing outward. The second integral on the right-hand side represents the flow of  $u$  across the boundary of domain  $\Sigma$ . Then by integrating over a time interval  $[t_1, t_2]$ , we have

$$\int_{t_1}^{t_2} \left[ \frac{d}{dt} \int_{\Sigma} u d\mathbf{x} + \int_{\partial\Sigma} \mathbf{F}(u) \cdot \mathbf{n} d\gamma \right] dt = 0$$

and by using the fundamental theorem of calculus, we get

$$\int_{\Sigma} u(t_2, \mathbf{x}) d\mathbf{x} = \int_{\Sigma} u(t_1, \mathbf{x}) d\mathbf{x} - \int_{t_1}^{t_2} \int_{\partial\Sigma} \mathbf{F}(u) \cdot \mathbf{n} d\gamma dt \quad (\text{A.2})$$

which immediately allows to understand why equations of type (A.1) are called conservation law. Indeed, if the flow of  $u$  across  $\partial\Sigma$  is null, then

$$\int_{t_1}^{t_2} \int_{\partial\Sigma} \mathbf{F}(u) \cdot \mathbf{n} d\gamma dt = 0 \quad (\text{A.3})$$

and therefore

$$\int_{\Sigma} u(t_2, \mathbf{x}) d\mathbf{x} = \int_{\Sigma} u(t_1, \mathbf{x}) d\mathbf{x}$$

which means that the quantity  $\int_{\Sigma} u(t, \mathbf{x}) d\mathbf{x}$  is conserved within the time interval  $[t_1, t_2]$ . On the other hand, if the quantity in (A.3) is not null, the variation of  $\int_{\Sigma} u(t, \mathbf{x}) d\mathbf{x}$  in  $[t_1, t_2]$  is equal to the balance between the incoming and outgoing flow across  $\partial\Sigma$ .

Eq.(A.2) is the starting point of each finite volume method. Therefore, the idea is to decompose the spatial domain  $\Omega$  in finite volumes, also called cells; then, in each cell it is imposed the conservation law (A.1), written in the integral form. In the following we will see how this method works in a two-dimensional and one-dimensional domain.

---

### A.0.1 Two-dimensional case

We imagine to have a domain  $\Sigma \subset \Omega$  with  $\Omega \subseteq \mathbb{R}^2$  and to decompose such domain in cells  $\Sigma_j$  with finite measure  $|\Sigma_j|$ , which intersect only at their boundaries  $\partial\Sigma_j$ . The discretization in time is made with a certain time step  $\Delta t \geq 0$ , with  $t^n = n\Delta t$ ,  $n \in \mathbb{N}$ .

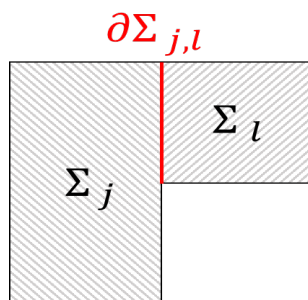


Figure A.1: Spatial discretization of a two-dimensional domain.

The first step consists in writing Eq.(A.2) for a generic cell  $\Sigma_j$  in the time interval  $[t^n, t^{n+1}]$

$$\int_{\Sigma_j} u(t^{n+1}, \mathbf{x}) d\mathbf{x} = \int_{\Sigma_j} u(t^n, \mathbf{x}) d\mathbf{x} - \int_{t^n}^{t^{n+1}} \int_{\partial\Sigma_j} \mathbf{F}(u) \cdot \mathbf{n}_j d\gamma dt. \quad (\text{A.4})$$

As shown in Fig.(A.1) we can define  $\partial\Sigma_{j,l} = \partial\Sigma_j \cap \partial\Sigma_l$  which is the common boundary between cells  $\Sigma_j$  and  $\Sigma_l$ , and write (A.4) as

$$\int_{\Sigma_j} u(t^{n+1}, \mathbf{x}) d\mathbf{x} = \int_{\Sigma_j} u(t^n, \mathbf{x}) d\mathbf{x} - \sum_{|\partial\Sigma_{j,l}| > 0} \int_{t^n}^{t^{n+1}} \int_{\partial\Sigma_{j,l}} \mathbf{F}(u) \cdot \mathbf{n}_j d\gamma dt.$$

The second step consists in introduce the cell average values of the exact solution and the average fluxes on cell boundaries

$$\begin{aligned} U_j^n &= \frac{1}{|\Sigma_j|} \int_{\Sigma_j} u(t^n, \mathbf{x}) d\mathbf{x} \\ F_{j,l}^n &= \frac{1}{\Delta t} \int_{t^n}^{t^{n+1}} \frac{1}{|\partial\Sigma_{j,l}|} \int_{\partial\Sigma_{j,l}} \mathbf{F}(u) \cdot \mathbf{n}_j d\gamma dt \end{aligned} \quad (\text{A.5})$$

and by substituting relations (A.5) in Eq.(A.4) we obtain

$$|\Sigma_j| U_j^{n+1} = |\Sigma_j| U_j^n - \Delta t \sum_{|\partial\Sigma_{j,l}| > 0} |\partial\Sigma_{j,l}| F_{j,l}^n.$$

If we divide by  $|\Sigma_j|$  and we define

$$\lambda_{j,l} = \Delta t \frac{|\partial \Sigma_{j,l}|}{|\Sigma_j|}$$

we finally obtain the relation

$$U_j^{n+1} = U_j^n - \sum_{|\partial \Sigma_{j,l}| > 0} \lambda_{j,l} F_{j,l}^n. \quad (\text{A.6})$$

Eq.(A.6) is the discrete form of Eq.(A.4); indeed, if the flow across cells  $\Sigma_j$  and  $\Sigma_l$  is null, then  $U_j^{n+1} = U_j^n$ ; this means that the quantity  $U$  in cell  $\Sigma_j$  is conserved within the time interval  $[t^n, t^{n+1}]$ . Thus, Eq.(A.6) suggests to define a numerical scheme in which the cell average values are update at each time step in order to the numerical flux values, easily obtained from the cell average values of the surrounding cells.

Till this point we have not introduced approximations, indeed Eq.(A.6) provides an exact solution. But for being able to implement equations as Eq.(A.1), approximations must be introduced. Therefore, we define a discrete cell average value  $u_j^n \simeq U_j^n$ , which is an approximation of the exact one; so,  $u_j^n$  represents the discrete cell average value of cell  $\Sigma_j$  at time  $t^n$ . Moreover, we introduce the so-called numerical flux  $f_{j,l}^n = f(u_j^n, u_l^n) \simeq F_{j,l}^n$ , which is an approximation of the average flux between two consecutive cells  $\Sigma_j$  and  $\Sigma_l$ , defined by using their discrete cell average values  $u_j^n$  and  $u_l^n$ .

Thanks to these considerations, we are able to write the numerical scheme of whatever finite volume method that operates on a two-dimensional domain, and is given by

$$u_j^{n+1} = u_j^n - \sum_{|\partial \Sigma_{j,l}| > 0} \lambda_{j,l} f_{j,l}^n. \quad (\text{A.7})$$

Once that the discretization is made and the time step  $\Delta t$  is chosen, the unique unknown quantity of the numerical scheme (A.7) is the numerical flux  $f_{j,l}^n$ . Hence, the unique difference among all finite volume methods relies on the choice of  $f_{j,l}^n$ . It is worth to point out that it does not exist a numerical flux which gives optimal results for all problems, but instead each application has its own optimal choice. Since the solution obtained depends mainly on the way in which the flux among cells is evaluated, it is recommended to make this choice carefully, possibly applying the scheme adopted on a benchmark model.

---

## A.0.2 One-dimensional case

In this context the domain to discretize is  $\Omega \subseteq \mathbb{R}$ . We introduce a spatial discretization with intervals of length  $\Delta x$ , as shown in Fig.(A.2). Since  $\Delta x$  is constant, all cell centers are equispaced, so  $x_j = j\Delta x, j \in \mathbb{Z}$ . Each cell is defined as  $\Sigma_j = [x_{j-1/2}, x_{j+1/2}]$ , where  $x_j$  represent the cell center and  $x_{j+1/2} = (j + \frac{1}{2})\Delta x$  is the boundary. As before, we divide the final time  $T$  in  $N$  time steps each long  $\Delta t > 0$ , so that  $T = N\Delta t$ , and  $t^n = n\Delta t, n \in \mathbb{N}$ .

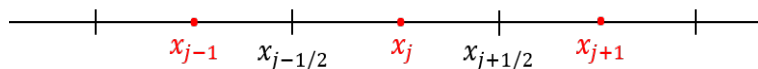


Figure A.2: Spatial discretization of a one-dimensional domain.

Consequently, Eq.(A.2) can be written as

$$\int_{x_{j-1/2}}^{x_{j+1/2}} u(t^{n+1}, x) dx = \int_{x_{j-1/2}}^{x_{j+1/2}} u(t^n, x) dx + \left( \int_{t^n}^{t^{n+1}} F(u(t, x_{j+1/2})) dt - \int_{t^n}^{t^{n+1}} F(u(t, x_{j-1/2})) dt \right) \quad (\text{A.8})$$

and by substituting in Eq.(A.8) the cell average values of the exact solution

$$U_j^n = \frac{1}{\Delta x} \int_{x_{j-1/2}}^{x_{j+1/2}} u(t^n, x) dx$$

and the average fluxes of  $u$  across the cell boundaries

$$F_{j+1/2}^n = \frac{1}{\Delta t} \int_{t^n}^{t^{n+1}} F(u(t, x_{j+1/2})) dt$$

we get

$$\Delta x U_j^{n+1} = \Delta x U_j^n - (\Delta t F_{j+1/2}^n - F_{j-1/2}^n).$$

If we divide by  $\Delta x$  and we define

$$\lambda_j = \frac{\Delta t}{\Delta x} > 0$$

we obtain the relation

$$U_j^{n+1} = U_j^n - \lambda_j (F_{j+1/2}^n - F_{j-1/2}^n). \quad (\text{A.9})$$

Each finite volume method defined on a one-dimensional domain is based on relation (A.9), where the unknown quantities are the discrete cell average values  $u_j^n$ , which are approximations of the exact cell average values  $U_j^n$ . Starting by the discrete cell average values, an approximation of the solution  $u(t^n, x)$  is reconstructed. Moreover, as in the two-dimensional case, also the quantity  $F_{j+1/2}^n$  must be approximated by a numerical flux  $f_{j+1/2}^n$ , which is defined by taking in consideration only the two cells with common interface  $x_{j+1/2}$ , so that

$$f_{j+1/2}^n = f(u_j^n, u_{j+1}^n).$$

Once that the expression of the numerical flux is chosen, relation (A.9) can be written as

$$u_j^{n+1} = u_j^n - \lambda_j (f_{j+1/2}^n - f_{j-1/2}^n). \quad (\text{A.10})$$

This scheme is common for all finite volume methods and is used for advancing in time. Since this will be the scheme adopted in the following, we will provide a trivial example for showing how it operates, and what means choose a numerical flux.

#### A.0.2.1 Example:

Let us consider the conservation law

$$\begin{cases} \frac{\partial u}{\partial t} + \frac{\partial}{\partial x} F(u) = 0 & \text{in } \Omega \times (0, T] \\ u(0, x) = u_0(x) & \text{in } \Omega \end{cases} \quad (\text{A.11})$$

where  $\Omega = [0, 2] \subset \mathbb{R}$ ,  $a$  is a zero constant and  $F(u) = au$  is the flow of  $u$ . Hence, Eq.(A.11) can be written also as

$$\begin{cases} \frac{\partial u}{\partial t} + a \frac{\partial u}{\partial x} = 0 & \text{in } \Omega \times (0, T] \\ u(0, x) = u_0(x). & \text{in } \Omega \end{cases} \quad (\text{A.12})$$

This initial-value problem is able to reproduce the propagation of a signal along the  $x$ -axis, which spreads with constant velocity  $|a|$ ; in particular the propagation is toward the right direction if  $a > 0$  or toward the left if  $a < 0$ .

Initial-value problem (A.12) admits an analytical solution. Indeed, if we fix arbitrarily a time  $\bar{t} > 0$  and a point  $\bar{x}$ , the characteristic line which passes by  $(\bar{t}, \bar{x})$  has equation

$$x(t) = \bar{x} + a(t - \bar{t}). \quad (\text{A.13})$$

Relation (A.13) crosses the  $x$ -axis in the point  $x(0) = \bar{x} - a\bar{t}$ ; therefore

$$u(\bar{t}, \bar{x}) = u(\bar{t}, x(\bar{t})) = u(0, x(0)) = u(0, \bar{x} - a\bar{t}) = u_0(\bar{x} - a\bar{t}).$$

Since the point  $(\bar{t}, \bar{x})$  is arbitrary, we can conclude that the solution of the initial-value problem (A.12) is given by

$$u(x, t) = u_0(x - at), \quad x \in \mathbb{R}, \quad t \geq 0. \quad (\text{A.14})$$

On the other hand, since (A.12) is a conservation law on a one-dimensional domain, it can be solved also numerically by using the numerical scheme (A.10). Therefore, we have to choose a suitable numerical flux. The most popular ones are the following:

- Lax-Friedrichs scheme:

The numerical flux  $f(u, v)$  is given by

$$f_{LF}(u, v) = \frac{a}{2}(u + v) + \frac{1}{2\lambda}(u - v)$$

which gives a numerical scheme that can be written as

$$\frac{u_j^{n+1} - u_j^n}{\Delta t} + a \frac{u_{j+1}^n - u_{j-1}^n}{2\Delta x} - \Delta x \frac{1}{2\lambda} \frac{u_{j+1}^n - 2u_j^n + u_{j-1}^n}{\Delta x^2} = 0.$$

Thus, this method corresponds to a finite-difference discretization in  $x_j$  at time  $t^n$  of the modified equation

$$\frac{\partial u}{\partial t} + a \frac{\partial u}{\partial x} - \Delta x \frac{1}{2\lambda} \frac{\partial^2 u}{\partial x^2} = 0 \quad (\text{A.15})$$

which has an additional diffusion term proportional to  $\Delta x \frac{1}{2\lambda}$  also denoted as numerical diffusion.

- Upwind scheme:

The numerical flux  $f(u, v)$  is given by

$$f_U(u, v) = \begin{cases} au & \text{if } a > 0 \\ av & \text{if } a < 0 \end{cases}$$

which gives a numerical scheme that can be written as

$$\frac{u_j^{n+1} - u_j^n}{\Delta t} + a \frac{u_{j+1}^n - u_{j-1}^n}{2\Delta x} - \Delta x \frac{|a|}{2} \frac{u_{j+1}^n - 2u_j^n + u_{j-1}^n}{\Delta x^2} = 0.$$

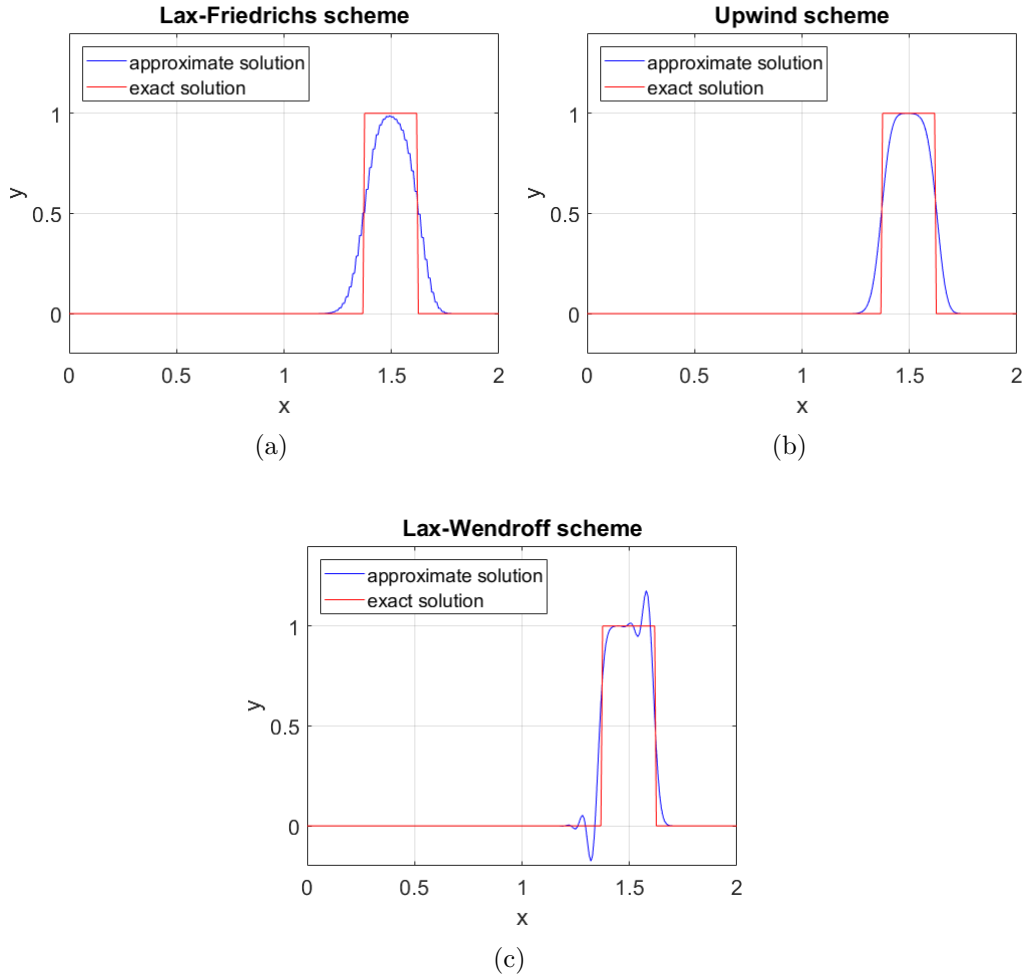


Figure A.3: Solutions of initial-value problem (A.12) plotted at time  $t = 4.5$  s and obtained with different numerical fluxes; the exact solution in red is given by (A.14).

Hence, this method corresponds again to a finite-difference discretization in  $x_j$  at time  $t^n$  of the modified equation (A.15). The unique difference is that now the numerical diffusion is proportional to  $\Delta x \frac{|a|}{2}$ .

- Lax-Wendroff scheme:

The numerical flux  $f(u, v)$  is given by

$$f_{LW}(u, v) = \frac{a}{2}(u + v) + \frac{1}{2}\lambda a^2(u - v)$$

which gives a numerical scheme that can be written as

$$\frac{u_j^{n+1} - u_j^n}{\Delta t} + a \frac{u_{j+1}^n u_{j-1}^n}{2\Delta x} - \Delta x \frac{\lambda a^2}{2} \frac{u_{j+1}^n - 2u_j^n + u_{j-1}^n}{\Delta x^2} = 0.$$


---

Thus, this method corresponds to a finite-difference discretization in  $x_j$  at time  $t^n$  of the modified equation (A.15), and introduces a numerical diffusion proportional to  $\Delta x \frac{\lambda a^2}{2}$ .

The behaviour of the solution provided by the numerical schemes above described is shown in Fig.(A.3). The initial condition is a function that assumes value 1 in the interval  $[0.25, 0.5]$ , 0 otherwise. For all cases,  $a = 1/4$  while the length of each cell is  $\Delta x = 1/128$ . In order to ensure the stability of the system, the time step  $\Delta t$  is chosen such that

$$\Delta t = Cour \frac{\Delta x}{a}.$$

In this way the CFL condition is satisfied. The Courant number used in Fig.(A.3) is  $Cour = 0.85$ . It is noticeable how the choice of the numerical flux strongly affect the performances of the method. In particular, the numerical diffusion of the Lax-Friedrichs and Upwind scheme is evident in Fig.(A.3a) and Fig.(A.3b), more accentuated in the first one; the dispersion of the Lax-Wendroff scheme is visible in Fig.(A.3c). Moreover, the Lax-Wendroff scheme does not even respect the maximum principle, indeed the approximated solution assumes values above 1 and under 0.

---



# Bibliography

- [1] Lorenzo Pareschi e Giuseppe Toscani, *Interacting multiagent systems*, Oxford university press, 2013.
- [2] F. Venuti, V. Racic, A. Corbetta, *Pedestrian-structure interaction in the vertical direction: coupled oscillator-force model for vibration serviceability assessment*, Proceedings of the 9th International Conference on Structural Dynamics, 2014.
- [3] L. Ambrosio, *Lecture notes on optimal transport problems*, 2000.
- [4] D. Helbing, P. Molnàr, *Social force model for pedestrian dynamics*, Phys. Rev. E 51, (1995) 4282– 4286.
- [5] W. Zeng, H. Nakamura, P. Cheng, *A modified social force model for pedestrian behavior simulation at signalized crosswalks*, The 9th International Conference on Traffic and Transportation Studies, 2014.
- [6] F. Johansson, A. Peterson, A. Tapani, *Waiting pedestrians in the social force model*, Physica A: Statistical Mechanics and its Applications, (419), (2015) 95-107.
- [7] Y.Han, H Liu, *Modified social force model based on information transmission toward crowd evacuation simulation*, Physica A 469 (2017) 499–509.
- [8] S. Okazaki, *A study of pedestrian movement in architectural space, Part 1: pedestrian movement by the application of magnetic model*, Trans. A.I.J. 283, (1979) 111–119.
- [9] S. Okazaki, *A study of pedestrian movement in architectural space, Part 2: concentrated pedestrian movement*, Trans. A.I.J. 284,(1979) 101–110.

- 
- [10] S. Okazaki, *A study of pedestrian movement in architectural space, Part 3: along the shortest path, taking fire, congestion and unrecognized space into account*, Trans. A.I.J. 285, (1979) 137–147.
- [11] S. Okazaki, S. Matsushita, *A study of pedestrian movement in architectural space, Part 5: a probing walk and a guide walk by a guideboard*, Trans. A.I.J. 302, (1981) 87–93.
- [12] S. Okazaki, C. Yamamoto, *A study of pedestrian movement in architectural space, Part 4: pedestrian movement represented in perspective*, Trans. A.I.J. 299, (1981) 105–113.
- [13] W.J. Yu, R. Chen, L.Y. Dong, S.Q. Dai, *Centrifugal force model for pedestrian dynamics*, Phys. Rev. E 72, 026112/1–7, 2005.
- [14] A. Kirchner, A. Schadschneider, *Simulation of evacuation processes using a bionics-inspired cellular automaton model for pedestrian dynamics*, Physica A 312, (2002) 260–276.
- [15] V.J. Blue, J.L. Adler, *Emergent fundamental pedestrian flows from cellular automata microsimulation*, Transp. Res. Rec. 1644, (1998) 29–36.
- [16] V.J. Blue, J.L. Adler, *Cellular automata microsimulation of bidirectional pedestrian flows*, Transp. Res. Rec. 1678, (1999) 135–141.
- [17] V.J. Blue, J.L. Adler, *Modeling four-directional pedestrian flows*, Transp. Res. Rec. 1710, (2000) 20–27.
- [18] C. Burstedde, K. Klauck, A. Schadschneider, J. Zittartz, *Simulation of pedestrian dynamics using a two-dimensional cellular automaton*, Physica A 295, (2001) 507–525.
- [19] Y. Gao, P.B. Luh, H. Zhang, T. Chen, *A modified social force model considering relative velocity of pedestrians*, IEEE International Conference on Automation Science and Engineering (CASE), 2013.
- [20] B. Maury, J. Venel, *A mathematical framework for a crowd motion model*, C. R. Acad. Sci. Paris Ser. I 346, (2008) 1245–1250.
-

- 
- [21] A. Corbetta, A. Tosin, *Comparing first-order microscopic and macroscopic crowd models for an increasing number of massive agents*, Advances in Mathematical Physics Volume 2016, Article ID 6902086.
- [22] A. Corbetta, *Multiscale crowd dynamics: physical analysis, modeling and applications*, PhD thesis, 2015.
- [23] G. Martalò, *Different scale modeling for crowd dynamics and multi-temperature gas mixtures*, PhD thesis, 2014.
- [24] H.P. Gavin, *Vibrations of single degree of freedom systems*, CEE 541. Structural Dynamics, 2016.
- [25] A. Tosin, *Un approccio multiscala alla dinamica delle folle mediante misure che evolvono nel tempo*, Bollettino dell'Unione Matematica Italiana, 2013.
- [26] J. Evers, *Modelling crowd dynamics: a multiscale, measure-theoretical approach*, Master's thesis, 2011.
- [27] I. Roos, *Human induced vibrations on footbridges - Application and comparison of pedestrian load models*, Master's thesis, 2009.
- [28] C. Dogbe, *On the modelling of crowd dynamics by generalized kinetic models*, J. Math. Anal. Appl. 387 (2012) 512–532.
- [29] E.S. Mashaly, T.M. Ebrahim, H. Abou-Elfath, O.A. Ebrahim, *Evaluating the vertical vibration response of footbridges using a response spectrum approach*, Alexandria Engineering Journal (2013) 52, (2013) 419–424.
- [30] G.W. Parry, *The Dynamics of Crowds*, Master's thesis, 2007.
- [31] M.J. Lighthill, G.B. Whitham, *On kinematic waves. II. A theory of traffic flow on long crowded roads*, Proc. R. Soc. Lond. Ser. A 229, (1955) 317–345.
- [32] P.I. Richards, *Shock waves on the highway*, Oper. Res. 4, (1956) 42–51.
- [33] H.J. Payne, *Models of freeway traffic and control*, Math. Models Publ. Syst. Simul. Counc. Proc. 28, 51–61, 1971.
-

- 
- [34] G.B. Whitham, *Linear and Nonlinear Waves*, Pure and Applied Mathematics. Wiley, New York, 1974.
- [35] D. Helbing, *A fluid-dynamic model for the movement of pedestrians*, Complex Syst. 6, (1992) 391–415.
- [36] R.M. Colombo, M.D. Rosini, *Pedestrian flows and non-classical shocks*, Math. Methods Appl. Sci. 28, (2005) 1553–1567.
- [37] R.M. Colombo, P. Goatin, G. Maternini, M.D. Rosini, *Macroscopic Models for Pedestrian Flows*, eventh Venice International Conference, 2010.
- [38] V. Coscia, C. Canavesio, *First-order macroscopic modelling of human crowd dynamics*, Math. Models Methods Appl. Sci. 18, (2008) 1217–1247.
- [39] N. Bellomo, C. Dogbè, *On the modelling crowd dynamics from scaling to hyperbolic macroscopic models*, Math. Models Methods Appl. Sci. 18, (2008) 1317–1345.
- [40] N. Bellomo, C. Dogbè, *On the modeling of traffic and crowds: a survey of models, speculations, and perspectives*, SIAM Rev. 53, (2011) 409–463.
- [41] D. Helbing, A. Johansson, H. Zein Al-Abideen, *Dynamics of crowd disasters: an empirical study*, Phys. Rev. E 75, 046109/1–7, 2007.
- [42] A. Seyfried, B. Steffen, W. Klingsch, M. Boltes, *The fundamental diagram of pedestrian movement revisited*, J. Stat. Mech. Theory Exp. 2005(10), P10002, 2005.
- [43] F. Venuti, L. Bruno, *Crowd-structure interaction in lively footbridges under synchronous lateral excitation: a literature review*, Phys. Life Rev. 6, (2009) 176–206.
- [44] W. Daamen, S.P. Hoogendoorn, *Experimental research of pedestrian walking behavior*, Transp. Res. Rec. 1828, (2003) 20–30.
- [45] B. Maury, A. Roudneff-Chupin, F. Santabrogio, *A macroscopic crowd motion model of gradient flow type*, Math. Models Methods Appl. Sci. 20, (2010) 1787–1821.
-

- 
- [46] B. Maury, A. Roudneff-Chupin, F. Santabrogio, J. Venel, *Handling congestion in crowd motion modeling*, *Netw. Heterog. Media* 6, (2011) 485–519.
- [47] E. Cristiani, B. Piccoli, A. Tosin, *Multiscale modeling of granular flows with application to crowd dynamics*, *Multiscale Model. Simul.* 9, (2012) 155–182.
- [48] L. Bruno, A. Corbetta, A. Tosin, *From individual behaviour to an evaluation of the collective evolution of crowds along footbridges*, arXiv:1212.3711, 2016.
- [49] L.D. Vanumu, K.R. Rao, G. Tiwari, *Fundamental diagrams of pedestrian flow characteristics: A review*, *Eur. Transp. Res. Rev.*, 2017.
- [50] E. Cristiani, B. Piccoli, A. Tosin, *Multiscale modeling of pedestrian dynamics*, Springer, 2014.
- [51] F. Venuti, L. Bruno, N. Bellomo, *Crowd dynamics on a moving platform: Mathematical modelling and application to lively footbridges*, *Mathematical and Computer Modelling* 45 (2006) 252–269.
- [52] L. Bruno, F. Venuti, *Crowd–structure interaction in footbridges: Modelling, application to a real case-study and sensitivity analyses*, *Journal of Sound and Vibration* 323 (2009) 475–493.
- [53] B. During, G. Toscani, *Hydrodynamics from kinetic models of conservative economies*, *Physica A* 384 (2007) 493–506.
- [54] F. Venuti, L. Bruno, *Mitigation of human-induced lateral vibrations on footbridges through walkway shaping*, *Engineering Structures* 56 (2013) 95–104.
- [55] S.P. Carroll, J.S. Owen, M.F.M. Hussein, *Modelling crowd–bridge dynamic interaction with a discretely defined crowd*, *Journal of Sound and Vibration* 331 (2012) 2685–2709.
- [56] F. Venuti, V. Racic, A. Corbetta, *Modelling framework for dynamic interaction between multiple pedestrians and vertical vibrations of footbridges*, *Journal of Sound and Vibration* 379 (2016) 245–263.
-

- 
- [57] L. Bruno, A. Tosin, P. Tricerri, F. venuti, *Non-local first-order modelling of crowd dynamics: A multidimensional framework with applications*, Applied Mathematical Modelling 35 (2011) 426–445.
- [58] L. Bruno, F. Venuti, *A new load model of the pedestrians lateral action*, Third international conference, 2008.
- [59] Y. Matsumoto, H. Shiojiri, T. Nishioka, *Dynamic design of footbridges*, IABSE proceedings P-17/78, 1978.
- [60] E. Shahabpoor, A. Pavic, V. Racic, *Identification of walking human model using agent-based modelling*, Mechanical Systems and Signal Processing 103 (2018) 352–367.
- [61] C. Dogbe, *On the modelling of crowd dynamics by generalized kinetic models*, J. Math. Anal. Appl. 387 (2012) 512–532.
- [62] S. Al-Nasur, P. Kachroo, *A Microscopic-to-macroscopic crowd dynamic model*, IEEE Conference on Intelligent Transportation Systems 606-611. Institute of Electrical and Electronics Engineers, 2006.
- [63] M.D. Rosini, *Macroscopic Models for Vehicular Flows and Crowd Dynamics: Theory and Applications*, Understanding Complex Systems. Springer, Switzerland, 2013.
- [64] A. Quarteroni, *Numerical Models for Differential Problems*, Springer, 2017.
- [65] C. Hirsch, *Numerical computation of internal and external flows*, Elsevier, 2007.
- [66] A. Quarteroni, R. Sacco, F. Saleri, *Numerical mathematics*, Spinger, 2000.
- [67] S. Bartels, *Numerical methods for non linear partial differential equations*, Springer, 2015.
- [68] A. Fasana, S. Marchesiello, *Meccanica delle vibrazioni*, Clut, 2006.
- [69] M. Colangeli, *From Kinetic Models to Hydrodynamics*, Springer, 2013.
-

- 
- [70] R.J. LeVeque, *Numerical Methods for Conservation Laws*, Springer, 1992.
- [71] M. Paz, W. Leigh, *Structural dynamics*, Springer, 2004.
- [72] S.S. Rao, *Mechanical vibrations*, Pearson, 2011.
- [73] C. Canuto, *Appunti per il corso di fluidodinamica e ingegneria del vento computazionali*, 2014.
- [74] D.H. Biedermann, C. Torchiani, P.M. Kielar, D. Willems, O. Handel, S. Ruzika, A. Borrmann, *A hybrid and multiscale approach to model and simulate mobility in the context of public events*, International Scientific Conference on Mobility and Transport Transforming Urban Mobility, mobil.TUM 2016, 6-7 June 2016, Munich, Germany.
- [75] L. Boltzmann, *Weitere studien uber das warmegleichgewicht unter gasmolekullen*, Lectures on gas theory, Berkeley: University of California Press, 1964.
- [76] L.F. Henderson, *On the fluid mechanics of human crowd motion*, Transp. Res. 8, (1974) 509–515.
- [77] N. Bellomo, A. Bellouquid, *On the modeling of crowd dynamics: looking at the beautiful shapes of swarms*, Netw. Heterog. Media 6(3), (2011) 383–399.
- [78] N. Bellomo, A. Bellouquid, *On multiscale models of pedestrians crowds: from mesoscopic to macroscopic*, COMMUN.MATH.SCI Vol. 13, No. 7, pp. 1649–1664, 2015.
- [79] C. Heinemeyer, M. Feldmann, *European design guide for footbridge vibration*, Third international conference - footbridge, 2008.
- [80] G. Naldi, *Mathematical modeling of collective behavior in socio-economic and life sciences*, Birkhäuser, 2010.
- [81] N. Bellomo, P. Degond, E. Tadmor, *Active particles, Volume 1: advances in theory, models, and applications*, Birkhäuser, 2017.
-

- 
- [82] N. Bellomo, A. Bellouquid, L. Gibelli, N. Outada, *A Quest Towards a Mathematical Theory of Living Systems*, Birkhäuser, 2017.
- [83] C. Butz, M. Feldmann, C. Heinemeyer, G. Sedlacek, B. Chabrolin, A. Lemaire, *Advanced load models for synchronous pedestrian excitation and optimised design guidelines for steel footbridges*, Tech. Rep. RFS-CR 03019, Research Fund for Coal and Steel, 2008.
- [84] R.L. Hughes, *A continuum theory for the flow of pedestrians*, Transportation Research Part B 2002; 36:507–35.
- [85] U. Weidmann, *Transporttechnik der Fussgänger*, Tech. Rep. n. 90, Zürich: ETH, 1993.
- [86] J.J. Fruin, *Pedestrian planning and design*, Elevator World Inc., 1971.
- [87] H.K. Lam, J.F. Morrall, H. Ho, *Pedestrian flow characteristics in Hong Kong*, Transportation Research Record; 1487:56–62, 1995.
- [88] S.J. Older, *Movement of pedestrians on footways in shopping streets*, Traffic Engineering and Control; 10:160–3, 1968.
- [89] J. Pauls, *Calculating evacuation times for tall buildings*, Fire Safety Journal; 12:213–36, 1987.
- [90] M.R. Virkler, S. Elayadath, *Pedestrian speed-flow-density relationships*, Transportation Research Record; 1438:51–8, 1994.
- [91] A. Polus, J. Schofer, A. Ushpiz, *Pedestrian flow and level of service*, Journal of Transport Engineering; 109:46–56, 1983.
- [92] A.K. Sarkar, K. Janardhan, *A study on pedestrian flow characteristics*, In: Proceedings 76th transportation research board annual meeting, Washington; 1997.
- [93] Y. Tanariboon, S. Hwa, C. Chor, *Pedestrian characteristics study in Singapore*, ASCE Journal of Transportation Engineering; 112:229–35, 1986.
-

- 
- [94] S.S. Vallender, *Calculation of the Wasserstein distance between probability distributions on the line*, Theory Probab. Appl., 18(4), (1974) 784–786.
- [95] V. Venuti, L. Bruno, *Crowd-structure interaction in lively footbridges under synchronous lateral excitation: a literature review*, Physics of Life Reviews 6 (2009) 176–206.
- [96] R. Clough, J. Penzien, *Dynamics of structures*, New York: McGraw-Hill; 1987.
- [97] M. Landajuela, *Burgers equation*, BCAM Internship, 2011.
- [98] P. Dallard, T. Fitzpatrick, A. Flint, A. Low, R.R. Smith, M. Willford, M. Roche, *London Millennium Bridge: pedestrian-induced lateral vibration*, Journal of Bridge Millennium, Volume 6 Issue 6, 2001.
- [99] C. Cremona, *Dynamic investigations of the Solferino footbridge*, 3rd International Operational Modal Analysis Conference, 2009.
- [100] E.T. Ingólfsson, C.T. Georgakis, J. Jönsson, *Pedestrian-induced lateral vibrations of footbridges: A literature review*, Engineering Structures 45 (2012) 21–52.
- [101] C.S. Oliveira, V.T. Camacho, *Data-base with in-situ vibration frequencies of bridges in Portugal*, J Civil Struct Health Monit 6:851–862, 2016.
- [102] D. Helbing, *A mathematical model for the behaviour of pedestrians*, Behav. Sci. 36 (1991) 298–310.
- [103] D. Helbing, L. Buzna, A. Johansson, T. Werner, *Self-organized pedestrian crowd dynamics: experiments, simulations and design solutions*, Transportation Sci. 39 (2005) 1–24.
- [104] R.L. Hughes, *The flow of human crowds*, Annu. Rev. Fluid Mech. 35 (2003) 169–183.
- [105] A. Festa, A. Tosin, M.T. Wolfram, *Kinetic description of collision avoidance in pedestrian crowds by sidestepping*, Kinetic and Related Models, American Institute of Mathematical Sciences Volume 11, Number 3, June 2018.
-

- 
- [106] S.I. Nakamura, T. Kawasaki, *Lateral vibration of footbridges by synchronous walking*, Journal of Constructional Steel Research 62 (2006) 1148–1160.
- [107] M. Bocian, J.H.G. Macdonald, J.F. Burn, *Biomechanically inspired modeling of pedestrian-induced vertical self-excited forces*, American Society of Civil Engineers, 2013.
- [108] C. Caprani, J. Keogh, P. Archbold, P. Fanning, *Characteristic vertical response of a footbridge due to crowd loading*, Proceedings of the 8th International Conference on Structural Dynamics EURODYN 2011, Leuven, Belgium, 2011.
- [109] H. Dang, S. Živanović, *Modelling pedestrian interaction with perceptibly vibrating footbridges*, FME Transactions 41 (2013) 271–278.
- [110] Technical guide, *Footbridges: Assessment of vibrational behaviour of footbridges under pedestrian loading*, published by the Sétra, 2006.
- [111] C.C. Caprani, E. Ahmadi, *Formulation of human–structure interaction system models for vertical vibration*, Journal of Sound and Vibration 377 (2016) 346–367.
- [112] J.M. Biggs, *Introduction to structural dynamics*, McGraw-Hill, NewYork, 1964.
- [113] D. O’Sullivan, C.C. Caprani, J. Keogh, *The response of a footbridge to pedestrians carrying additional mass*, Bridge and Concrete Research Ireland Conference, Dublin, 2012.
- [114] V. Racic, A. Pavic, J.M.W. Brownjohn, *Experimental identification and analytical modelling of human walking forces: Literature review*, Journal of Sound and Vibration 326 (2009) 1–49.
- [115] V. Racic, J.M.W. Brownjohn, *Stochastic model of near-periodic vertical loads due to humans walking*, Advanced Engineering Informatics 25 (2011) 259–275.
- [116] M. Willford, P. Young, *A design guide for footfall induced vibrations of structures*, The Concrete Centre, Slough, 2006.
-